Universitat Autònoma de Barcelona

FLEXOELECTRICITY IN SINGLE CRYSTALS

Jackeline Narvaez Morales

FLEXOELECTRICITY IN SINGLE CRYSTALS

Jackeline Narvaez Morales

Programa de Doctorat en Física-Departament de Física

Universitat Autònoma de Barcelona

Director: Prof. Gustau Catalan Bernabé

Co-Director: Dr. Neus Domingo

Memòria presentada per l'obtenció de la titulació de Doctor

Bellaterra December, 2015

CSIC Consejo Superior de Investigaciones Científicas

UAB Universitat Autònoma de Barcelona

ICN2 Institut Català de Nanociència i Nanotecnologia

Excelencia Severo Ochoa

Prof. Gustau Catalan, profesor de investigación ICREA, **Neus Domingo**, investigadora Ramon y Cajal y el **Prof. Jordi Sort**, catedrático de la Universidad Autónoma de Barcelona,

CERTIFICAN:

Que Jackeline Narvaez Morales, Licenciada en Física, ha realizado bajo su dirección el trabajo de investigación titulado: "**Flexoelectricity in single crystals**". Dicho trabajo ha sido desarrollado dentro del programa de doctorado de Física de la Universidad Autónoma de Barcelona.

Y para que así conste, firman el presente certificado:

Prof. Gustau Catalan Dra Neus Domingo Prof. Jordi Sort

Jackeline Narvaez

Bellaterra, Enero 20 del 2016

ACKNOWLEDGEMENTS.

I would like to start by offering my acknowledgements to my supervisor. Prof. Gustau Catalan Bernabé, for giving me the opportunity to work in the laboratory of Oxide Nanoelectronics at the Catalan Institute of Nanoscience and nanotechnology. I also thank the expertise he has provided to my thesis and to teach me how to work effectively. In this gratitude I should include Dr Neus Domingo for her valuable comments during these years.

I appreciate the support of Professor Massimiliano Stengel for the theoretical calculation, Francisco Belarre on sample preparation (polishing and cutting samples), Jaume Roqueta for his training and support in Pulsed Laser Deposition and Pablo Garcia for support in X Ray Diffraction. Additionaly I would like to extend this gratitude to the people of the maintenance division, Ismael Galindo and Dani Peruga. They always had very good attitude and disposition to help.

Special acknowledgements are deserved by the members of oxide nanoelectronics group for their support and patience during these years, especially Umesh Bhaskar, Kumara Cordero, Fabian Vásquez, James Zapata and Sahar Saremi for innumerable comments and help in this period. Additionally, I thank all my friends that accompanied me during these years.

Finally, I would like to express my gratitude to my family because they gave me all the support and motivation to enhance my knowledge despite all the difficulties in our lives. And my last and deepest words are to express my gratitude to my daughter Catalina Narvaez, who is the sense and motor of my life, and has been patient and understanding with me during every stage of my Ph.D.

The doctoral work leading to this thesis has been financially supported by a grant from Spanish government (JAE-Predoc fellowship)

ABSTRACT

In general terms, flexoelectricity is the response of polarization to a strain gradient. In contrast to the piezoelectric effect, this effect is present in all materials regardless of their crystal structure. In this doctoral dissertation, we studied the bending-induced polarization in dielectric and semiconductor single crystals that arises from two mechanisms: bulk flexoelectricity and surface flexoelectricity. Both mechanisms are of the same order in ordinary dielectrics and, before this work, their respective contributions were considered indistinguishable one from another. The research in this thesis shows that it is possible to separate the two contributions. Additionally, we show that bending-induced reorientation of polar nanoregions can also enhance the effective flexoelectric coefficients well above the intrinsic value.

Polarization can be generated by dielectric separation of bound charge within atoms or unit cells, but also by a space charge separation of free carriers. Until now, when referring to flexoelectricity, only the response from bound charge was taken into account (chapter 3 and 4); however, in this thesis dissertation we report that free charge also can also contribute, generating very big effective flexoelectric responses in semiconductor materials (chapter 5).

We have divided this thesis dissertation as follows:
Chapter 1 is an introduction to the physics of polarization and flexoelectricity, while Chapter 2 describes the experimental procedure that has been used to develop this work; there are details about the set-up specifically developed for the flexoelectric measurement, required for this project.

In chapter 3, we have measured and analyzed the bending-induced polarization of $Pb(Mg_{1/3}Nb_{2/3})O_3$-$PbTiO_3$ single crystals with compositions at the relaxor-ferroelectric phase boundary. The crystals display flexocoupling coefficients $f > 100$ V, an order of magnitude bigger than the theoretical upper limit set by the theories of Kogan and Tagantsev. This enhancement persists in the paraphase up to a temperature T* = 500 ± 25K that coincides with the disappearance of anelastic softening in the crystals; above T*, the true (lattice-based) flexocoupling coefficient is measured as $f_{13} \approx 10$V. Cross-correlation between flexoelectric, dielectric, and

elastic properties indicates that the enhancement of bending-induced polarization of relaxor ferroelectrics is not caused by intrinsically giant flexoelectricity but by the reorientation of polar nanodomains that are ferroelastically active below T*.

In chapter 4, we have studied the bending-induced polarization of barium titanate single crystals that have been measured with an aim to elucidate the origin of the large difference between the theoretically predicted and experimentally measured magnitudes of flexoelectricity in this material. The results point toward precursor polar regions (short range order) that exist above T_C and up to T* ≈ 200-225ºC and align themselves with the strain gradient, thus increasing the effective flexoelectricity, just like in the case of relaxors. Above T*, the flexovoltage coefficient drops down to intrinsic-like values, but still show an unexpectedly large anisotropy for a cubic material, with (001)-oriented crystals displaying 10 times more flexoelectricity than (111)-oriented crystals. Theoretical analysis shows that this anisotropy cannot be a bulk property, and we therefore interpret it as indirect evidence for the theoretically predicted but experimentally elusive contribution of surface piezoelectricity to macroscopic bending polarization.

In chapter 5, we have studied the flexoelectricity of reduced barium titanate single crystals, where introduction of oxygen vacancies increases the carrier density, turning them into n-type semiconductors. Semiconductors appear to also redistribute their charge in response to strain gradients, just like the dielectric materials studied in previous chapters. The crucial difference between a dielectric and a semiconductor is that, while in the former only bound charge responds to gradients, in the latter free charge can also move, leading to much bigger responses and hence offering a potential solution to the principal problem of flexoelectricity, which is its small magnitude compared to piezoelectricity. Quantitatively, we have found that, by vacancy-doping an insulating dielectric such as $BaTiO_3$ in order to increase its conductivity, its effective flexoelectricity is enhanced by more than 10000%, reaching the highest effective coefficient reported for any material.

Chapter 6 concludes this thesis with a discussion of the results and potential lines of future work.

Before this research, there were numerous controversies regarding the true magnitude of flexoelectricity and the origin of discrepancies between theoretically predicted values and actual experimentally measured ones. The present work has seeked to address this situation by quantifying the true value of the intrinsic flexoelectiricy and identifying the origin of additional contributions. The take-home message from this thesis is that true bulk flexoelectricity remains a relatively small effect with a stringent upper bound of $f \approx 10\text{V}$ for the flexocoupling coefficient of even the best materials, but that there are a number of other gradient-induced polarization phenomena that can greatly enhance the total response: polar nanoregions, surface piezoelectricity and movement of free charges are the three we have identified, but we do not discard the existence of others. Among these, the incorporation of free carriers to the total flexoelectric response in semiconductors is quantitatively the largest, and it also offers most promising route to elevating flexoelectricity to a level where it can compete with piezoelectricity even in bulk applications.

RESUMEN

En términos generales, la flexoelectricidad es la respuesta de la polarización a un gradiente de deformación. A diferencia del efecto piezoeléctrico, este efecto está presente en todos los materiales independientemente de su estructura cristalina. En esta tesis doctoral, hemos estudiado la polarización inducida por deformación en cristales dieléctricos y semiconductores, la cual surge desde dos mecanismos: flexoelectricidad macroscópica y flexoelectricidad superficial. Los dos mecanismos son del mismo orden en dieléctricos normales y hasta ahora sus respectivas contribuciones han sido indistinguibles entre ellas. La investigación desarrollada en esta tesis muestra que es posible separar las dos contribuciones, además de mostrar que la deformación induce reorientación de las nanoregiones polares las cuales también pueden incrementar el coeficiente flexoelectrico efectivo sobre el valor intrínseco.

La polarización puede ser generada por la separación de las cargas enlazadas entre los átomos o la celda unidad, pero también por la separación de cargas superficiales debido a las cargas libres. Hasta ahora cuando se refiere a flexoelectricidad, únicamente es tomada en cuenta la respuesta de las cargas enlazadas (capitulo 3 y 4); sin embargo, en esta tesis doctoral se ha reportado que la polarización debida a las cargas libres también pueden contribuir, generando una gran respuesta flexoeléctrica efectiva en materiales semiconductores (capitulo 5)

Esta tesis está distribuida de la siguiente manera:

El capítulo 1 es una introducción de la física de la polarización y la flexoelectricidad, mientras el capítulo 2 describe el procedimiento experimental que ha sido usado para desarrollar este trabajo; se encuentran los detalles del montaje experimental para las medidas flexoeléctricas requeridas para este proyecto.

En el capítulo 3, se ha medido y analizado la polarización inducida debido a la deformación de cristales relaxores ferroeléctricos de $Pb(Mg_{1/3}Nb_{2/3})O_3$-$PbTiO_3$ con diferentes composiciones cercanos a los límites de fase relaxor-ferroelectrico. Los cristales tienen un coeficiente de flexoacoplamiento $f > 100$V, un orden de magnitud más que los predichos teóricamente por Kogan y Tagantsev. Este incremento

persiste en la parafase hasta una temperatura T* = 500 ± 25 K que coincide con el inicio de reblandecimiento inelástico en los cristales; por encima de T*, el coeficiente de flexoacoplamiento real es medido como f_{13} ≈10V. Relacionando las propiedades flexoeléctricas, dieléctricas y elásticas; muestra que el incremento de la polarización inducida por la deformación de un ferroeléctrico relaxor no es consecuencia directa de una flexoelectricidad gigante intrínseca pero si debido a la reorientación de nanodominios polares que son ferroelásticamente activos por debajo de T*.

En el capítulo 4, se ha estudiado la polarización inducida debida a la deformación de cristales de $BaTiO_3$. El objetivo principal de este capítulo es encontrar una explicación a la gran diferencia entre las magnitudes del coeficiente flexoeléctrico predicho teóricamente y el medido experimentalmente en este material. Los resultados indican la existencia de regiones polares precursoras (orden de corto alcance), las cuales existen por encima de T_c y por debajo de T* ≈ 200-225ºC y alineadas con el gradiente de deformación, incrementan la flexoelectricidad efectiva, de la misma forma que en el caso de los relaxores. Por encima de T*, el coeficiente de flexovoltaje cae a un valor intrínseco, pero muestra una gran anisotropía la cual es inesperada en un material cubico, con un valor del coeficiente flexoeléctrico diez veces más grande en cristales orientados en la dirección (001) que en cristales orientados en la dirección (111). Análisis teóricos muestran que la anisotropía no puede venir de propiedades macroscópicas, y se ha interpretado esto como una evidencia indirecta de la piezoelectricidad superficial predicha teóricamente pero experimentalmente alusiva a polarizaciones macroscópicas inducidas por deformación.

En el capítulo 5, se ha estudiado la flexoelectricidad de un cristal de $BaTiO_{3-\delta}$ reducido, introduciendo vacantes de oxigeno las cuales incrementan la densidad de portadores, convirtiendo el cristal en un semiconductor tipo n. Los semiconductores también redistribuyen sus cargas en respuesta a un gradiente de deformación de la misma manera que los materiales dieléctricos estudiados en los capítulos previos. La diferencia crucial entre un dieléctrico y un semiconductor es que; en los dieléctricos únicamente las cargas enlazadas responden a gradientes de deformación, en los semiconductores las cargas libres también se mueven, produciendo respuestas mucho más grandes y por lo tanto ofrecen una solución potencial al principal

problema de la flexoelectricidad, el cual es su pequeña magnitud en comparación a la piezoelectricidad. Cuantitativamente, hemos encontrado que por el dopaje de vacantes de oxígeno en un dieléctrico aislante tal como el $BaTiO_3$ este incrementa su conductividad, su flexoelectricidad efectiva es incrementada por más de un 10000%, alcanzando el coeficiente flexoeléctrico efectivo más alto reportado para ningún otro material.

El capítulo 6 concluye esta tesis con una discusión de los resultados y líneas potenciales de futuros trabajos.

Antes de esta investigación, habían numerosas controversias respecto a la verdadera magnitud del coeficiente flexoelectrico y el origen de la discrepancia entre los valores predichos teóricamente y experimentalmente. En el presente trabajo hemos buscado dilucidar esta situación y cuantificar el valor intrínseco del coeficiente flexoelectrico e identificar el origen de contribuciones adicionales a este. El mensaje principal de esta tesis es que el coeficiente macroscópico flexoeléctrico efectivo permanece en valores relativamente pequeño con un riguroso límite superior de $f \approx$ 10V para el coeficiente de flexoacoplo de incluso los mejores materiales, pero hay otra gran cantidad de fenómenos de polarización inducida debida a gradientes de deformación que pueden incrementar la respuesta total de este: nanoregiones polares, piezoelectricidad superficial y movimiento de cargas libres son las tres que hemos identificado, pero no descartamos la existencia de otras. Entre estos, la incorporación de cargas libres a la respuesta flexoeléctrica total en semiconductores es cuantitativamente la más grande y la más prometedora dando lugar a aplicaciones macroscópicas debida a su elevada magnitud del coeficiente flexoeléctrico y permitiendo a su vez que compita con la piezoelectricidad.

TABLE OF CONTENTS

1 INTRODUCTION

Electric materials can be divided into three general categories according to the value of their electrical conductivities: conductors, insulators and semiconductors. In a strict physical sense, there is not much difference between a semiconductor and an insulator, since they both have zero conductivity at a temperature of zero kelvin, but the distinction between semiconductors and insulators is useful at finite temperatures and in real devices, and it essentially describes whether, when an oscillating electric field is applied, the free charge current that is generated is bigger (semiconductors) or smaller (insulators) than the dielectric displacement current generated by the small relative displacements of bound charge.

Electrical conductivity of a material is defined as the ability for transport of electric charge. This property is one of the properties of materials that varies most widely, from values of 10^{+7}(S/m) typical for metals to 10^{-20}(S/m) for good electrical insulators. Semiconductors have conductivities in the range 10^{-6} to 10^{4}(S/m). These conductivities only take into account the contribution from electrons (or holes) as charge carriers. On the other hand, ionic conduction can also exist, as a result from the net motion of charged ions. Movement of different particles in various materials depend on more than one parameter. These include: atomic bonding, imperfections, microstructure, ionic compounds, diffusion rates and temperature.

In solids, electrons of atoms form bands. The bands are separated by gaps, with forbidden energies for the electrons. The precise location of the bands and band gaps depend on the type of atom, the distance between atoms in the solid, and the atomic arrangement. Narrow energy band gap i.e. size < 2 eV, is found in semiconductors, while broader energy band gap i.e. size > 4 eV, is found in insulators. In a semiconductor or insulator, this bandgap defines the energy that an electron has to acquire to move from the highest-energy bound state (valence band) to a conduction band in which it is free to travel. According to Bolztmann statistics, there is a finite probability that an electron can jumps the forbidden gap from the valence band to the conduction band, and this probability is given by an exponential, $e^{-\frac{\Delta E}{kT}}$, where ΔE is the bandgap energy, k is Boltzmann's constant and T is temperature; we therefore see that at 0 K the probability of having a free electron in the conduction band is zero, while at any finite temperature it is nonzero, meaning that both

insulators and semiconductors are perfectly insulating at 0K, and both can conduct, albeit by different amounts, at finite temperatures.

Every insulator is also a dielectric. When a dielectric material is placed in an electric field, practically no current flows through it because, unlike metals, they have almost no loosely bound, of free electrons able to move through the material. Instead, *electrical polarization due to bound charge separation* occurs. When we refer to dielectric materials, is important to know the polarization concepts and its mechanisms.

1.1 POLARIZATION AND PERMITTIVITY.

When an electric field is applied to an insulator, the electronic distribution and the nuclear position are altered and the charges in the molecules are displaced. This displacement creates small electric dipoles within the material, which is represented in Figure 1.1a [1]. Electric dipoles are atomic structures that have a difference in charge from one end to the other. As opposed to a conductor, the displaced charges, also called bound charges, do not escape the molecules. This displacement can be thought of as two opposite charges, +q and -q, which are separated by a distance **a**, which is represented in Figure 1.1b. The dipole can be represented by a vector $\vec{\boldsymbol{p}}$ that points from the negative charge to the positive charge and has a magnitude of the distance **a** between them. This vector is called the electric dipole moment [2]. The direction of the dipole moment is always in the direction of the applied field

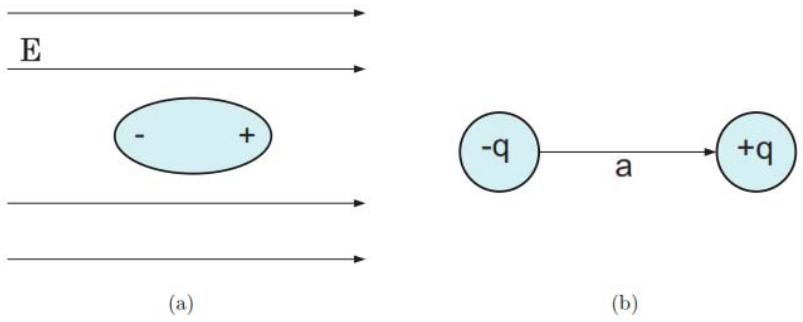

Figure 1.1. (a) An electric dipole induced in an applied electric field and (b) an electric dipole moment can be represented as a vector which points in the direction of –q to +q and a magnitude of the distance (a) between them.

Another way of illustrating an electric dipole is to use two spheres of charge; one positive and one negative. The two spheres are the same size and are superimposed on top of one another. This superposition helps to show the idea of bound charge. In

the absence of an external electric field, the two spheres cancel each other's charge and are, overall, electrically neutral. When an external electrical field is applied, the negative sphere shifts one direction and the positive sphere shifts the other direction, as illustrated in Figure 1.2. The charges of the two spheres no longer cancel each other. As a result, an electric dipole is created, where one side is slightly positive in charge and the other side is slightly negative in charge [4]. The amount of uncancelled charge is called the bound surface charge σ_b [4]. In an atom, the two spheres essentially represent the nucleus, which is positively charged, and the centre of an electron cloud, which is negatively charged [5].

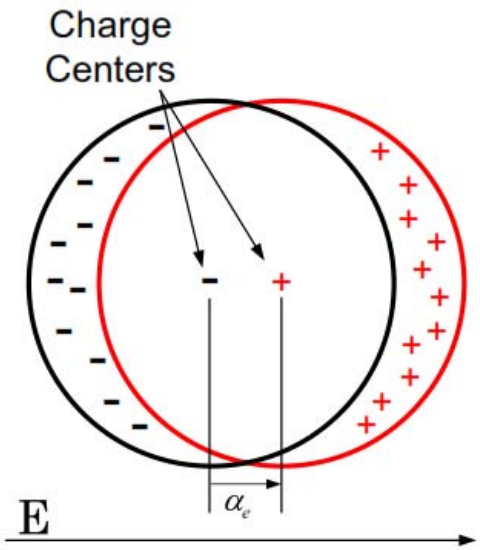

Figure 1.2 Two displaced charge spheres illustrating an electric dipole [4] creating electric dipoles within a materials through an application of an electric

Polarization is mathematically defined as $\boldsymbol{P}$ and is the number of induced dipole moments per unit volume. The amount of polarization depends on the electric field $\boldsymbol{E}$ and the quantity called the polarizability α, which is shown by [4,2].

$$P = \alpha E \qquad (C/m^2) \qquad 1.1$$

To better define charge displacement, a term called the electric displacement, $\boldsymbol{D}$, is defined as total charge displacement induced in the material. Maxwell defines the electric displacement mathematically as [4].

$$D = \varepsilon_0 E + P \qquad (C/m^2) \tag{1.2}$$

Electric displacement consists of two parts, the displacement of charge which is a result of the applied electric field and the displacement caused by polarization. The induced dipole from the polarization induces its own electric field which further contributes to the electric displacement.

The polarizability $\boldsymbol{\alpha}$ of a dielectric can be divided into the electric susceptibility $\boldsymbol{\chi_e}$ and permittivity of free space $\boldsymbol{\varepsilon_0}$ [4]. The electric susceptibility is the dielectric's ability to be polarized, and the permittivity of free space is a universal polarizability constant that is defined for all of free space. Incorporating the electronic susceptibility, the number of induced dipoles per unit volume, Equation 1.1, then turns into [4].

$$P = \chi_e \varepsilon_0 E \qquad (C/m^2) \tag{1.3}$$

Substituting Equation 1.3 into Equation 1.2 yields [4].

$$\begin{aligned} D &= \varepsilon_0 E + \chi_e \varepsilon_0 E \\ &= \varepsilon_0 (1 + \chi_e) E \qquad (C/m^2) \end{aligned} \tag{1.4}$$

The permittivity of the material ε is defined as [4]

$$\varepsilon = \varepsilon_0 (1 + \chi_e) \qquad (F/m) \tag{1.5}$$

Substituting Equation 1.5 into Equation 1.4 yields

$$D = \varepsilon E \qquad (C/m^2) \tag{1.6}$$

As defined earlier, ε is the permittivity of the material and by dividing the permittivity by the permittivity of free space yields the relative permittivity or the dielectric constant, ε_r, and is defined as

$$\varepsilon_r = 1 + \chi_e = \frac{\varepsilon}{\varepsilon_0} \tag{1.7}$$

The dielectric constant is one of the central themes in this study and is a key characteristic in capacitor materials. The equations above illustrate the fact that the dielectric constant defines how the dielectric material reacts to the introduction of an

electric field: the higher dielectric constant in a capacitor material causes a higher electric energy density in the capacitor. Additionally, the dielectric constant also affects the flexoelectric coefficient [6,7,8]: flexoelectricity is directly proportional to permittivity. From a thermodynamical point of view, is flexoelectricity is one mechanism for converting electric energy density into elastic energy density and vice-versa, so anything that increases one should also increase the other. Ultimately, both permittivty and flexoelectricity are measures of the polarizability of a material.

1.1.1 ELECTRONIC POLARIZATION.

Following the simple Bohr model of the atom, an applied electric field displaces the electron orbit slightly (see Figure 1.3). This produces a dipole, equivalent to a polarization. There are quantum mechanical treatments of this effect (using perturbation or variational theory) which all give the result that the effect is both, small and occurs very rapidly (on the timescale equivalent to the reciprocal of the frequency of the X-ray or optical emission from excited electrons in those orbits). Therefore we expect no delay in the occurrence of polarization after the application of an electric field, and thus no dissipation phenomena, except at frequencies which are resonant with the electron transition energies.

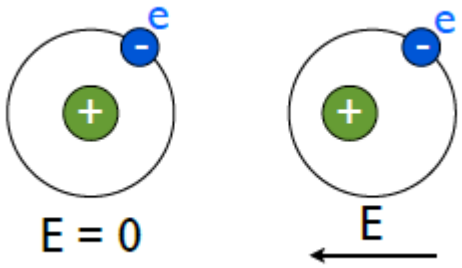

Figure 1.3. Electronic (atomic) polarization

After equilibrium is reached, the two forces acting on the electrons are the coulombic attraction called the restoring force and the force due to the electric field that keeps the electron cloud shifted. The average induced polarization per molecule due to electronic polarization is [3] Thus:

$$P_e = \alpha_e E \qquad (C/m^2) \qquad 1.8$$

As reflected earlier, the induced electronic dipole moment $\boldsymbol{\alpha_e}$ due to electronic polarization is proportional to the electric field $\boldsymbol{E}$. This equation is valid only under equilibrium or static conditions.

1.1.2 ELECTRONIC POLARIZATION IN COVALENT SOLIDS.

A covalent bond is a chemical bond that involves the sharing of electron pairs between atoms. These electrons and their resulting wave functions are referred to as delocalized. When an electric field is applied, two different types of electronic polarizations can occur. The weaker one happens when the individual nuclei experiences a shift within its own electron shell that is not shared with the lattice bonds. The dominant one is the electronic polarization, based on the shifting of the atom's valence electrons and the lattice bonds surrounding the nuclei within the material [9].

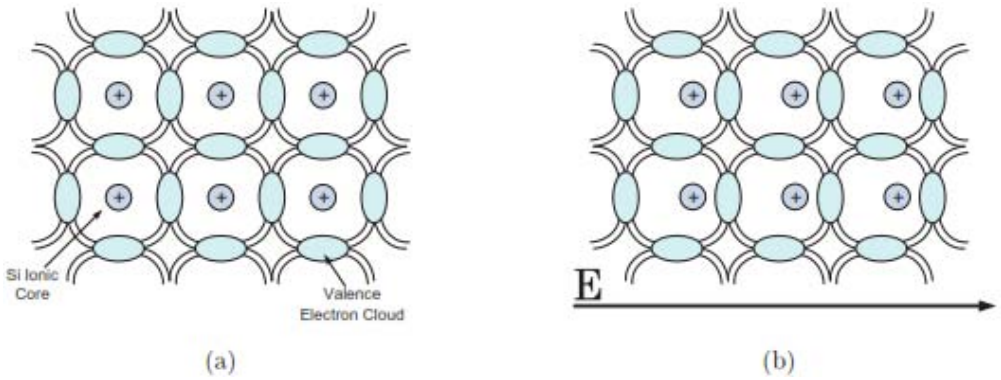

Figure 1.4 An illustration of electronic polarization in a Si covalent lattice (a) before the application on an electric field and (b) after a field is applied [9].

1.1.3 IONIC POLARIZATION.

Ionic polarization occurs in crystal lattices of ionic molecules such as NaCl. Although each individual molecule has a dipole moment, the net dipole moment of the material is zero because the individual molecules are lined up head to head and tail to tail, as shown in Figure 1.5. When an electric field is applied, cations and ions are pushed in opposite directions, creating a net polarization in the material. The average induced polarization per molecule due to ionic polarization is [9,10].

$$P_i = \alpha_i E \qquad 1.9$$

Where α_i is the ionic polarization of the material, and $\boldsymbol{E}$ is the applied electric field.

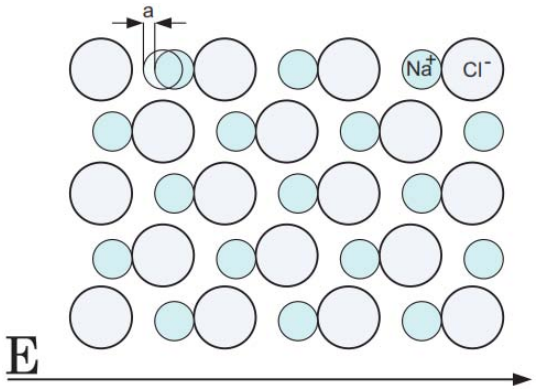

Figure 1.5. Ionic polarization in NaCl [10]

1.1.4 ORIENTATIONAL POLARIZATION.

Polar molecules such as water have permanent dipole moments. In the liquid or gas phase, these polar molecules can move around and are randomly orientated. When an electric field is applied to a polar material, the dipoles experience a torque which aligns them in the direction of the applied field. This process is called orientational polarization [4, 9, 10].

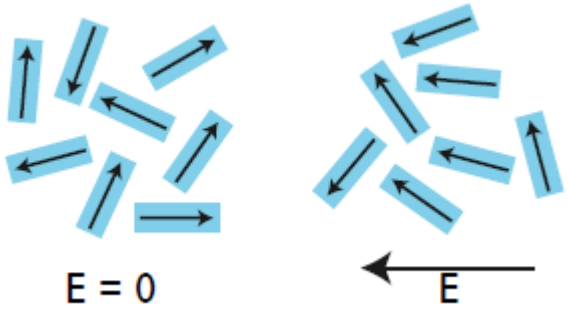

Figure 1.6. A dielectric medium consisting of polar molecules (a) that are ramndomly oriented before an electric field is applied and (b) after a field is applied

Some solids are made up of polar molecules which are normally randomly orientated. There are materials such as certain plastics can be softened by heating and exposed to an electric field in order to align the dipoles. The electric field is left on as the material cools which solidifies the direction of the dipole moments. This process is used to produce materials that have a permanent dipole moment. Electrets and have many uses especially in high fidelity microphones [11].

The average induced polarization per molecule due to orientational polarization is [9, 10]

$$P_0 = \alpha_0 E \qquad 1.10$$

Where α_0 is the orientational polarization of the material, and E is the applied electric field. As we shall see in chapters 3 and 4, the orientational polarization of polar nanoregions that exist in relaxors and even standard ferroelectrics greatly enhances their flexoelectric response.

1.1.5 INTERFACIAL POLARIZATION.

Even in the most pure of crystals and materials, there are defects and impurities that generate charge carriers such as electrons, holes, and ions. These charge carriers can move within the material and build up at different boundaries such as the dielectric-electrode boundary or at grain boundaries within the material itself. This accumulation also contributes to the dielectric constant of the material [3].

All of the above mechanisms of polarization are additive and define the total polarization of the material. The average induced dipole moment per molecule is [3].

$$P_{av} = \alpha_e E + \alpha_i E + \alpha_0 E \qquad (C/m^2) \qquad 1.11$$

where $\boldsymbol{\alpha_e}$ is the electronic polarization, $\boldsymbol{\alpha_i}$ is the ionic polarization, $\boldsymbol{\alpha_0}$ is the orientational polarization, and $\boldsymbol{E}$ is the applied electric field. The interfacial polarization is not added to the above equation because it occurs at interfaces and does not correlate to an average polarization in the bulk material. This is again a simplification because the electric field $\boldsymbol{E}$ in the above equation is the local field experienced by the individual molecules and not the applied electric field [1, 3].

The take-home message from all the previous discussion is that polarization is a complex magnitude that has several different contributions, all of which may be potentially sensitive to strain gradients. Thus, the definition of flexoelectricity as a dielectric (electronic+ionic) polarization generated by a strain gradient is insufficient when attempting to correlate the actual experimental results (which incorporate all possible contributions to the polarization) to their microscopic origin.

As will be seen, orientational and interfacial polarization can in some cases largely dominate the total flexoelectric response of a material.

1.2 DIELECTRIC CONSTANT VS FREQUENCY.

The aforementioned polarization assumes a static electric field which does not vary with time. The introduction of a time varying electric field adds a little more complexity to the idea of polarization. The mechanics of polarization depends on the movement of particles with mass. Particles have to be accelerated and shifted back and forth as the electric field changes, which cannot occur instantaneously. Since certain movements of particles involve the movement of different masses and different distances, the different types of polarization will have different rates at which polarization occurs. When a time varying electric field is applied, the dielectric constant depends on the frequency of the field. As the frequency increases, the different polarizations progressively show difficulties to follow the changes of the electric field and start to relax. As a result, the slower processes cease to contribute to the dielectric constant [1] as shown in Figure 1.7 [3]. At low frequencies, all of the polarization types have time to reach their relaxed state. This is important for our work because all our flexoelectric measurements have been performed at low frequencies (of the order of 13Hz), and thus the measured flexoelectric response is in principle sensitive to all polarization mechanisms.

1.3 DIELECTRIC LOSS.

An ideal dielectric material is a perfect insulator that only permits a displacement of the charge by an electric field via polarization. In this sense, the impedance response of a dielectric material is capacitive, and hence the generated displacement current leads the voltage by 90°, or similarly is out of phase by a quarter-cycle. Real materials always have dissipation and thus the phase angle between the current and voltage is not exactly 90°; the current leads the voltage by 90- δ, where δ is defined as the angle of lag. The angle of lag, δ, is the measure of the dielectric power loss.

$$Power\ Loss = \pi f V_0^2 \varepsilon_1 tan\delta \qquad 1.12$$

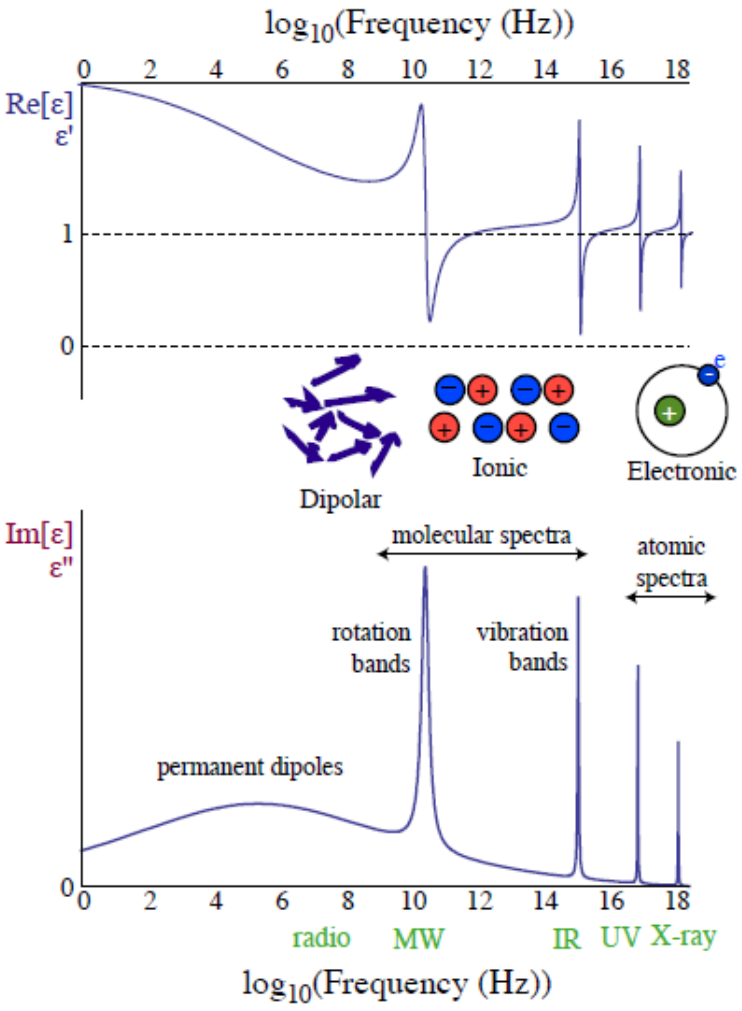

Figure 1.7. The real and imaginary part of the dielectric constant versus frequency of an applied electric field, showing the contribution of the with different physical polarizations over the frequency ranges**.**

The product "$\varepsilon_r \tan\delta$" is called the *loss factor* and "$\tan\delta$" is referred to as the *loss tangent* or the dissipation factor. The loss tangent consequently characterizes the usefulness of a material as a dielectric or as insulator; a low loss tangent is thus desirable for a better dielectric behaviour [12].

The dielectric loss results from several energy-dissipating mechanisms: (1) ion migration; (2) ion vibration and deformation; (3) electronic hopping. The most important mechanism in most ceramics is leakage current, which includes both electronic and ionic charge transport. Ion migration is strongly influenced by temperature and frequency. These losses increase at low frequencies and as the temperature increases [13].

Getting back to polarization, there are three main phenomena related to electric dipoles: ferroelectricity, piezoelectricity and flexoelectricity. Ferroelectricity can exist when there is a spontaneous alignment of electric dipoles by their mutual interaction in the absence of an applied electric field, and is defined as the reorientation ("switching") of this spontaneous polarization upon application of a finite electric field smaller than the breakdown strength of the material. Piezoelectricity is defined as polarization induced by the application of external force. The aforementioned properties are limited to materials with a non-centrosymmetric crystal structure. In contrast, flexoelectricity is a universal property, present in every material irrespective of their symmetry, and is defined as the linear response of polarization to strain gradient. Polarization can, as discussed earlier, be generated by dielectric separation of bound charge within atoms or unit cells, or by a space charge separation of free carriers. To the best of our knowledge, until now, when referring to flexoelectricity, only the response from bound charge (electronic displacement within atoms or ionic displacement within unit cells) has been taken into account. One of the main advances contained in this thesis and developed in Chapter 5 is the observation that free carriers also respond to strain gradients.

1.4 FERROELECTRICITY.

Ferroelectric materials (named "ferroelectrics") have a spontaneous electric polarization which can be switched by an external electric field. The spontaneous polarization is produced by the arrangement of ions in the crystal structure, as in conventional ferroelectrics, or on charge ordering as in electronic ferroelectrics [14,15]. Only materials with a non-centrosymmetric point group which contains alternate atom positions or molecular orientations to permit the reversal of the dipole and the retention of polarization after voltage removal are ferroelectric. Ferroelectricity is closely related to piezoelectricity and pyroelectricity; all ferroelectric materials are also piezoelectric and pyroelectric, but not all piezoelectrics are pyroelectric, and not all pyroelectrics are ferroelectric.[14]

The ferroelectric phase is typically reached by cooling from a high-symmetry, non-polar phase through its Curie point (T_c), reducing the symmetry of the system and permitting the polarization to align along any one of the crystallographically

equivalent directions. The ferroelectric phase can be represented by only minor perturbations in the structure of the high-symmetry prototype phase, which is paraelectric[14]. The paraelectric to ferroelectric phase transformation at T_c can be either first order where the volume, strain, polarization and crystal structure of the system change discontinuously at the transition point or second order where the aforementioned parameters change continuously [17].

The Curie point is marked by a large dielectric anomaly, often in the form of a diverging relative permittivity (ε_r). This can result in the appearance of a large peak in permittivity at T_c. Many systems obey the Curie-Weiss law, which gives the permittivity as a function of temperature above T_c as follows:

$$\varepsilon_r = \frac{C}{T - T_0} \qquad 1.13$$

Where C is the Curie constant and T_0 is the Curie temperature [16]. T_0 is slightly lower than Tc in the case of a first-order phase transition but is coincident with T_c in a second-order phase transition [17]. Below T_c, the spontaneous polarization in the ferroelectric generally increases with decreasing temperature (i.e. $\frac{dP_S}{dT} < 0$). This behaviour is summarized in Figure 1.8.

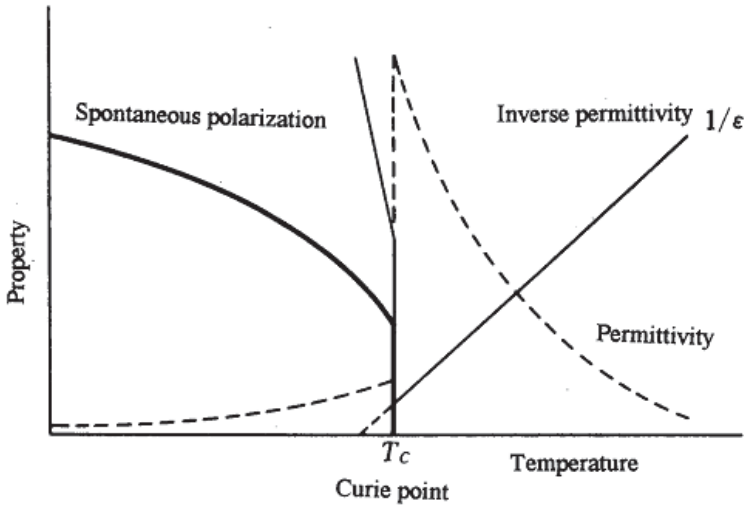

Figure 1.8 Temperature dependence of the spontaneous polarization and permittivity in the ferroelectric material [16].

1.5 PIEZOELECTRICITY.

Piezoelectricity (following direct translation from Greek word piezein, “pressure electricity”) was discovered by Jacques Curie and Pierre Curie as early as in 1880 (Curie and Curie 1880). This effect was distinguished from other similar phenomena such as “contact electricity” (friction-generated static charge). Even at this stage, it was clearly understood that symmetry plays a decisive role in the piezoelectric effect, as it was observed only for certain crystal cuts and mostly in pyroelectric materials in the direction normal to polar axis. However, the Curie brothers did not predict a converse piezoelectric effect, i.e., deformation or stress under applied electric field. This important property was then mathematically deduced from the fundamental thermodynamic principles by Lippmann (1881). The existence of the converse effect was immediately confirmed by Curie brothers. Since then, the term *piezoelectricity* has thus been used for more than a century to describe the ability of materials to develop electric displacement D that is directly proportional to an applied mechanical stress σ (Fig. 1.9a). Following this definition, the electric charge appeared on the electrodes reverses its sign if the stress is changed from tensile to compressive. As follows from thermodynamics, all piezoelectric materials are also subject to a converse piezoelectric effect (Fig. 1.9b), i.e., they deform under applied electric field. Again, the sign of the strain S (elongation or contraction) changes to the opposite one if the direction of electric field E is reversed. Shear piezoelectric effect (Fig. 1.9c) is also possible, and it linearly couples shear mechanical stress or strain with the electric charge.

Piezoelectric coupling is described by a linear relationship between the first-rank tensor or vector (D or E) and the second-rank tensor (σ or S), the corresponding coupling coefficients d_{kij} (also called charge piezoelectric coefficients) form a third-rank tensor. Hence, the piezoelectric equations may be written in the following form ($i, j, k = 1, 2, 3$):

$$S_{ij} = d_{kij}E_k \qquad 1.14$$

$$D_k = d_{kij}\sigma_{ij} \qquad 1.15$$

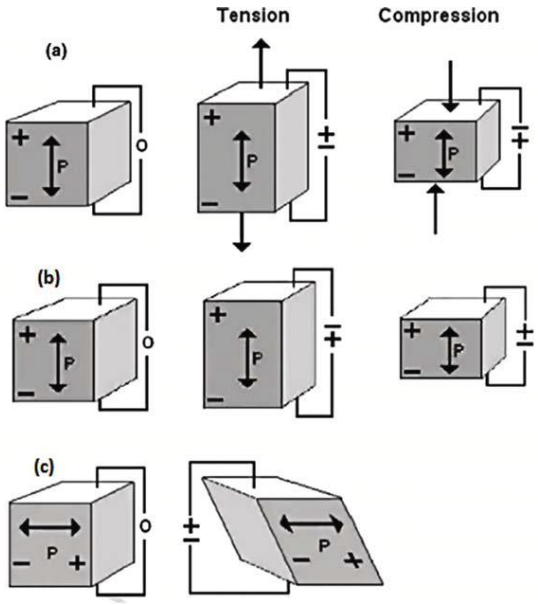

Figure 1.9 Schematic representation pf longitudinal direct (**a**) converse (**b**) and shear (**c**) piezoelectric effect.

where the Einstein's summation rule for repeated indices is implied. Both direct and converse piezoelectric effects are frequently expressed using the reduced matrix notation d_{km}, where k denotes the component of electric displacement D or field E in the Cartesian reference frame (x_1, x_2, x_3), and the index $m = 1, \ldots, 6$ is used to define the mechanical stress or strain. In this case, $m = 1, 2$, and 3 correspond to the normal stresses along the x_1, x_2, and x_3 axes, respectively, whereas $m = 4, 5$, and 6 denote the shear stresses S_{23}, S_{13}, and S_{12}.

The main point to remember from this section is that piezoelectricity defines a polarization induced by a homogeneous deformation. This is fundamentally different from polarization induced by an inhomogeneous deformation – flexoelectricity- which we discuss in the next section, and in the rest of the thesis.

1.6 FLEXOELECTRICITY.

Flexoelectricity is the main topic in this doctoral dissertation. The flexoelectric effect in solids was first predicted in 1964 [19], but only very limited attention was put to it up to the end of last century, mainly because the effect was expected to be extremely weak.

The flexoelectricity by definition is the response of electric polarization to a strain gradient:

$$P_i = \mu_{klij} \frac{\partial u_{kl}}{\partial x_j} \qquad 1.16$$

In contrast with the piezoelectricity, this effect is not limited to non-centrosymmetric crystal structures, making it a more universal property. Homogeneous stress and strain cannot by themselves break centrosymmetry. If the material is centrosymmetric(Figure 1.10a) and we apply a stress, the displacements of ions are also symmetric and compensate each-other between them, so the result is a null polarization (Figure 1.10b). In contrast, if the material is centrosymmetric and we apply strain gradient, the displacement of ions is uncompensated and therefore a net polarization can appear which is dictated by the direction of the strain gradient (Figure 1.10c).

Estimation of flexoelectric coefficients was of the order of ***e/a***, where ***e*** is the electronic charge and ***a*** is the lattice parameter; it is a very small value of around 10^{-10} C/m for almost all insulators [19]. Bursian and Trunov [20], and then Tagantsev [21], later predicted an enhancement of flexoelectric effect in materials with high dielectric permittivity, a prediction backed up by first principle calculations [6,7,8] and validated by multiple experimental work on relaxor ferroelectrics and ferroelectric materials, such as Lead Magnesium Niobate ceramic (PMN) [22], Barium Strontium Titanate ceramic (BST) [23], Lead Zirconate Titanate ceramic (PZT)[24], Strontium Titanate single crystal (STO) [25] and Barium Titanate ceramic (BTO) [26]. Measurements on BST and BTO also revealed a remarkable magnitude of the flexoelectric coefficient in the order 10^{-5} C/m, which is 10^3-10^5 times larger than the flexoelectric coefficient estimated by Kogan and is too large even when the dielectric constant is factored in. With the exception of $SrTiO_3$[25], in fact, for most perovskites, the experimentally measured flexoelectricity exceeds theoretical expectations by one to three orders of magnitude[27, 30]. The origin of this enormous flexoelectric coefficient is not known; the principal motivation for this thesis is precisely the remarkable lack of fundamental knowledge about the intrinsic value of the effective flexoelectric

coefficients—the constants of proportionality between strain gradient and induced polarization.

This thesis addresses this question for paradigmatic materials (morphotropic phase boundary relaxors and high-k perovskite ferroelectrics), for which possible explanations for the enhancement of flexoelectic coefficient values are proposed.

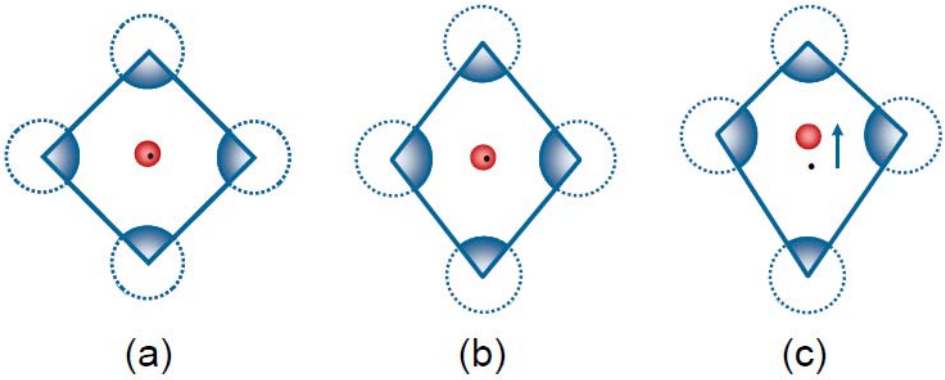

Figure 1.10. A centrosymmetric crystal such as NaCl: (a) undeformed, (b) under homogeneous strain, and (c) inhomogeneously strained. Negative ions shown in blue, positive in red; black dot represents the centre of negative charge; arrow indicates the direction of the flexoelectric polarisation.

The flexoelectric phenomena can be divided into two types; static flexoelectricity such as that present in a bent plate and dynamic flexoelectricity, caused by acceleration of the ions during deformation, and corresponding to gradients generated by waves travelling in the solid [18]. The subject of the research in the present doctoral dissertation is static flexoelectricity. Static (or, strictly, quasistatic) flexoelectricity arises from three mechanisms: bulk flexoelectricity, surface flexoelectricity and surface piezoelectricity. An additional consideration here is the size dependence of flexoelectricity. In general, the maximum achievable strain gradients increase in inverse proportion to sample size, and therefore, flexoelectricity can be very large at the nanoscale [18]. The relative contributions of bulk flexoelectricity and surface piezoelectricity have been shown to be of the same order in ordinary dielectrics and independent of sample thickness, which makes them indistinguishable one from another [21]. The reason for this scaling is that, while the thickness ratio of surface to bulk decreases as thickness increases, this is compensated by the fact that, for a given amount of bending, the strain on the

surface (and thus its piezoelectricity) increases with sample thickness. Thus, the two thickness dependences (surface-to-bulk ratio and of strain-induced polarization) cancel each other, and the surface-piezoelectric contribution is therefore independent of thickness. In contrast, surface flexoelectricity decreases in inverse proportion to sample thickness, and can in principle be neglected from the analysis of bulk samples; in this thesis, therefore, we have only dealt with bulk flexoelectricity and surface piezoelectricity.

The impossibility of distinguishing between bulk flexoelectricity and surface piezoelectricity by thickness-dependent studies has also meant that, so far, they have been lumped together in effective coefficients that contain the contributions of both. In this thesis, and for the first time, we provide direct experimental evidence for the existence and magnitude of the surface piezoelectric effect. We have achieved this by two different means: by changing the type of surface while leaving the bulk contribution unchanged (chapter 4), and by screening the bulk contribution by making the crystals conductive (chapter 5).

1.6.1 STATIC BULK FLEXOELECTRIC EFFECT.

This section describes the phenomenology of bulk flexoelectricity, which is the principal topic of this doctoral dissertation. Static flexoelectricity has a different treatment of dynamic flexoelectricity [31, 32].

For static case, the constitutive equation for electric polarization in a general medium (including piezoelectricity) is [33]:

$$P_i = \chi_{ij} E_j + e_{ijk} u_{jk} + \mu_{klij} \frac{\partial u_{kl}}{\partial x_j} \qquad 1.17$$

Where E_i, u_{jk} and $\partial u_{jk}/\partial x_j$ are the macroscopic electric field, the strain tensor, and its spatial gradient, respectively. In the equation 1.17, the first and the second terms refer to dielectric and piezoelectric contributions with a second rank tensor χ_{ij} and third rank tensor e_{ijk} respectively. The last term corresponds to the response of polarization to a strain gradient- the flexoelectric effect- which is dictated by a fourth rank tensor μ_{klij}. The flexoelectric tensor is allowed in any material, in contrast with piezoelectricity which is limited to non-centrosymmetric materials.

Both flexoelectricity and piezoelectricity can describe properties of the materials in the absence of a macroscopic electric field, so one can be define the following tensor for piezoelectricity and flexoelecticity as:

$$e_{ijk} = \left(\frac{\partial P_i}{\partial u_{jk}}\right)_{E=0} \tag{1.18}$$

$$\mu_{klij} = \left(\frac{\partial P_i}{\left(\partial u_{kl}/\partial x_j\right)}\right)_{E=0} \tag{1.19}$$

Piezoelectricity and flexoelectricity are electromechanical phenomena that can be described by thermodynamics. Therefore we can define the thermodynamic potential density in terms of polarization, strain and their derivatives as [34].

$$\Phi = \frac{\chi_{ij}^{-1}}{2} P_i P_j + \frac{c_{ijkl}}{2} u_{ij} u_{kl} + \frac{g_{ijkl}}{2} \frac{\partial P_i}{\partial x_j} \frac{\partial P_k}{\partial x_l}$$

$$-\frac{f_{ijkl}}{2}\left(P_k \frac{\partial u_{ij}}{\partial x_l} - u_{ij} \frac{\partial P_k}{\partial x_l}\right) - P_i E_i - u_{ij}\sigma_{ij} \tag{1.20}$$

Where f_{ijkl} is called the flexocoupling tensor and has units of volts; this magnitude, as we shall see, has a more universal value than the flexoelectric coefficient μ. Static bulk flexoelectricity was introduced by Indenbom [35], as a free energy in form of equation 1.20.

Equations 1.20 contains again gradient terms. To find the equation of state it is necessary to minimize the thermodynamic potential of the sample as a whole, making a integration over volume of the sample as: $\int \Phi dV$. For the latter procedure one can use Euler equation $\partial\Phi/\partial A - \frac{d}{dx}(\partial\Phi/\partial(\partial A/\partial x)) = 0$, where A can be replaced by P and *x* by *u*. In this way, the constitutive electromechanical equations as proposed by Mindlin are[36]:

$$E_i = \chi_{ij}^{-1} P_j - f_{klij} \frac{\partial u_{kl}}{\partial x_j} - g_{ijkl} \frac{\partial^2 P_i}{\partial x_j \partial x_l} \tag{1.21}$$

$$\sigma_{ij} = c_{ijkl} u_{kl} + f_{ijkl} \frac{\partial P_k}{\partial x_l} \tag{1.22}$$

Considering the polarization and strain gradient as homogeneous, the flexoelectric effect described in equation 1.21 is the same as in equation 1.17 with:

$$\mu_{klij} = \chi_{is} f_{klsj} \tag{1.23}$$

Equation 1.23 couples the flexoelectric tensor to flexocoupling tensor through to susceptibility of the material. The most important consequence of this equation is that the flexoelectric coefficient is found to be proportional to the permittivity. Therefore, materials with high dielectric constants such as ferroelectrics are good candidates to study flexoelectricity. Additionally, Eq. 1.21 highlights that flexoelectric coupling acts as an electric field (this can be seen by just moving the second term of the right hand side to the left of the equality). This equivalence is also important to understand that, just like all the components of the polarization of a material (electronic, ionic, space-charge etc.) are sensitive to electric fields, they can in principle be also responsive to *flexoelectric* fields, hence yielding a bigger response than may have been anticipated from the ideal dielectric case considered by Kogan.

On the other hand, equation 1.22, describes the contribution to mechanical stress generated by a gradient of polarization, i.e. converse flexoelectricity.

From constitutive equation 1.21 and 1.22, and assuming the strain gradient is small enough that the rhs term is vanished in equation 1.21, the equations of state can be rewritten as.

$$P_i = \chi_{ij} E_j + \mu_{klij} \frac{\partial u_{kl}}{\partial x_j} \tag{1.24}$$

$$\sigma_{ij} = \mu_{ijkl} \frac{\partial E_k}{\partial x_l} + c_{ijkl} u_{kl} \tag{1.25}$$

These constitutive equations are convenient in the case of the extrinsic gradient, such as mechanical bending of the sample as induced in the investigations of this thesis, in contrast to the intrinsic strong gradient such as that at domain boundaries or dislocations.

1.6.2 SURFACE PIEZOELETRIC EFFECT.

Surface contributions are always present in any phenomena on finite samples. In general, this is small or even negligible because it is controlled by the ratio between surface and volume; however in the present work, this effect is comparable to a bulk effect and plays an important role in this doctoral dissertation. The relevant example for this thesis is the surface piezoelectric effect, which is present even in centrosymmetric materials; in these, the surface is breaks the symmetry and thus the surface becomes a piezoelectric layer, with a thickness of λ.

Let's discuss this effect with the example of cylindrical bending of a thin parallel plate capacitor, as drawn in Figure 1.11. Since the normal to the surface defines the direction and sign of the piezoelectric coefficient e_{ijk}, it has opposite directions at the top and bottom sides of the sample. Meanwhile, the application of a strain gradient induces opposite strains on the two surfaces: tensile at the convex side, compressive at the concave side. Since the induced polarization is the product of piezoelectric coefficient times strain, the opposite signs of both magnitudes cancel each other, and therefore the induced polarizations in these layers have the same direction in the top and bottom surfaces, thus giving an overall net contribution.

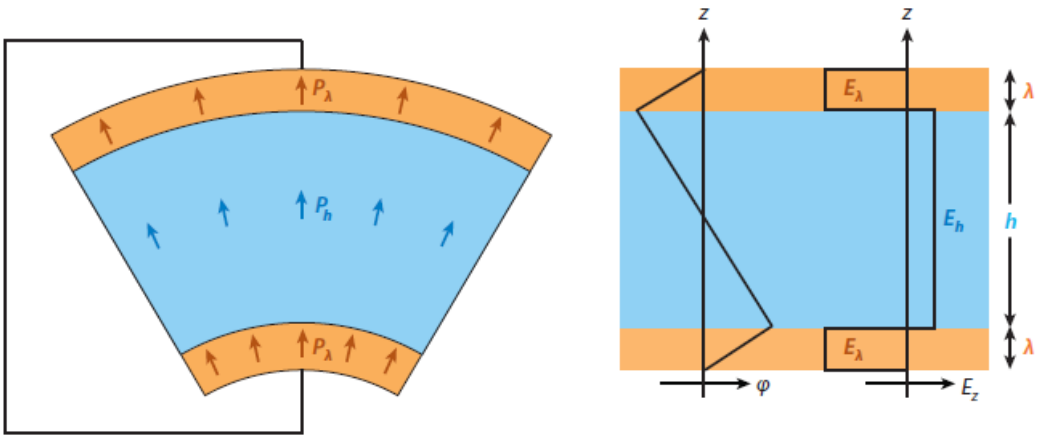

Figure 1.11. Surface piezoelectricity upon bending, as shown on the left, the tensile/compressive strains in the top/bottom surface layers give rise to a polarization P_λ in the piezoelectric surface layers of thickness λ. Because the normal component of the electric displacement must remain constant, this surface polarization gives rise to electric fields E_h and thus to a polarization P_h within the nonpiezoelectric bulk. The measured average polarization of the whole structure therefore depends

not only on the dielectric properties of the piezoelectric surface layers but also on those of the bulk. The potential ϕ and field E profiles along the sample thickness are shown on the right [18].

Additionally, the normal component of the electric displacement as described in the equation 1.2, must be conserved across any dielectric interface, i.e., $D_z = P_\lambda + \varepsilon_0 E_\lambda = P_h + \varepsilon_0 E_h$, where ε_0 is the vacuum permittivity. Thus, internal fields appear in the sample due to the presence of polarization P_λ within the surface layers. For a short-circuited capacitor, the potential difference $\Delta\phi = 2\lambda E_\lambda + hE_h$ across the capacitor must vanish; here h is the thickness of the nonpiezoelectric bulk (see Figure 1.11). The electric displacement induced by the strain gradient can then be calculated as [37]

$$D = e\lambda \frac{h\varepsilon_h}{2\lambda\varepsilon_h + h\varepsilon_\lambda} \frac{\partial u_{11}}{\partial x_3} \qquad 1.26$$

Where $\varepsilon_\lambda = \varepsilon_0 + \chi_\lambda$ is the dielectric constant of the surface layer and ε_h is that of the bulk. For thin-enough surface layers $(\lambda/h \ll \varepsilon_\lambda/\varepsilon_h)$, and defining the effective flexoelectric coefficient as the derivative of the displacement field with respect to the strain gradient, Equation 1.26 yields an effective flexoelectric coefficient associated with surface piezoelectricity:

$$\mu_{1133}^{eff} = e\lambda \frac{\varepsilon_h}{\varepsilon_\lambda} \qquad 1.27$$

The two ouststanding features of this equation are that (i) the polarization raising from *surface* piezoelectriciticty is related with the *bulk* value of the dielectric constant, and (ii) the effective flexoelectricity due to surface piezoelectricity is independent of the thickness of the bulk (h). This means that, even for macroscopically thick (bulk) samples, bending will provoke a surface response that can in principle be as big as *or even bigger than* the actual bulk flexoelectricity of the crystal. Moreover, for a quantitative evaluation of surface piezoelectric effect, one can estimate the effective flexocoupling coefficient $f^{eff} \equiv \mu^{eff}/\chi_h \approx e\lambda/\varepsilon_\lambda$. For a conservative lower limit estimation, we consider the surface layer to be atomically thin (λ = a few angstroms). Then, using $e \sim 1$ C m^{-2} and $\varepsilon_\lambda/\varepsilon_0 \sim 10$, we find f^{eff} of the order of a few volts. This value is of the same order of magnitude as

the value of the components of the flexocoupling tensor f_{ijkl}~1–10 V. Thus, surface piezoelectricity can readily compete with bulk flexoelectricity.

The above features render surface piezoelectricity is qualitatively indistinguishable from bulk flexoelectricity. The only way to separate the two effects (bulk flexo and surface piezo) are therefore to either (i) change the nature of the surface, so that its surface-piezoelectric coefficient *e* is changed while preserving the same value of the bulk flexoelectric coefficient [38] or (ii) screen the bulk flexoelectricity by making the bulk conducting while keeping the interface insulating. The first route is described in chapter (4) and the second in chapter (5) of this thesis.

1.7 MATERIALS.

Below the Curie temperature T_C, ferroelectric materials undergo a phase transition from paraelectric to ferroelectric [39, 40]. In proper ferroelectrics (i.e., those where polarization is the primary order parameter), the dielectric constant shows a peak at the Curie temperature. Meanwhile, relaxors show a more diffuse phase transition with a high but broad dielectric peak, persistence of polar nanoregions even in the nominally paraelectric phase, and lack of spontaneous (i.e. not field-induced) long-range order. Solid solutions between ferroelectrics and relaxors can yield morphotropic phase boundary materials that are at the frontier between ferroelectric and relaxor behaviours.

The transformation plasticity associated with such morphotropic phase boundaries renders these frontier materials as the best electromechanical ceramics known to man [41].

The high dielectric constant of relaxor-ferroelectric and ferroelectric materials also makes them good candidates to obtain high flexoelectric performance. Therefore, for this thesis we investigated archetypical examples of each type: (1-x)$Pb(Mg_{1/3}Nb_{2/3})O_3$-x$PbTiO_3$, with x = 0.28 and 0.34 (hereafter, labelled PMN-28%PT and PMN-34%PT) as morphotropic phase boundary Relaxor Material (Chapter 3) and $BaTiO_3$ (Chapter 4) as Ferroelectric Material.

In Chapter 5, we have studied the role of conductivity. We have used oxygen reduction and annealing in determining the flexoelectric coefficient values in (001)-

oriented BTO single crystal. When reduced, more electrons per unit volume are available to carry a current under applied field. In these conditions, the current in the reduced material can be expressed as the sum of two contributions: the displacement current, resulting from changes in dielectric polarization, and the free charge current resulting from the movement of free carriers (oxygen vacancies) in response to the applied strain gradient. In the conductive conditions we found a colossal flexoelectric values and therefore conclude that the flexoelectric property is not limited to dielectric materials, but should be extended to semiconductor materials. Based on this observation, we have also initiated the study of flexoelectricity in an archetypical semiconductor such as silicon, which is discussed in chapter 6.

1.8 REFERENCES.

1. L. V. Azaroff and J. J. Brophy, Electronic Processes in Materials. McGraw Hill, 1963.

2. P. W. Atkins, Physical Chemistry, 4th Ed. W.H. Freeman and Company, 1990.

3. S. O. Kasap, Principles of electrical engineering materials and devices. McGraw Hill, 2000.

4. D. J. Griffiths, Introduction to Electrodynamics, 2nd Ed. Prentice Hall, 1989.

5. F. T. Ulaby, Fundamentals of Applied Electromagnetics. Pearson Prentice Hall, 2004.

6. I. Ponomareva, A. K. Tagantsev, and L. Bellaiche, *Phys. Rev. B.* **85**, 104101 (2012).

7. J. Hong and D. Vanderbilt, *Phys. Rev. B.* **88**, 174107 (2013).

8. M. Stengel, *Phys. Rev. B.* **88**, 174106 (2013).

9. S. O. Kasap, Principles of electrical engineering materials and devices. McGraw Hill, 2000.

10. W. D. J. Callister, Materials Science and Engineering, 3rd Ed. John Wiley and Sons, Inc., 1994.

11. D. K. Cheng, Field and Wave Electromagnetics, 2nd Ed. Addison-Wesley Publishing Company, 1992

12. R. M. Rose, L. A. Shepard, and J. Wulff, “The structure and properties of materials”, Wiley Eastern private limited, (1971).

13. D. W. Richerson, "Modern ceramic engineering: Properties, processing, and use in design", Second Edition, Marcel Dekker, inc., (1992).

14. M. E. Lines and A.M. Glass, “Principles and Spplications of Ferrroelectric and related Materials”Oxford (1977)

15. K. M. Rabe, M. Dawber, C. Lichtensteiger, C. H. Ahn and J-M. Triscone, “Modern Physics od Ferroelecttrics: Essential Background”, Springer, 2007

16. K. Uchino, “Piezoelectric actuators and ultrasonic motors”. Boston: Kluwer Academic Piblisers. (1997)

17. T. Mitsui, I. Tatsuzaki, and E. Nakamura, “An introduction to the physics of ferroelectrics.” New York: Gordon and Breach Science Publishers (1976)

18. P. Zubko, G. Catalan and A. K. Taganstsev, *Annu. Rev. Mater. Res*. **43** (2013).

19. S. M. Kogan Sov. *Phys.Solid. State*. **5**, 2069 (1964).

20. E. V. Bursian, N.N. Trunov, *Sov. Phys. Sol. State*. **16**, 760 (1974).

21. A. K. Tagantsev, *Phys. Rev. B*. **34**, 5883 (1986).

22. W. Ma and L. E. Cross, *Appl. Phys. Lett*. **78**, 2920 (2001).

23. W. Ma and L. E. Cross, *Appl. Phys. Lett*. **81**, 3440 (2002).

24. W. Ma and L. E. Cross, *Appl. Phys. Lett.* **82**, 3293 (2003).

25. P. Zubko, G. Catalan, A. Buckley, P. R. L Welche, and J. F Scott., *Phys. Rev. Lett.* **99**, 167601 (2007).

26. W. Ma and L. E. Cross, *Appl. Phys. Lett.* **88**, 232902 (2006).

27. R. Marangati and P. Sharma, *Phys. Rev. B.* **80**, 054109 (2009).

28. J. Hong, G.Catalan, J.F.Scott and E. Artacho, *J. Phys.: Condens. Matter.* **22**, 112201 (2010).

29. J. Hong and D. Vanderbilt, *Phys. Rev. B.* **88**, 174107 (2013).

30. L. Shu, X. Wei, L. Jin, Y. Li, H. Wang, and X. Yao, *Appl. Phys. Lett*. **102**, 152904 (2013).

31. A. K. Tagantsev, *Phase. Transit*. **35**, 119 (1991)

32. A. K. Tagantsev, *Phys. Rev. B*. **34**, 5883 (1986)

33. S. M. Kogan, *Phys. Solid. State.* **5**, 2069 (1964)

34. P. V. Yudin and A. K Tagantsev, *Nanotechnology,* **24**, 432001 (2013)

35. V.L. Indenbom, E. B. Loginov and M. A. Osipov, *Kristalografija*, **26**, 1157 (1981)

36. R. D. Mindlin. *Int. J. Solids Struct.* **4**, 637 (1968)

37. A.K. Tagantsev, A.S. Yurko., *J. Appl. Phys*. **112**, 044103 (2012)

38. M. Stengel, *Phys. Rev. B.* **90**, 201112(R) (2014).

39. A. F. Devonshire, *Philos. Mag.* **40**, 1040, (1949).

40. A. Von. Hippel, *Rev. Mod. Phys*. **22**, 221 (1950).

41. S-E Park and T. R. Shrout. *J. Appl. Phys*. **82**, 1804 (1997)

2 EXPERIMENTAL PROCEDURES

As a starting point, it is important to emphasize that there is not any commercial standard equipment in the market for flexoelectric measurements, such as there is for example to perform dielectric measurements (LCR-Meter), polarization loops (RT66B), etc. Therefore, the first step of this thesis work was to implement our own system to measure flexoelectricity. The designed set-up was based on a Dynamical Mechanical Analyzer (DMA) on which we implemented the simultaneous detection of bending induced current with external instrumentation such as a home-made signal amplifier and a lock-in amplifier. Every aforementioned instrument was controlled with programs made in LabView software. LabView allows us to obtain a versatile and user-friendly interface for integrating electric, mechanical and electromechanical measurements as a function of various parameters, including temperature. In the following, each step of this hardware and software development is exposed.

2.1 MECHANICAL MEASUREMENTS BY DYNAMIC MECHANICAL ANALYSIS

A dynamic mechanical analyser (DMA) is an instrument that allows us measure the mechanical response (deformation and mechanical loss) of a material as it is subjected to a periodic force. The material response is expressed in terms of a dynamic young's modulus and a dynamic loss modulus (a mechanical damping term). Typically, the values of dynamic moduli depend upon the type of material, temperature, and frequency of the measurement.

For an applied sinusoidal stress, a material will respond with a sinusoidal strain for low amplitudes of stress. The sinusoidal variation in time is usually described as a rate specified by the frequency (f = Hz; ω = rad/sec). The strain of a material is out of phase with the stress applied, by the phase angle, δ. This phase lag is due to the excess time necessary for molecular motions and relaxations to occur. The dynamic stress thus precedes the strain by δ, and the dynamic stress, σ, and strain, ε, are given as:

$$\sigma = \sigma_0 \sin(\omega t + \delta) \quad 2.1$$

$$\varepsilon = \varepsilon_0 \sin(\omega t) \quad 2.2$$

where ω is the angular frequency. Stress can be divided into an "in-phase" component ($\sigma_0 \cos \delta$) and an "out-of-phase" component ($\sigma_0 \sin \delta$) and rewritten as.

$$\sigma = \sigma_0 \sin(\omega t) \cos \delta + \sigma_0 \cos(\omega t) \sin \delta \quad 2.3$$

Dividing stress by strain yields to the Young's modulus E of the sample and using the symbols E' and E'' for the in phase (real) and out-of-phase (imaginary) components yields to:

$$\sigma = \varepsilon_0 \, \mathrm{E}' \sin(\omega t) + \varepsilon_0 \, \mathrm{E}'' \cos(\omega t) \quad 2.4$$

$$E' = \frac{\sigma_0}{\varepsilon_0} \cos \delta \qquad E'' = \frac{\sigma_0}{\varepsilon_0} \sin \delta \quad 2.5$$

In the frequency domain, this relationship can be expressed as:

$$\varepsilon = \varepsilon_0 \exp(i\omega t) \qquad \sigma = \sigma_0 \exp(\omega t + \delta) i \quad 2.6$$

$$E^* = \frac{\sigma}{\varepsilon} = \frac{\sigma_0}{\varepsilon_0} e^{i\delta} = \frac{\sigma_0}{\varepsilon_0} (\cos \delta + i \sin \delta) = E' + iE'' \quad 2.7$$

where E' is the Young's modulus and E'' is the loss modulus. The phase angle δ is given by

$$\tan \delta = \frac{E''}{E'} \quad 2.8$$

Equation 2.7 shows that the complex modulus obtained from a dynamic mechanical test consist of "real" and "imaginary" parts. The real (storage) part describes the ability of the material to store potential energy and release it upon deformation, i.e., it describes the elastic part of the mechanical response. The imaginary (loss) portion is associated with energy dissipation in the form of heat upon deformation.

The storage modulus is often times associated with "stiffness" of a material and is related to the Young's modulus, E. The dynamic loss modulus is often associated with "internal friction" and is sensitive to different kinds of molecular motions, relaxation processes such as dislocations or twin formation, transitions, morphology and other structural heterogeneities. Thus, the dynamic properties provide information at the molecular level to understand the material mechanical behaviour.

The DMA model 8000 from Perkin Elmer was used in this thesis and is shown in Figure 2.1. In the present case, the sinusoidal deformation applied to a sample is done in a three point bending configuration on samples of rectangular shape. The sample can be submitted to a controlled stress or a controlled strain. By applying a known stress, the sample will then deform by a certain amount, related to sample stiffness. A force motor is used to generate the sinusoidal wave and this is transmitted to the sample via a drive shaft. The response from the sample is detected by Lineal Vertical Displacement Transducer (LVDT) that converts a linear displacement into and electric signal for recording. The sample displacement ranges from 0μm to 1000μm; the amplitude used in our study was typically 2 μm, and the accuracy of the displacement measurements is 1nm. Its frequency of operation ranges from 0Hz to 600Hz, but mechanical resonances of the sample + DMA system

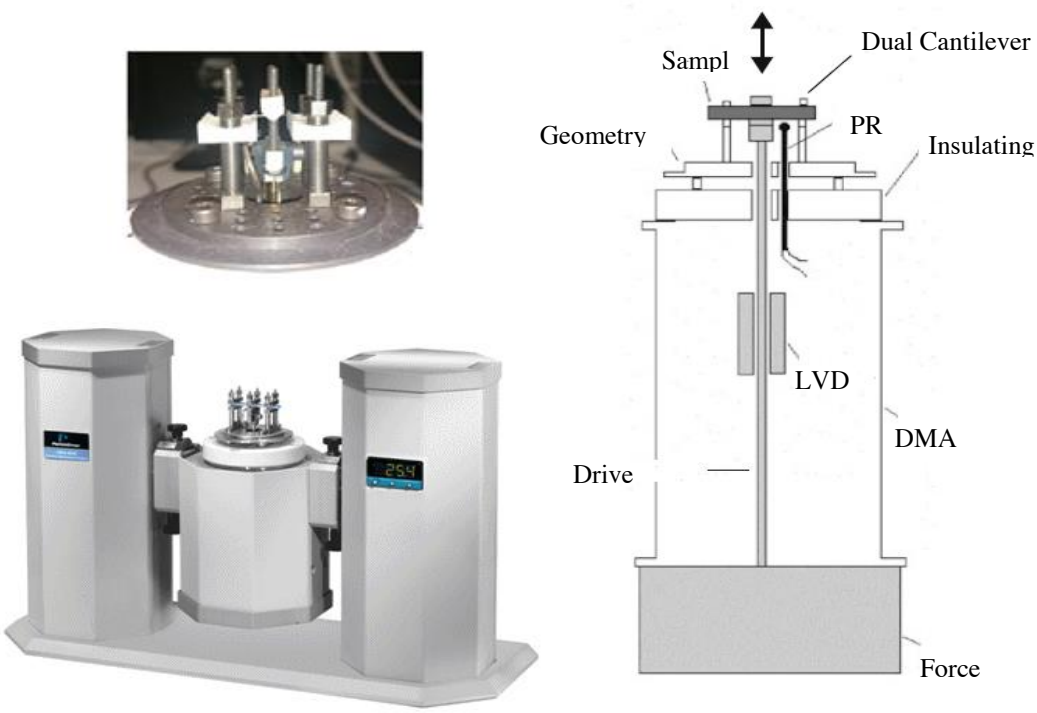

Figure 2.1 Perkin Elmer DMA 8000

typically prevented us from reaching beyond a few tens of Hz. For each measurement it is necessary to perform two types of instrument calibration: Balance/Zero calibration is used to determine and record the zero displacement position and Force Factor calibration is used to determine and record the conversion factor from machine units (DAC bits) into Newtons.

Finally, the DMA is embedded in a wide range furnace machinery capable of operating at temperatures between -150ºC and 600ºC. This includes a standard furnace configuration for heating and a cooling circuit for liquid nitrogen assisted cooling and controlled temperature ramping. Liquid nitrogen is driven through accessory circuit from a liquid nitrogen storage dewar of 50L placed by the set up. The temperature change rate of DMA can be varied by setting it from 1ºC/min to 10ºC/min. It must be mentioned, however, that although this the temperature range in which *mechanical* measurements can be made, *electromechanical* measurements such as flexoelectricity require making electrical connections to the sample, and not all wires can resist exposure to high temperatures. This wiring is not part of the as-purchased DMA and we had to implement it ourselves; details are described in the next section.

2.2 FLEXOELECTRIC MEASUREMENTS.

2.2.1 STRAIN GRADIENTS BY DYNAMIC MECHANICAL ANALYSIS

The main experimental task of this thesis was to measure the flexoelectric response of single crystals. In order to generate flexoelectric polarization, a strain gradient was applied by bending the samples.

The strain gradient along the direction of thickness was induced by a three-point bending motion, as illustrated in Figure 2.2. Samples are supported (but not clamped) on both ends by fixed sharp bars, and the drive shaft applies the deformation by pressing in the middle of the sample. The maximum dynamic displacement delivered to the middle of the samples was around 2 μm.

The strain of each measurement was calculated from the usual equation for a bent beam:

$$\epsilon_{11} = \frac{24x_3}{L^3}\left(\frac{L}{2} - x_1\right)z_0 \qquad 2.8$$

where z_0 is the displacement applied to the sample from the DMA, L is the length between the shafts, and x_1 and x_3 are spatial coordinates. Therefore, the strain gradient in the normal to the surface is:

$$\frac{\partial \epsilon_{11}}{\partial x_3} = \frac{24 z_0}{L^3}\left(\frac{L}{2} - x_1\right) \qquad 2.9$$

Assuming that the size of electrodes is always bigger than the length between the shafts, we have:

$$\frac{\partial \epsilon_{11}}{\partial x_3} = \frac{6 z_0}{L^2} \qquad 2.10$$

Considering that the distance between the shafts is of the order of mm, and the displacement applied to the sample is of the order of μm, typical strain gradient values are of the order 1 m^{-1}.

The sinusoidal movement of the drive shaft can be applied at frequencies between 0 and 600 Hz. As we will see later on, for low frequencies, the flexoelectric signal is too small to be detected (the flexoelectric current is linearly proportional to the frequency), and for too high frequencies, mechanical resonances appear and the samples easily exceed their mechanical stability and break. For a good compromise, the drive frequency of DMA was set to 13 Hz for all measurements. 13 Hz was chosen because it is a prime number and is therefore incommensurate with the frequency of the power supply (50Hz); this eliminates the risk of interference between the ac power supply and the small ac signals that we measure.

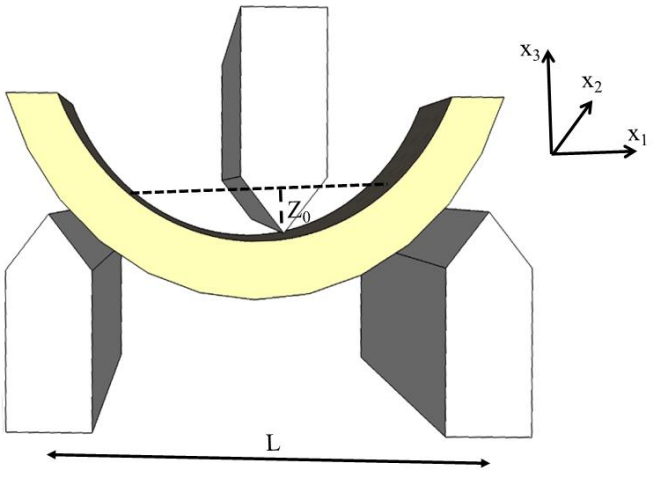

Figure 2.2. Three point bending configuration

2.2.2 FLEXOELECTRIC POLARIZATION.

The flexoelectric polarization (P_3) induced by mechanical strain gradient $\partial\varepsilon_{11}/\partial x_3$ in the single crystals was measured using the method described by Zubko et al [1], based on the detection of the displacement current induced by the flexoelectric polarization during the bending process.

The generated polarization can be calculated from the displacement current using the following equation:

$$P_3 = {}^{I}/_{2\pi\nu A} \qquad 2.11$$

where ν is the frequency of the bending force and A the area of the electrodes. Since this displacement current is proportional to the *derivative* of the polarization over time, it is a transient magnitude that linearly depends on the frequency of operation.

2.2.3 FLEXOELECTRIC COEFFICIENT.

In three-point bending, the strain gradient is not homogeneous along the length of the beam: it is maximum at the centre and zero at the clamping points. The charge per unit area collected by the electrodes is therefore an average of the flexoelectric polarization, which in turn is related to the average strain gradient by the effective flexoelectric coefficient μ_{13}^{eff} [1]:

$$\overline{P_3} = \mu_{13}^{eff}\,\overline{\frac{\partial\epsilon_{11}}{\partial x_3}} \text{ and } \overline{\frac{\partial\epsilon_{11}}{\partial x_3}} = \frac{12z_0}{L^3}(L-a) \qquad 2.12$$

where L is the separation between the standing points of the crystal, a is the half-length of electrodes, and z_0 the displacement applied in the middle of the samples, which is 2 μm in all our experiments.

The measured polarization is a combination of the non-zero flexoelectric tensor components and not the actual flexoelectric tensor components defined by [1]:

$$P_i = \mu_{ijkl}\frac{\partial\epsilon_{kl}}{\partial x_j} \qquad 2.13$$

Zubko et al [1] has in fact shown that the individual tensor components cannot be measured separately, so from an experimental point of view the effective coefficients are the relevant magnitude.

2.2.4 CURRENT SIGNAL DETECTION.

In order to measure the displacement current by the DMA, we used the following approach: extra wiring was added to the DMA to contact sample top (black line in Figure 2.3) and bottom electrodes (red line in Figure 2.3) in order to pick up the displacement current between the top and bottom surfaces of the samples, which was subsequently measured by an external lock-in amplifier. As mentioned earlier, these wires must be able to withstand quite extreme temperatures under most forms of electrically insulating coatings either crack or melt. Therefore, the parts of the wire that are inside the thermal chamber were bare platinum, threaded through ceramic alumina tubes. These wires were connected outside the chamber to coaxial cables.

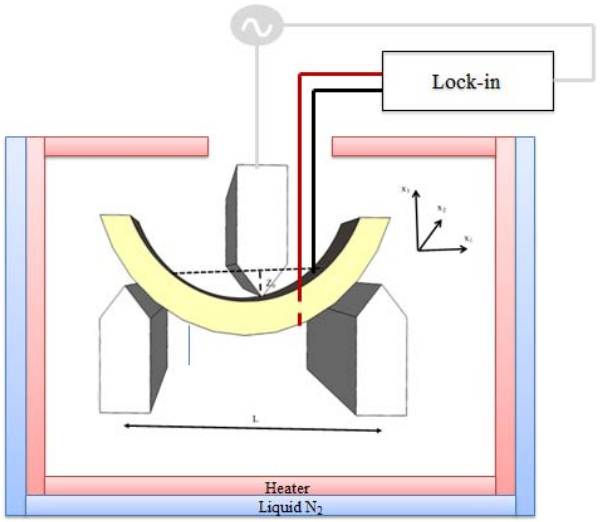

Figure 2.3 Experimental set-up for flexoelectric measurement

The lock-in uses the sinusoidal sample deformation signal extracted from the DMA (grey line in Figure 2.3) as a reference signal. The lock-in amplifier uses a technique known as phase-sensitive detection to single out the component of the signal at a specific reference frequency and phase. It works by multiplying the signal input to be analysed (the displacement current) by an oscillatory reference signal (the DMA induced deformation) and integrating over a time constant much longer than the

period of oscillation. If the input contains any signal that has the same frequency and constant phase difference with respect to the reference, the integrated signal will be the product of the two times the sinus of the constant phase difference, while any spurious signal (noise) that has a random spectrum of frequencies and phases will be averaged out to zero and thus are filtered out of the measurement. The lock-in can thus extract the amplitude and phase lag out of a small oscillatory signal even when the signal to noise ratio is very small.

In our experimental set up, the sinusoidal signal extracted from the DMA as a reference signal was itself too small (~0.2mV) and unstable to be read by an external Lock-in amplifier (Stanford, model SR830), so it was necessary to use a preamplifier. This preamplifier was home-made using a voltage divider and an active low pass filter, as shown in Figure 2.4.

Resistor voltage dividers are commonly used to create reference voltages, or to reduce the magnitude of a voltage so that it can be measured, and may also be used as signal attenuators at low frequencies, as in this case. The active low pass filter eliminates signals above the cut-off frequency, and allows signals below the cut-off frequency to pass. Additionally, the operational amplifier used in this circuit produces an output potential (relative to circuit ground) that is typically five orders of magnitude larger than the potential difference of its input signals. In this way, it is possible to obtain a signal detectable by the lock-in amplifier as reference input.

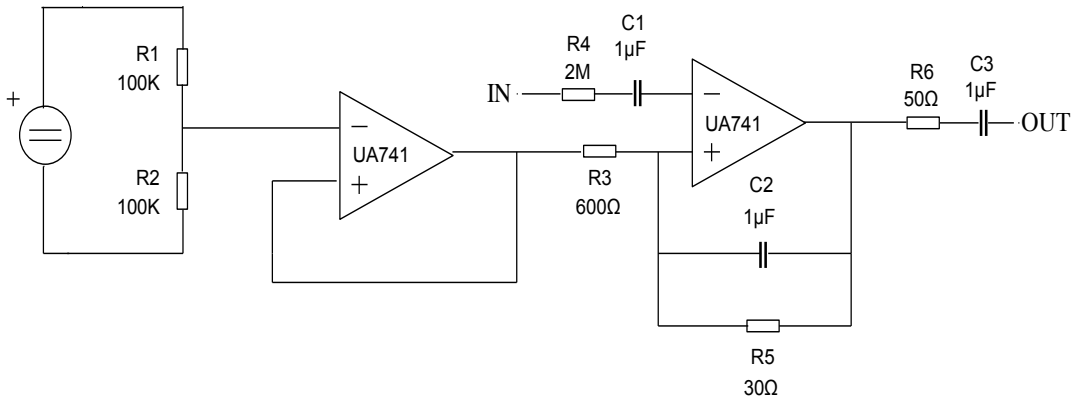

Figure 2.4 Scheme of home-made preamplifier circuit used to make output signal (~5V) of the DMA sufficiently large and stable for the lock-in to use it as a reference.

2.2.5 DATA ACQUISITION.

The magnitude of displacement current obtained from the Lock-in amplifier, together with the temperature, was integrated in a single software interface build up in LabView, which is shown in Figure 2.4. The Labview algorithm takes the current measured by the lock-in and the strain measured by the DMA, divides one over the other and the result is divided by the frequency and by the appropriate (user-determined) geometric factor in order to calculate the effective flexoelectric coefficient, which is plotted in real time as a function of temperature using the readout from the DMA thermocouple.

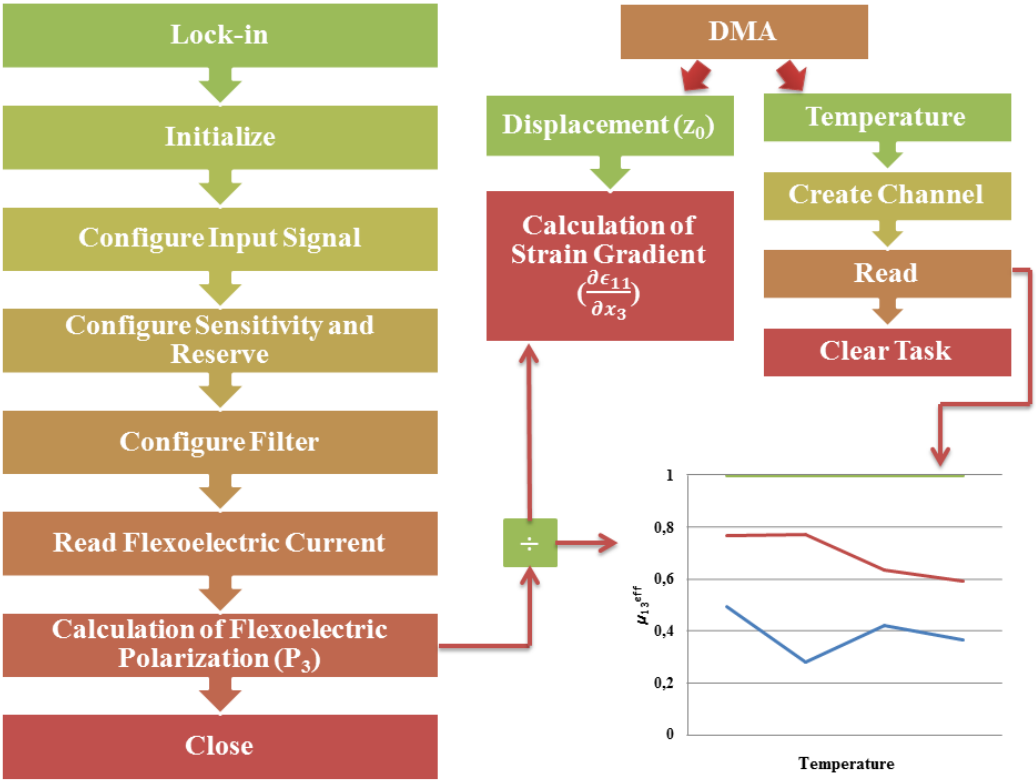

Figure 2.5 Schema of block diagram by flexoelectric measurements

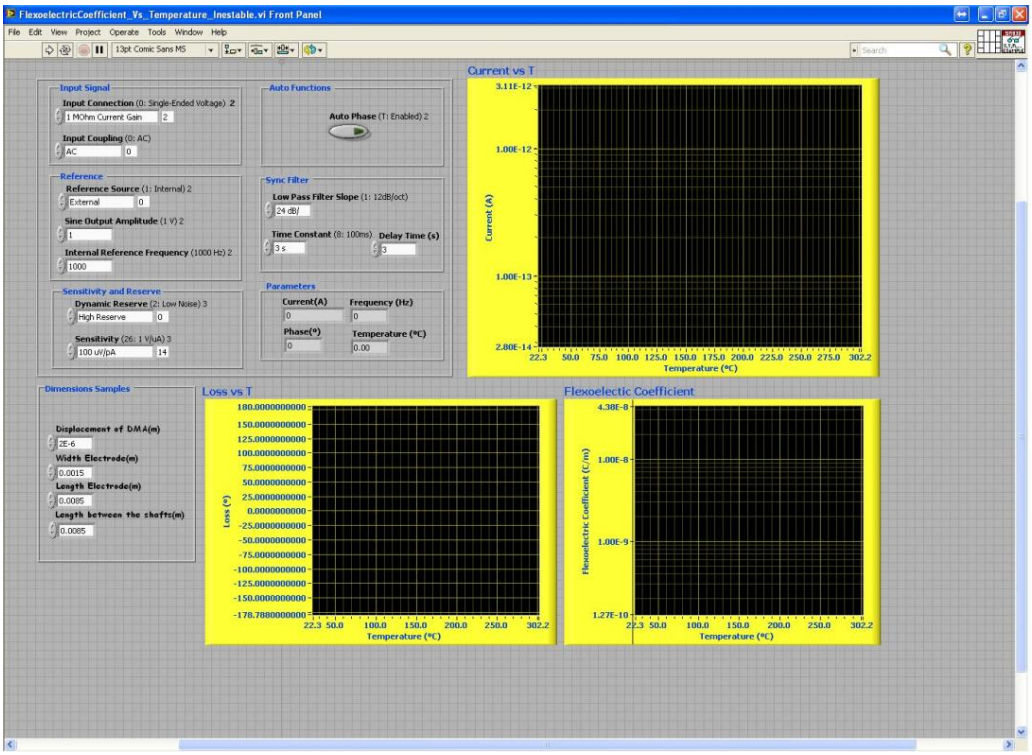

Figure 2.6. Interface user of LabView program for flexoelectric measurements

2.3 DIELECTRIC MEASUREMENTS.

The flexoelectric coefficient is expected to be proportional to the dielectric constant [2, 3, 4].

$$\mu_{klij} = \chi_{is} f_{klsj} \qquad 2.15$$

The latter condition already implies materials with high dielectric constant such as ferroelectric materials, are good candidates to study flexoelectricity. In order to correlate the flexoelectric characterization with the dielectric properties of the material, it is useful to measure the dielectric constant using the same configuration and the same conditions than for the flexoelectric measurements, that is, the same range of temperature (0ºC to 300ºC) under the same ramp rate of 3ºC/min.

Dielectric characterization set up was therefore implemented in the same DMA platform essentially used as a furnace, but in this case integrated with an Agilent Precision LCR Meter (Model E-4980A), which was connected to the sample using the electrodes in the same configuration as of the flexoelectric measurements. The LCR Meter applies a sinusoidal voltage with amplitude of 1 V and a frequency of 1

KHz, and measures the capacitance and dielectric loss of the sample. The capacitance was converted to dielectric constant using the relation:

$$\varepsilon_r = \frac{dC}{A\varepsilon_0} \qquad 2.9$$

where d is the thickness of the crystal, A is the area of the electrodes and ε_0 is the dielectric permittivity of vacuum.

Since in this measurement the DMA was used as a furnace, the temperature data was straightforward measured by the DMA. Therefore, the data from DMA and LCR Meter were collected by a LabView program is a similar way to that of the flexoelectric measurement. In this case, the program was made following the block diagram schematized in Figure 2.7. The user interface is shown in Figure 2.8

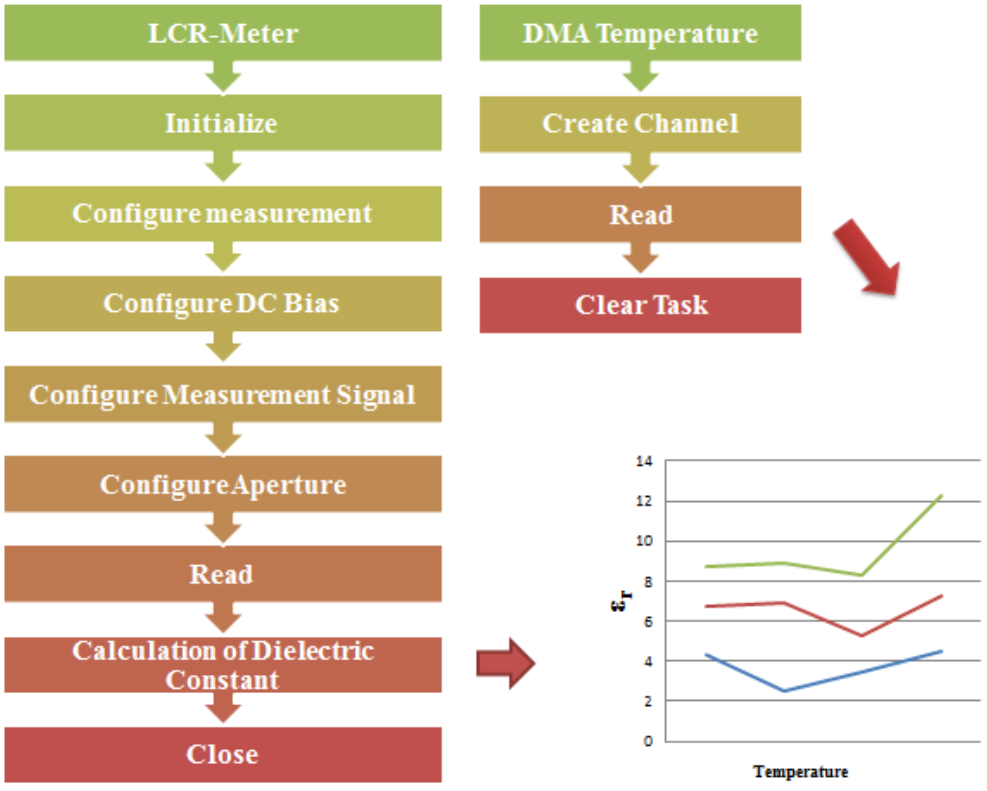

Figure 2.7 Scheme of block diagram for dielectric measurements

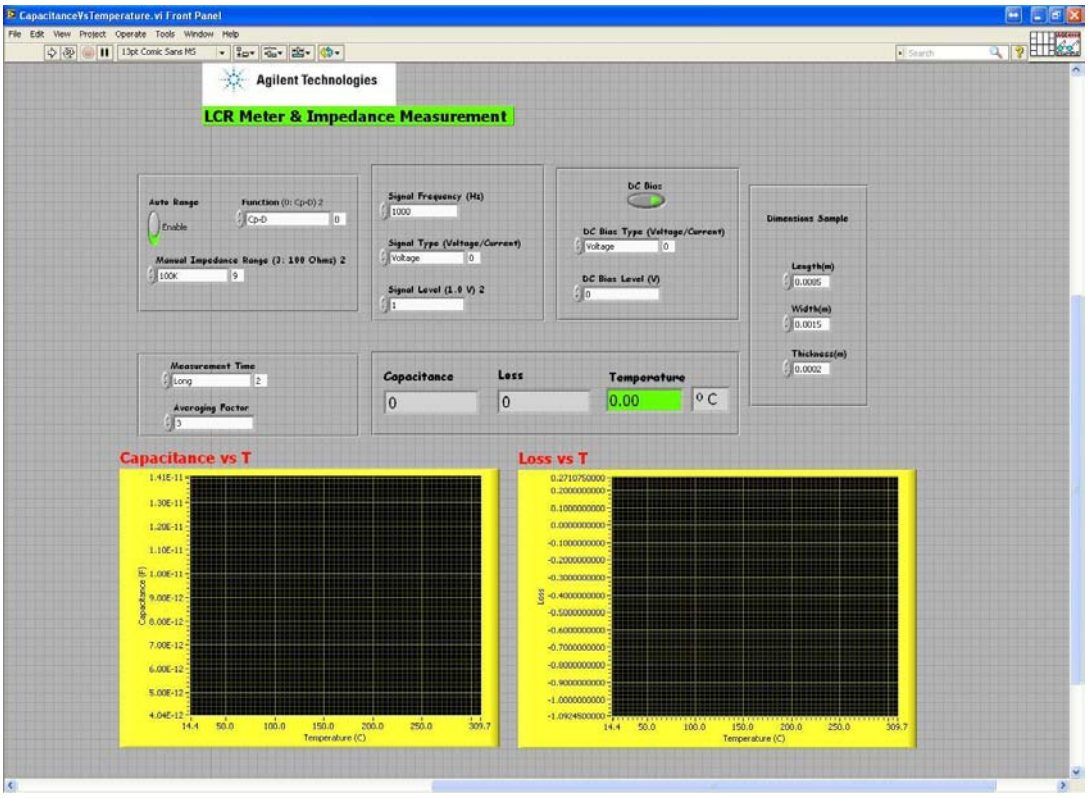

Figure 2.8 Interface user of LabView program for dielectric measurements

2.4 SAMPLES

All samples are rectangular bars, usually with a width around 1.5mm, a length more than 9mm and a thickness of 0.5mm.

In order to perform the flexoelectric characterization, it was essential to place rectangular electrodes on the top and bottom surfaces as illustrated in Figure 2.9.

It is important to achieve intimate contact between electrodes and surfaces, because otherwise air gaps or impurities can affect the measurements. Gold and platinum electrodes were deposited on the single crystals. Top and bottom electrodes were applied using:

- Electron Beam evaporation
- Pulsed Laser Deposition (PLD)

Even both techniques were used, we noticed that the PLD technique offered a better adhesion of the electrode with the materials, thus giving better stability for the

measurements. Eventually, we settled with PLD deposition (at room temperature and in vacuum) as the standard for most of our electrodes

Eventually, platinum wires of 0.05 mm in diameter were attached to the electrodes using very small drops of silver paste as illustrated in Figure 2.9. These wires facilitate connection of the electrodes to the internal DMA wires for flexoelectric and capacitance measurements respectively.

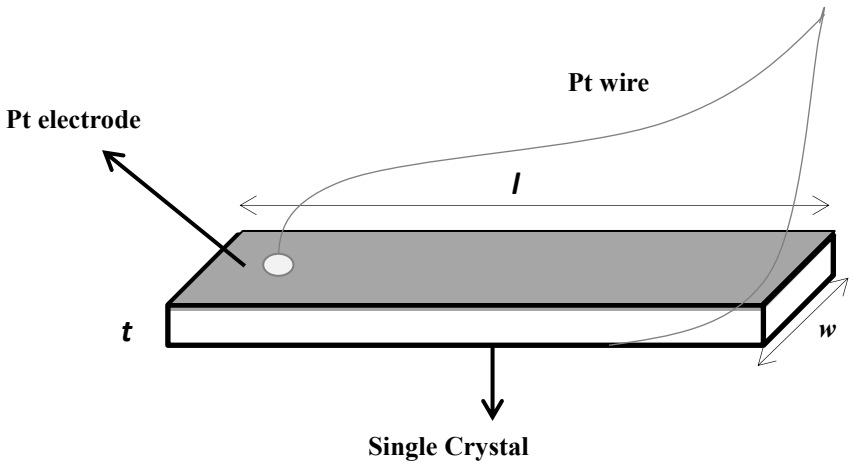

Figure 2.9 Geometry of samples

2.4.1 ELECTRON BEAM EVAPORATION (E-BEAM EVAPORATION)

Electron beam evaporation (Figure 2.10) is a technique in which a target material is exposed to an electron beam arising from the application of a huge voltage between the sample (used as the anode) and a filament under high vacuum conditions. The electron beam causes atoms from the source material to evaporate into the gaseous phase. These atoms then precipitate into solid form, coating all the present surfaces in the vacuum chamber with a thin layer of the anode material. A clear advantage of this process is that it allows for direct transfer of energy to the target through the induced heating and is very efficient in depositing pure evaporated material onto the substrate. Also, the deposition rate in this process can be as low as 1nm per minute or as high as few micrometers per minute. The efficiency in material use is high as

compared to other methods and the process offers good lateral control of the shape or homogeneity of the deposited films.

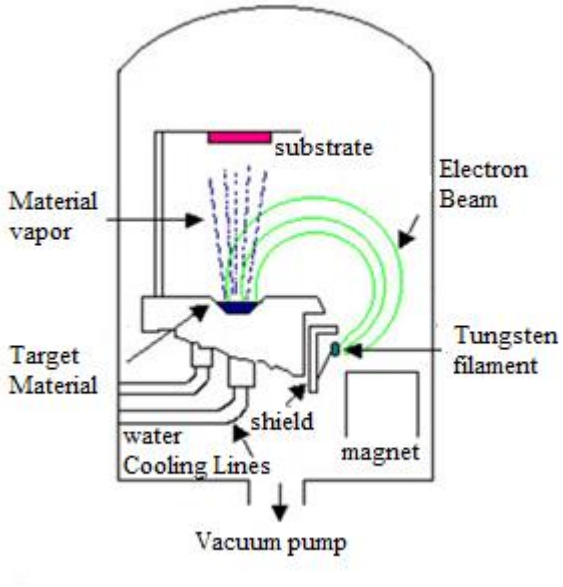

Figure 2.10 Scheme of Beam electron Evaporation

2.4.2 PULSED LASER ELECTRON BEAM EVAPORATION

Pulsed laser deposition (PLD) is a laser-based technique used to grow thin films of complex materials on substrates like our single crystals (Figure 2.11). The platinum (obtained from the target) is vaporized under argon atmosphere at pressure of 50mTorr by short and intense laser pulses at 10Hz –and 15000 pulses –forming plasma with the shape of a plume, and deposits on the substrate creating a platinum layer as electrode. For each laser shot, therefore, a layer of only 1.5 Angstrom of material is deposited by from the plasma plume in a process that typically lasts a few tens of picoseconds [5, 6]. To enable this process, nanosecond pulses with energies of 70 mill joules are necessary and UV wavelengths are usually preferred, for reach enough power to melt, evaporate and ionize material from the surface of the target. Though crystallization of ceramics and complex crystals requires deposition at high temperature, for base metals the deposition can be and was done at room temperature.

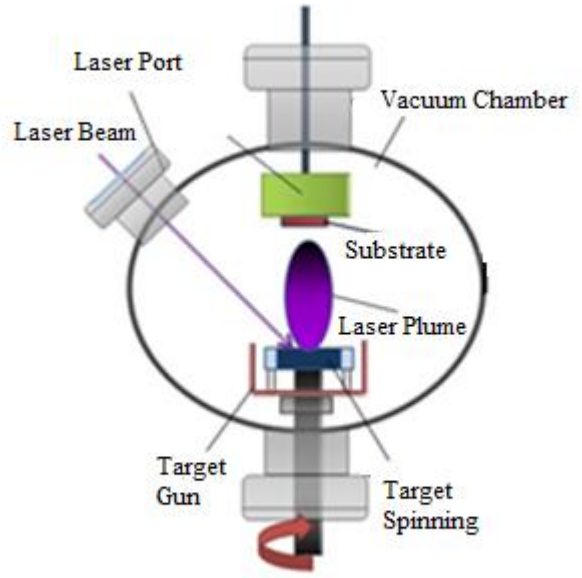

Figure 2.11 Scheme of Pulsed Laser Deposited

2.5 REFERENCES

1. P. Zubko, G. Catalan, A. Buckley, P. R. L. Welche, and J. F. Scott, *Phys. Rev. Lett.* **99**, 167601 (2007).

2. S. M. Kogan; Piezoelectric effect during inhomogeneous deformation and acoustic scattering of carriers in crystals, *Sov. Phys. Solid. State.* **5**, 2069 (1964).

3. E. V. Bursian, N.N. Trunov; Nonlocal piezoelectric effect, *Sov. Phys. Sol. State.* **16**, 760 (1974).

4. P. Zubko, G. Catalan and A. K. Taganstsev; Flexoelectric Effect in Solids, *Ann. Rev. Mater. Res.* **43** (2013).

5. http://www.andor.com/learning-academy/pulsed-laser-deposition-an-introduction-to-pulsed-laser-deposition

6.https://www.coherent.com/applications/index.cfm?fuseaction=Forms.page&PageID

3 FLEXOELECTRICITY OF RELAXOR FERROELECTRIC PMN-PT

3.1 INTRODUCTION.

The solid solutions formed between classical relaxor ferroelectrics such as lead magnesium niobate $PbMg_{1/3}Nb_{2/3}O_3$ (PMN) and the archetypal ferroelectric lead titanate $PbTiO_3$ (PT), i.e $(1-x)PbMg_{1/3}Nb_{2/3}O_3$-$xPbTiO_3$ (PMN-PT), have recently become one of the most intensively studied materials within solid state physics, due to their excellent piezoelectric and electromechanical properties as well the complexity and subtlety of its phase diagram and the various length scales involved in the structural and functional behavior of these materials.[1, 2, 3]

Relaxor ferroelectrics (relaxors) form a special class of ferroelectric materials. They have been extensively studied both experimentally and theoretically since the 1950s [4-7]. Relaxors are distinguished from the normal ferroelectrics by a few characteristic features [1, 8]:

- Relaxor exhibit a very broad peak of dielectric permittivity ε (T), often referred as a diffuse phase transition. The temperature of maximum ε (T) , called T_m, is strongly frequency dependent; namely, it shifts to higher temperatures with increasing frequencies. Below T_m, relaxors show a very strong dielectric dispersion. In contrast, the normal ferroelectrics exhibit a sharp, frequency independent peak of ε(T) at the Curie temperature (Tc). The examples of characteristic dielectric responses for relaxor and ferroelectric materials are shown in Figure 3.1.

- The temperature dependence of ε' in the case of normal ferroelectrics obeys the Curie-Weiss law, as show in Figure 3.1.

$$\varepsilon_r = \frac{C}{T - T_0} \qquad 3.1$$

Where C is the Curie constant and T_0 is the Curie temperature. In contrast the relaxors show strong deviations from this law above T_m. The linear dependence of 1/ε' Vs. T is obtained only at very high temperatures in relaxors, often hundreds of degrees above T_m.

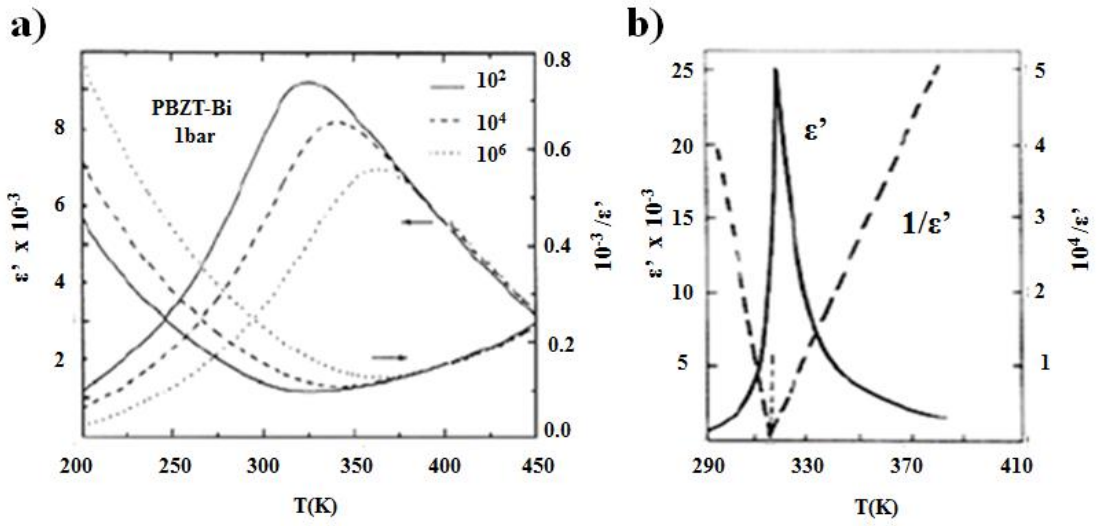

Figure 3.1 . Representative dielectric responses of a) relaxors (PBZT-Bi) and b) ferroelectrics (PZT) [8]

- The maximum of the dielectric permittivity observed in the relaxors is not linked to a structural phase transition. In contrast, the ferroelectrics show a sharp 1st or 2nd order structural phase transition at T_c. In the more paradigmatic cases such as $PbTiO_3$ or $BaTiO_3$, this transition is from a cubic to a tetragonal structure.

- In ferroelectric materials, polarizations versus electric field loops with stable remnant polarization are observed. In contrast, relaxors exhibit slim loops with weak "remnant" polarization that decays over time –i.e., it is not truly a thermodynamically stable polarization.

- In contrast to normal ferroelectrics, relaxors exhibit a weak optical anisotropy, consistent with the absence of a macroscopic polar axis.

In order to describe the relaxor behavior a few models were proposed. The first was offered by Smolenskii [9]. This author stated that the origin of the phase transition diffuseness can be related to the chemical heterogeneity on the cation site which results in a smearing of local Curie temperatures. Further studies performed by many authors showed that relaxor state is directly connected to the presence of the polar and chemically ordered clusters [10-14]. In 1987 Cross and co-authors introduced the so-called superparaelectric model [1]. The superparaelectric theory

described the regions of short-range chemical order as nanoscale polar clusters; the dipole moment of the clusters thermally switches between equivalent directions so macroscopic polar domains never form after the structural transition, as in classical ferroelectrics. Relaxors and their polar nanoregions are analogous to the spin cluster behavior in superparamagnets. Later, Viehland et al.[15] proposed a modified model, so called dipolar glass, in which correlation between polar clusters was taken into account in analogy to the spin glass system. The chief innovation from Viehland's analysis is the identification of a "freezing temperature", analogous to the Vogel-Fulcher glass transition, in which the polar nanoregions become "frozen" and no longer fluctuate in time. This freezing temperature can be identified by plotting an Arrhenius-like graph of $1/T_m$ as a function of frequency.

In 1992 Westphal et al. [16] postulates that the ground state of relaxors might be ferroelectric and the random fields induced by the compositional fluctuation led to the occurrence of the random domain state. Further on, Glinchuk and Farhi [17] offered a model of ferroelectric relaxors which based on the framework of the random field theory. In this model, the relaxors are considered as systems with random sites and orientations of electric dipoles, lattice vacancies, antisite ions and other defects as well as impurities embedded into the paraelectric phase which is proposed to be the host lattice for these materials. Recently, Pirc and Blinc[18] proposed the so called spherical random bond random field model which incorporates the two previous ones: dipolar glass and random field descriptions. In this hybrid model the dynamic of the polarization is controlled by the random/spherical bond characteristics, which are induced by the random fields. Multiple competing ordering of the polarization along multiple directions are allowed.

The bottom line is that relaxors are complex and the models used to describe them become increasingly sophisticated, but a common feature of all of them is the existence of some form disorder (chemical, structural, electrical) at the nanoscale that disrupts the formation of a long-range polar state, but with short-range polar order existing even above T_m. The existence of short-range order, as will be seen, is important also to understand the flexoelectric response of these materials.

The solid solutions between relaxors and ferroelectrics are also very interesting from the fundamental point of view. The addition of ferroelectric $PbTiO_3$ strongly affects the host lattice polarizability, and in consequence changes the characteristic relaxor behavior [8]. The Ti addition gradually transforms the typical relaxor behavior into the normal ferroelectric one, and makes possible the occurrence of structural phase transitions of different types. The phase diagram of PMN-PT [19-24] can be primarily divided into cubic (high temperature phase common to all compositions), rhombohedral – low temperature or room temperature phase for relaxor compounds with a small concentration of PT , and the tetragonal –ferroelectric phase, characteristic for solid solutions with high content of PT as is shown in Figure 3.2. In between tetragonal and rombohedral, however, there is a morphotropic phase boundary (MPB) that separates these two phases, and becomes the focus of our interest because it is where the highest electromechanical responses are found.

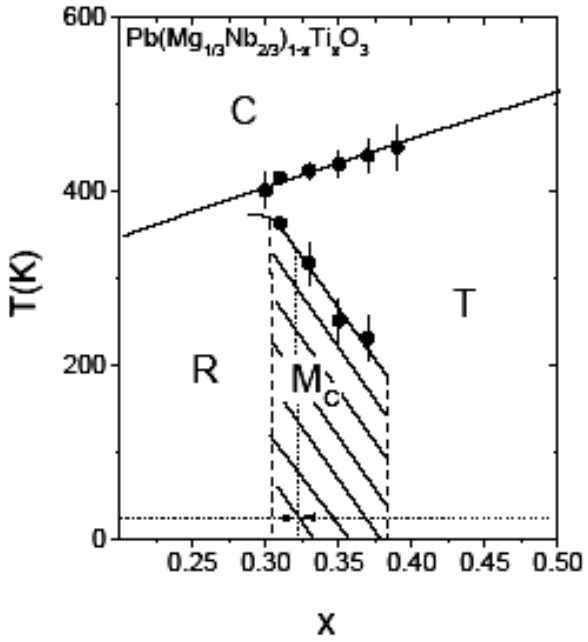

Figure 3.2 Phase Diagram Of $Pb(Mg_{1/3}Nb_{2/3})_{1-x}Ti_xO_3$ [21]

The existence of the MPB seems to be a common feature of the Pb(B' B'')O_3-$PbTiO_3$ system, where B' is a low valence cation, eg, Mg^{+2}, Ni^{+2}, Fe^{+3} and B'', a high valence cation, eg, Nb^{+5}, Ta^{+5}, W^{+6} [2, 25, 26]. The concept of the morphotropic phase boundary was introduced for the first time by Jaffe et al [25] in the case of $PbZr_{1-x}Ti_xO_3$ (PZT). The authors described the MPB as an almost vertical boundary, nearly temperature independent, between the rhombohedral and

tetragonal phases. However, the MPB is now considered rather as a region in which low symmetry phases, i.e. monoclinic or orthorhombic are present [21, 27, 28]. These low symmetry phases act as structural bridges between the tetragonal and rhombohedral ends of the phase diagram, and enable a continuous rotation of polarization between them, thus resulting in an enhanced piezoelectric response. The easy polar rotation is also important to understand the flexoelectric response of these materials, as we will see.

The giant electromechanical performance of relaxor-based ferroelectrics [29] and the complex physics associated with their inherently nanoscopic phase separation have inspired much research into these compounds [30]. The archetypal relaxor, $Pb(Mg_{1/3}Nb_{2/3})O_3$ (PMN), was also the first ceramic for which bending-induced polarization (flexoelectricity) [31, 32] was ever measured [33] and it was the unexpectedly large value of its flexoelectric coefficient that triggered the investigation of flexoelectricity in other perovskite ferroelectrics such as $Pb(Zr,Ti)O_3$[34, 35], $BaTiO_3$ [36], and $(Ba,Sr)TiO_3$ [37]; these investigations, together with the realization that very large flexoelectric effects can be achieved in the nanoscale [38-40], are ultimately behind the current surge of interest in this phenomenon [41].

Yet, for all the research, we still do not know something as basic as the intrinsic value of the effective flexoelectric coefficients—the constants of proportionality between strain gradient and induced polarization. With the exception of $SrTiO_3$ [42], in fact, the experimentally measured flexoelectricity of most perovskites exceeds theoretical expectations by between one and three orders of magnitude [43-46]. And differences are not merely between theory and experiment: experimental results can also substantially disagree among themselves. In $Pb(Mg_{1/3}Nb_{2/3})O_3$-10%$PbTiO_3$, for example, there is a discrepancy of three orders of magnitude between flexoelectric coefficients measured by two different methods [47]. Meanwhile, the expected contribution of polar nanoregions to the flexoelectricity of relaxor ferroelectrics [31] has not been established.

Before this investigation, in fact, there were no measurements for compositions at or near the morphotropic phase boundary either, even though their otherwise record-

high electromechanical performance [29] might suggest the possibility of similarly enhanced flexoelectric effects. To further complicate the picture, most flexoelectric measurements have been performed in ceramics, and, before our investigation of the PMN-PT system, there were no experimental reports for single crystals other than $SrTiO_3$ [42, 48], and this is relevant because grain boundaries have their own piezoelectric properties [49, 50] that can add an extrinsic contribution to the bending-induced polarization.

In this context, we studied the bending-induced polarization of single crystal relaxor-ferroelectrics with compositions $(1-x)Pb(Mg_{1/3}Nb_{2/3})O_3$-$xPbTiO_3$, with x = 0.28 and 0.34 (hereafter, labelled PMN-28%PT and PMN-34%PT). The dimensions are 6.58 × 2.54 × 0.5mm, and their surface is parallel to the $\{100\}_{pseudocubic}$ planes, with the edges parallel to the ⟨100⟩ crystallographic axes. These crystals, commercially available (TRS Technologies, Inc.), are at the morphotropic boundary that separates a relaxor-like rhombohedral phase for PMN-rich compositions from a ferroelectric tetragonal phase for PT-rich compositions [21]. We have found that not only the flexoelectricity is large, but the flexocoupling voltage is also large, exceeding theoretical expectations by an order of magnitude [41].

Deformation-induced polarization may arise from extrinsic origins such as defect dipoles, built-in pyroelectricity or even microcracking, so careful analysis was required to clarify the origin of the observed enhancement. Close inspection of the temperature dependence revealed a direct correlation between the enhancement of apparent flexoelectricity and the onset of anelastic softening in the materials. The mechanical softening and enhanced flexoelectric response are both consistent with the onset of ferroelasticity within polar nanodomains at a temperature T* higher than the dielectric peak [51, 52]. Our conclusion, as discussed below, is that "giant" bending-induced polarization of relaxor ferroelectrics is thus not due to an intrinsically giant flexoelectricity, but to a bending-induced reorientation of polar nanodomains.

3.2 DIELECTRIC CHARACTIZATION OF (1-*x*)PMN-*x*PT.

As discussed at the introduction, flexoelectricity is proportional to dielectric permittivity [31, 32, 41, 54], so it is useful to start by characterizing the dielectric constant of the crystals. The dielectric constant and loss as a function of temperature (Figure 3.3) have been measured at 1 kHz. The heating and cooling ramps were identical to those of the flexoelectric measurements (3 K/min). The dielectric losses are low (tan d<0.05) for both samples throughout the entire temperature range of the experiments: this ensures that the impedance response is predominantly dielectric even at the highest recorded temperatures, where dielectric losses start to rise due to increased conductivity.

Both samples display a clear dielectric maximum, but with differences: the peak of PMN-34%PT is sharper and at higher temperature than that of PMN-28%PT. This is to be expected and it correlates directly with the concentration of $PbTiO_3$ (PT), which is a standard ferroelectric with a high Curie temperature (T_C = 492ºC) [55]: PMN-34%PT has a dielectric response closer to that of standard ferroelectric $PbTiO_3$ (sharp peak and a higher Curie temperature T_C = 150 ºC) while the PMN-28%PT sample has response closer to that of conventional relaxor $Pb(Mn_{1/2}Nb_{2/3})O_3$, with increased diffuseness and broad maximum at a lower temperature (T_m = 125 ºC).

Although PMN-34%PT is more ferroelectric-like and PMN-28%PT more relaxor-like, the inverse permittivity (inset of Figure 3.3) departs from linear Curie-Weiss behavior below T* ~ 250 ºC for both compositions. Such departure is interpreted as an indicator of the existence of polar nanoregions or polarization fluctuations, characteristic of relaxors [56]. Thus, irrespective of whether the transition is diffuse or sharp, the high temperature phase is relaxor-like for both PMN-28%PT and PMN-34%PT. Transitions from a high temperature relaxor-like phase to a long-range ferroelectric phase are typical for compositions near the boundary between the two states [21].

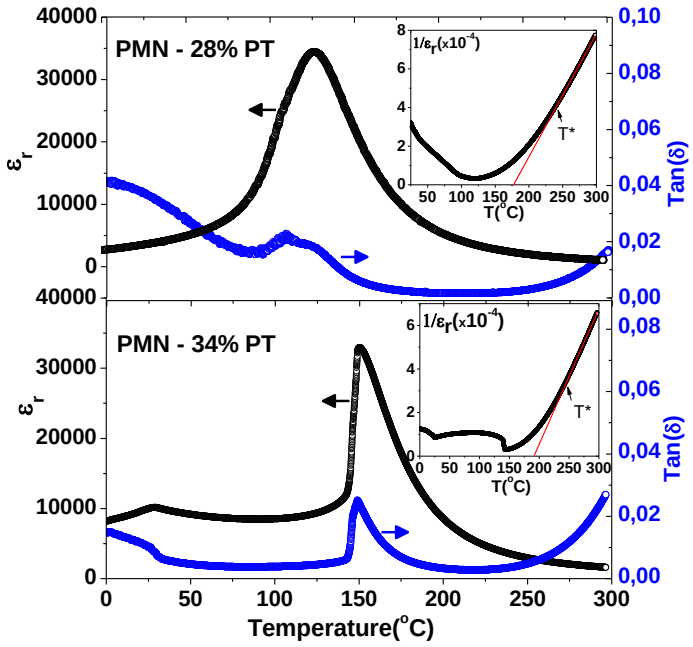

Figure 3.3. Relative dielectric constant (black) and loss tangent (blue) of PMN-28%PT and PMN-34%PT. Insets: inverse of the relative permittivity, showing a departure from linear Curie-Weiss behavior below T*

3.3 Flexoelectric And Elastic Characterization Of (1-x)PMN - xPT.

The effective flexoelectric coefficients as a function of temperature are shown in Figure 3.4, together with the simultaneously measured Young's modulus. Flexoelectricity and permittivity peak at the same temperature, with flexoelectric maxima of 30–40 ºC/m. There are no other single crystal values in the literature, but for ceramics of pure PMN the flexoelectric maximum is 8 μC/m [33]. Though the 5× bigger flexoelectricity of our PMN-PT crystals may in principle be influenced by the different sample morphology between crystals and ceramics, we think that the large difference is unlikely to be solely due to the single crystal vs ceramic difference (reported permittivity, for example, differs only by a factor of <2 between the two types of samples); rather, it seems that closeness to the morphotropic phase boundary may indeed contribute to enhance the effective flexoelectric coefficients. These, however, are still below those the current record-holders, barium titanate-based solid solutions [37, 41, 46, 57].

Importantly, the large flexoelectric coefficients are dependent on the thermal history of the sample: up to T* ~225–250 ºC, flexoelectricity is higher on heating than on

cooling, and this suggests a presence and participation of domains. The thermal hysteresis is more pronounced in PMN-28%PT, which is also consistent with bigger fraction metastable domains in the more relaxor-like compound.

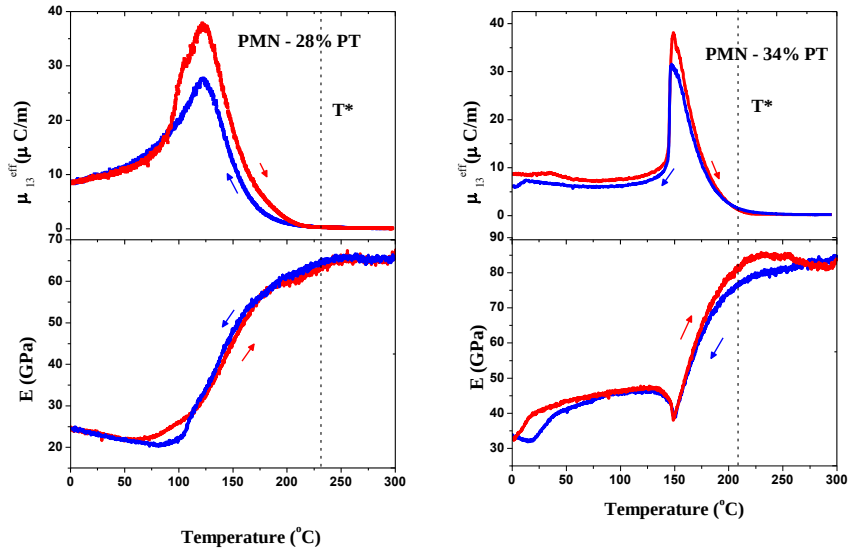

Figure 3.4 Temperature dependence of the flexoelectric coefficients and elastic Young's modulus of PMN-28%PT and PMN-34%PT.

Further evidence for the participation of domains comes from analysis of the elastic behavior in Figure 3.4 At high temperatures, the Young's modulus E is relatively constant, but around 200–250 ºC the lattice begins to soften, with the Young's modulus decreasing from 60GPa above T* to 20GPa below T_m for PMN-28%PT, and from 80GPa to 40GPa for PMN-34%PT. This softening is anelastic, as indicated by the increase in mechanical losses and a classic indication of the onset of ferroelastic domain activity, with the twin wall motion being both a way to relax the stress and a mechanical energy dissipation mechanism.

3.4 FLEXOCOUPLING CHARACTERIZATION OF (1-X)PMN-XPT.

In order to gain further insight into the high values of flexoelectricity, we now examine the flexoelectric coefficient normalized by the dielectric constant (Figure 3.5). Theoretically, this so-called flexo-coupling (or flexo-voltage [40]) coefficient, *f*, should be of the order of 1–10 V[41]. Experimentally, instead, the measured

coefficients reach up to f ~100–300 V, an order of magnitude bigger than the theoretical upper limit.

At low temperatures (i.e., below the Curie temperature), some or most of the bending-induced polarization may be attributed to piezoelectricity. In PMN-34%PT, long range polarization appears at $T_C = T_m = 150$ ºC. In PMN-28%PT, which is more relaxor-like, spontaneous long range order does not appear at any critical temperature, and the flexocoupling coefficient grows continuously upon cooling. On heating, though, a residual anomaly appears around T_f =100ºC < T_m =125ºC, which we interpret as the relaxor freezing temperature below which stable polarization and thus piezoelectricity can appear.

At temperatures above T*, however, the flexocoupling coefficient goes down to a stable value $f \leq$ 10V that is not hysteretic, is constant with temperature, and is consistent with theoretical expectations. This is therefore likely to be the true intrinsic value of the flexocoupling coefficient.

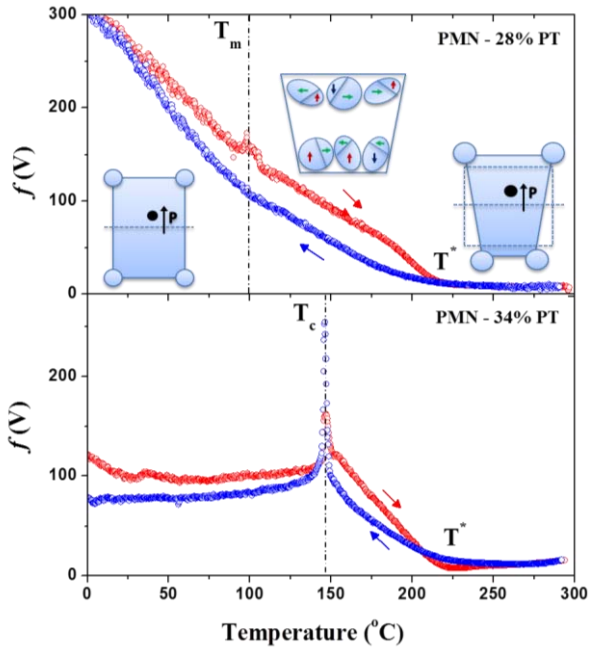

Figure 3.5 Flexocoupling coefficients of PMN-28%PT and PMN-34%PT

3.5 DISCUSSION

Relaxor ferroelectrics are known to display a peak in acoustic emission at a relatively composition-independent temperature T*~ 500 ± 30K [24, 25]. Acoustic emission is caused by a sudden release of elastic energy, so T* must signal an elastic discontinuity, in perfect agreement with our results and also with analysis of resonant ultrasound spectroscopy made by Carpenter et al. [58].

The origin of the peak in acoustic emission and of mechanical anelastic softening below T* is attributed to a ferroelastic transition within the relaxor polar nanoregions. These regions are known to appear at a higher temperature, the so-called Burns temperature (Tb ≥ 600K [52]) but only become ferroelastically active at T* ~ 500K [51, 52, 58, 59]. The exitence of nanodomains is also, as discussed before, consistent with the thermal history dependence of the bending-induced polarization, which is higher on heating than on cooling, indicative of a bigger volume fraction of nanodomains when heating from the ferroelectric polar state than when cooling from the non-polar paraphase.

The appearance and subsequent growth of nanotwins below T* has consequences for the electromechanical response of the material, because external stress can cause a ferroelastic reorientation of the nanodomains. Under bending stress, local compression of the x-y plane at the concave side will increase the proportion of domains with perpendicular polarization. The bending strains reach a maximum of ϵ_{11} ~ (near the center of curvature) at the surface; multiplied by the Young's modulus of PMN-PT (20–80 GPa), this is equivalent to a stress of 2–8 MPa, which is sufficient to cause ferroelastic switching[25] . However, an electric bias is still necessary in order to remove the degeneracy between the +*z* and -*z* directions:[25] though stress can rearrange ferroelastic domains and locally favour vertical polarization, the coupling is to the square of polarization (electrostriction) and thus it cannot favour one polarity over its opposite [40, 41]; this is the reason why mechanically assisted poling is always done in the presence of an electric bias[60]. Since we are not applying any external voltage in our experiments, and the electrodes are symmetric, the biasing may be provided by the flexoelectric field, although recent experiments by the group of Damjanovic suggest that another

potential source of bias may also be defect gradients, which are inherent in all crystals even when they are nominally centrosymmetric [61]. The average strain gradient in the bent crystals is of the order of $\overline{\frac{\partial \epsilon_{11}}{\partial z}}$ = 0.2 m^{-1}, and the intrinsic (high temperature) flexocoupling coefficient is of the order of $f \sim 10$ V, so the equivalent flexoelectric field is of the order of $E = f\overline{\frac{\partial \epsilon_{11}}{\partial z}}$ = 2 V/m. This is too small compared to typical coercive fields in ferroelectrics (kV/cm), so it is clear that the flexoelectric field by itself cannot cause switching; at most, as discussed, it provides a background bias that favours one polarity over the other when the polarization is ferroelastically switched. Ferroelasticity and flexoelectricity must therefore work in tandem to achieve the enhancement: the first causes the switching, and the second dictates the polarity of the switched state. Defect gradients may of course also cause a similar bias, but in that case it will probably be active only for a given orientation of the crystal and not for the opposite, as we discuss in the next chapter.

The effective flexoelectricity caused by this cooperative "flexoferroelastic" switching is not bound by the Kogan-Tagantsev limit and can therefore yield domain-based effective flexocoupling coefficients orders of magnitude larger than the intrinsic lattice-based flexoelectricity, which we have measured as an almost constant f_{13}=10V above T*. Though the potential practical usefulness of giant flexoelectricity for electromechanical transduction is mostly unaffected by its origin, the small thermal hysteresis, typical of domain-based properties, is undesirable and should be minimized.

Perhaps more importantly, these results are evidence that giant bending-induced polarization can be obtained without an intrinsically giant flexoelectricity, and this observation is a first step towards reconciling some of the discrepancies about the true magnitude of the flexoelectric coefficient. In the next chapter, we will see that nanodomain contribution to effective flexoelectricity is a pervasive phenomenon that affects not only relaxors but also very standard ferroelectrics, and we will also see that there is at least another source of bending-induced polarization that further modifies the intrinsic bulk value; namely, surface piezoelectricity.

3.6 REFERENCES.

1. L.E. Cross, Ferroelectrics **76**, 241 (1987)

2. J. Kuwata, K. Uchino and S. Nomura, *Ferroelectrics* **37**, 579 (1981)

3. J. Kuwata, K. Uchino and S. Nomura, *Jpn. J. Appl. Phys*. **21**, 1298 (1982)

4. G. Shirane and A. Takeda, *J. Phys. Soc. Jpn*. **7**, 5 (1952)

5. G. Shirane and K. Suzuki, *J. Phys. Soc. Jpn*. **7**, 333 (1952)

6. G. A. Smolenskii and A. I. Agranovskaya, *Sov. Phys. Tech. Phys.* **3**, 1380 (1958)

7. V. A. Bokov and I. E. Mylnikova, *Fiz. Tverd. Tela* **2**, 2728 (1960)

8. G. A. Samara, *J. Phys.: Condens. Matter* **15**, R367 (2003)

9. G. A. Smolenskii, *J. Phys. Soc. Jpn.* **28**, 26 (1970)

10. G. Burns and B. A. Scott, *Solid State Commun.* **13**, 417 (1973)

11. N. A. Setter and L. E. Cross, *J. Appl. Phys.* **51**, 4356 (1980)

12. C. G. Stenger and A. F. Burgraaf, *Phys. Status Solidi (a)* **61**, 275, (1980)

13. G. Burns and F. H. Dacol, *Phys. Rev. B* **28**, 2527 (1983)

14. X. Yao, Z. L. Chen and L. E. Cross, *J. Appl. Phys.* **54**, 3399 (1984)

15. D. Viehland, S. J. Jang, L. E. Cross and M. Wutting, J. Appl. Phys. **68**, 2916 (1990)

16. V. Westphal, W. Kleemann and M. D. Glinchuk, *Phys. Rev. Lett.* **68**, 847 (1992)

17. M. D. Glinchuk and R. Fahri, *J. Phys.: Condens. Matter* **8**, 6985 (1996)

18. R. Pirc and R. Blinc, *Phys. Rev. B* **60**, 13470 (1999)

19. W. Choi, T.R. Shrout, S. J. Jang and A.S. Bhalla, *Ferroelectrics* **100**, 29 (1989)

20. O. Noblanc, P. Gaucher and G. Calvarin, *J. Appl. Phys.* **79**, 4291 (1996)

21. B. Noheda, D. E. Cox, G. Shirane, Z.-G. Ye and *J. Gao, Phys. Rev. B*. **66**, 054104 (2002)

22. P. M. Gehring, W. Chen, Z. G. Ye and G. Shirane, *J. Phys.: Condens. Matter.* **16**, 7113 (2004)

23. D. Zekria, V. A. Shuvaeva and A. M. Glazer, *J. Phys.: Condens. Matter* **17**, 1593(2005)

24. V. A. Shuvaeva, A. M. Glazer and D. Zekria, *J. Phys.: Condens. Matter* **17**, 5709(2005)

25. B. Jaffe, W. R. Cook, and H. Jaffe, Piezoelectric ceramics (Academic Press, London, 1971)

26. T. Shrout, Z.P. Chang, N. Kim and S. Markgraf, *Ferroelectr. Lett. Sect.* **12**, 63(1990)

27. D. La-Orauttapong, B. Noheda, Z.-G. Ye, P. M. Gehring, J. Toulouse and D. E. Cox, *Phys. Rev. B* **65**, 144101 (2002)

28. B. Noheda, *Curr. Opin. Solid State Mater.* **6**, 27 (2002)

29. S. E. Park and T. R. Shrout, *J. Appl. Phys*. **82**, 1804–1811 (1997).

30. A. A. Bokov and Z.-G. Ye, *J. Mater. Sci*. **41**, 31–52 (2006).

31. S. M. Kogan, *Sov. Phys. Solid State.* **5**, 2069–2070 (1964).

32. A. K. Tagantsev, *Phys. Rev. B.* **34**, 5883–5888 (1986).

33. W. Ma and L. E. Cross, *Appl. Phys. Lett.* **78**, 2920–2921 (2001).

34. W. Ma and L. E. Cross, *Appl. Phys. Lett*. **82**, 3293–3295 (2003).

35. W. Ma and L. E. Cross, *Appl. Phys. Lett*. **86**, 072905 (2005).

36. W. Ma and L. E. Cross, *Appl. Phys. Lett*. **88**, 232902 (2006).

37. W. Ma and L. E. Cross, *Appl. Phys. Lett*. **81**, 3440–3442 (2002).

38. G. Catalan, L. J. Sinnamon, and J. M. Gregg, *J. Phys.: Condens. Matter.* **16**, 2253–2264 (2004).

39. G. Catalan, A. Lubk, A. H. G. Vlooswijk, E. Snoeck, C. Magen, A. Janssens, G. Rispens, G. Rijnders, D. H. A. Blank, and B. Noheda, *Nat. Mater.* **10**, 963–967 (2011).

40. H. Lu, C.-W. Bark, D. Esque de los Ojos, J. Alcala, C. B. Eom, G. Catalan, and A. Gruverman, *Science*. **336**, 59–61 (2012).

41. P. Zubko, G. Catalan, and A. K. Tagantsev, Annu. Rev. Mater. Res. **43**, 387–421 (2013).

42. P. Zubko, G. Catalan, A. Buckley, P. R. L. Welche, and J. F. Scott, Phys. Rev. Lett. 99, 167601 (2007).

43. R. Maranganti and P. Sharma, *Phys. Rev. B.* **80**, 054109 (2009).

44. J. Hong, G. Catalan, J. F. Scott, and E. Artacho, J. Phys.: Condens. Matter **22**, 112201 (2010).

45. J. Hong and D. Vanderbilt, *Phys. Rev. B.* **88**, 174107 (2013).

46. L. Shu, X. Wei, L. Jin, Y. Li, H. Wang, and X. Yao, *Appl. Phys. Lett.* **102**, 152904 (2013).

47. P. Hana, *Ferroelectrics.* **351**, 196–203 (2007).

48. P. Zubko, G. Catalan, A. Buckley, P. R. L. Welche, and J. F. Scott, *Phys. Rev. Lett.* **100**, 199906 (2008).

49. A. Kholkin, I. Bdikin, T. Ostapchuk, and J. Petzelt, *Appl. Phys. Lett.* **93**, 222905 (2008).

50. J. Petzelt, T. Ostapchuk, I. Gregora, I. Rychetsk_y, S. Hoffmann-Eifert, A. V. Pronin, Y. Yuzyuk, B. P. Gorshunov, S. Kamba, V. Bovtun et al., *Phys. Rev. B*. **64**, 184111 (2001).

51. M. Roth, E. Mojaev, E. Dul'kin, P. Gemeiner, and B. Dkhil, *Phys. Rev. Lett*. **98**, 265701 (2007).

52. B. Dkhil, P. Gemeiner, A. Al-Barakaty, L. Bellaiche, E. Dul'kin, E.Mojaev, and M. Roth, *Phys. Rev. B*. **80**, 064103 (2009).

53. M. Stengel, Phys. Rev. B 88, 174106 (2013).

54. E. V. Bursian and O. I. Zaikovskii, Sov. *Phys. Solid State.* **10**, 1121–1124 (1968).

55. M. J. Haun, E. Furman, S. J. Jang, H. A. McKinstry, and L. E. Cross, *J. Appl. Phys*. **62**, 3331–3338 (1987).

56. D. Viehland, S. J. Jang, L. E. Cross, and M. Wuttig, *Phys. Rev. B* **46**, 8003–8006 (1992)

57. L. E. Cross, *J. Mater. Sci*. **41**, 53–63 (2006).

58. M. A. Carpenter, J. F. J. Bryson, G. Catalan, S. J. Zhang, and N. J. Donnelly, *J. Phys.: Condens. Matter.* **24**, 045902 (2012).

59. M. A. Carpenter, J. F. J. Bryson, G. Catalan, and C. J. Howard, *J. Phys.: Condens. Matter.* **24**, 045901 (2012).

60. A. E. McLaughlin, T. Liu, and S. C. Lynch, *Acta Mater.* **53**, 4001–4008 (2005).

61. A. Biancoli, C. M. Fancher, J. L. Jones and D. Damjanovic, *Nat. Mater.* **14**, 224-229 (2015)

4 FLEXOELECTRICITY OF SINGLE CRYSTAL $BaTiO_3$

4.1. INTRODUCTION.

Barium titanate ($BaTiO_3$) has a typical perovskite structure, which is shown in Figure 4.1. Perovskite materials, with a general stoichiometry of ABO_3, represent a unique class of crystalline solids that demonstrate a variety of interesting dielectric, piezoelectric, flexoelectric, ferroelectric and electro-optic properties.

The cubic perovskite phase (space group Pm3m) is only stable above 120ºC, with Ba^{2+} ions in the large eightfold coordinated site at (0,0,0), Ti^{4+} ions in the octahedrally coordinated site at (1/2, 1/2, 1/2), and O^{2-} ions around each titanium ion at the equipoint (1/2, 1/2, 0). The cubic lattice parameter ***a*** is 3.996 Å, and Ti^{4+} is small as 61 pm in radius so that there is room for it to move inside the O_6 cage[1]. X-ray diffraction experiments [2] show a diffuse scattering that is interpreted as evidence that the Ti^{+4} ions are not static in the centre of the unit cell but rather "rattle" along the <111> diagonals of the cube. As we shall argue later in this chapter, the existence of these dynamically fluctuating dipoles is relevant to understand the flexoelectricity of BTO in its paraelectric phase.

At temperatures below 120ºC, the structure changes to tetragonal phase (space group P4mm) in which Ti atom moves off-centre along Ti-O bond, giving a polarization along the [0 0 1] with a value of 26 $\mu C/cm^2$. The original cubic symmetry is distorted with the lengthening of ***c*** lattice parameter, and the ***c/a*** ratio is 1.011. By choosing the origin at O_{II} position (Figure 4.1), the displacement data for Ba^{2+}, Ti^{4+} and O_I^{2-} atoms along the c-axis are +0.06 Å, +0.12 Å and -0.03 Å, respectively[3].As temperature falls below 0ºC, and orthorhombic phase (space group C2mm) becomes stable. It is ferroelectric with the spontaneous polarization parallel to the pseudo- cube edge direction [1 1 0][3].At -90ºC, the third phase transition occurs and the lattice symmetry changes to rhombohedral (space group Rm3) with a = b = c = 4.001 Å and $\alpha = 89.87^\circ$ [4]. The ferroelectric polar axis lies along one of the pseudo-cube diagonal directions [111]

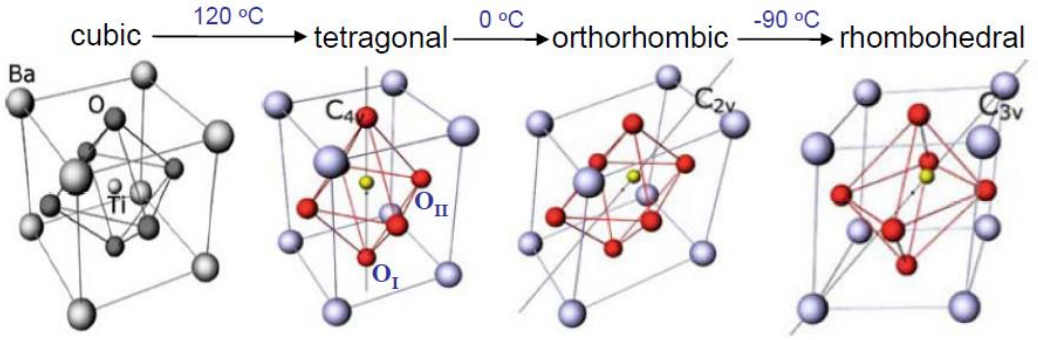

Figure 4.1 Structural transition in $BaTiO_3$ [5]

The crystal structure and dielectric characteristics of $BaTiO_3$ strongly depend on temperature. The temperature dependence of the relative permittivity of $BaTiO_3$ measured in the ***a*** and ***c*** directions is shown in Figure 4.2.

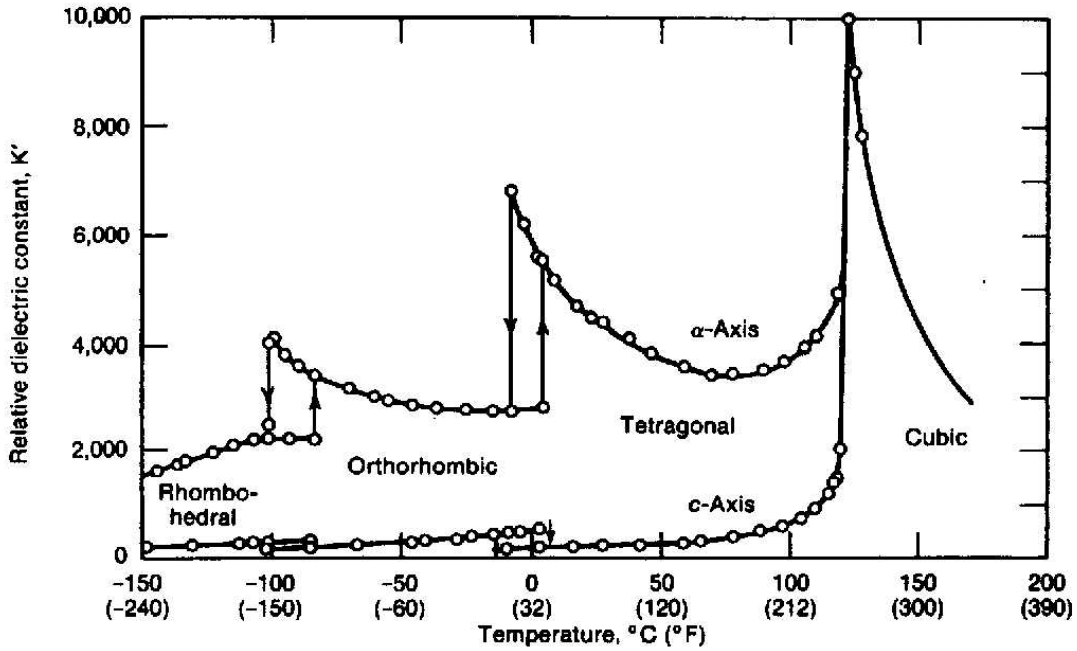

Figure 4.2 Temperature dependence of relative permitivity of $BaTiO_3$ single crystal [6]

The high dielectric constant of $BaTiO_3$ makes it a good candidate to obtain high flexoelectric performance. However, even factoring in the large permittivity, the experimentally measured flexoelectric coefficient of $BaTiO_3$ [7] is still between one and two orders of magnitude too high compared to theoretical predictions [8, 9]. Recently, two different explanations have been put forward for the discrepancy.

Biancoli et al. [10] have observed net polarization in nominally paraelectric $SrTiO_3$ and (Ba,Sr)TiO_3. Such built-in macroscopic polarizations are inherent to fabrication processes and common to all materials and may therefore explain the large bending-induced polarization of $BaTiO_3$. In contrast, Bersuker's theoretical analysis concludes that the large flexoelectric response is due instead to a flexoelectrically-induced alignment of precursor polarization that exists in the paraelectric phase of $BaTiO_3$ [11]. In this scenario, $BaTiO_3$ would behave similar to relaxor ferroelectrics, as we have described in the previous chapter [12]. The investigation on the magnitude and origin of the enhanced flexoelectricity in $BaTiO_3$ single crystals is the subject of the research presented in this chapter.

In order to identify different contributions to the total bending-induced polarization, we have studied the flexoelectricity of $BaTiO_3$ single crystals of different orientation in the temperature range between 25 ºC and 300 ºC. The samples were commercially acquired from SurfaceNet and MTI crystal, and their dimensions were 10 mm long, 1mm wide and 0.5 mm thick. In order to characterize anisotropy, we examine crystals with surfaces parallel to the (111), (110) and (001) crystallographic planes respectively. We found that the enhancement is consistent with the existence of precursor polarization in the paraelectric phase, but we additionally find a strong anisotropy that cannot be a bulk effect. We attribute this anisotropy to the predicted [13, 14] but experimentally unconfirmed contribution of surface piezoelectricity to the total flexoelectricity of even bulk crystals.

4.2. Dielectric Characterization Of $BaTiO_3$.

Figure 4.3 shows the dielectric constant and dielectric loss as a function of temperature for (001), (011) and (111)-$BaTiO_3$ oriented single crystals. A sharp peak in dielectric constant, corresponding to the first order transition between the paraelectric and ferroelectric phase, is observed around T_C~120-125 ºC for all samples. The cubic phase is orthotropic and the dielectric constant above T_C is the same for these three orientations, while in the ferroelectric phase (below T_C) it is sensitive to both crystal orientation and domain configuration [15]. The dielectric

loss is increased by domain wall motion below T_C and falls sharply on entering the cubic phase, before increasing again at high temperatures due to rising conductivity.

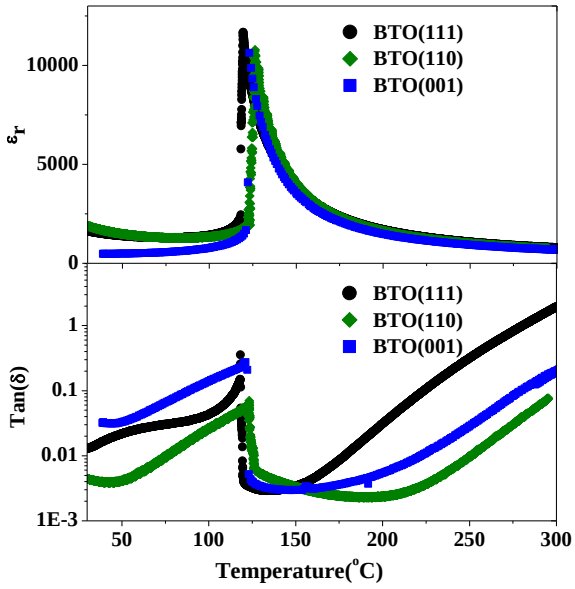

Figure 4.3 Dielectric constant and dielectric loss as a function of temperature for (111), (110) and (001)-oriented BTO.

Though barium titanate is usually regarded as an archetypal ferroelectric, it displays precursor polar behaviour (short range order) in its paraelectric phase [16 - 20], which result in enhanced flexoelectricity. It is interesting, however, that the effect of precursor polarization is evident in the electromechanical response (see next section) but not in dielectric measurements; unlike relaxors, for which we observed a deviation from Curie Weiss around the temperature where nanotwin activity begins, the dielectric constant (Figure 4.4) and inverse permittivity (Figure 4.5) of BTO do not significantly deviate from Curie-Weiss behaviour, nor change when we apply up to 40V DC bias during measurement (Figure 4.4). This insensitivity of the paraelectric permittivity with DC bias contrasts with the sensitivity of the ferroelectric phase. We therefore speculate that the polar nanoregions in $BaTiO_3$ can only be statically collapsed by strain gradient fields rather than electrostatic fields. This, however, is only speculation, and in our opinion the contrasting difference between the flexoelectric response (Figure 4.6) (sensitive to precursor polarization in the paraphase) and the dielectric response (insensitive) calls for further research.

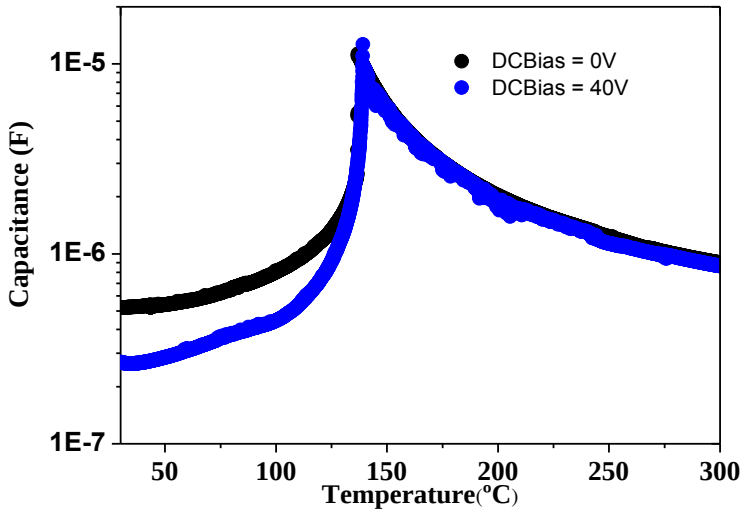

Figure 4.4 Capacitance as a function of temperature for (001)-oriented $BaTiO_3$ at 0V and 40V

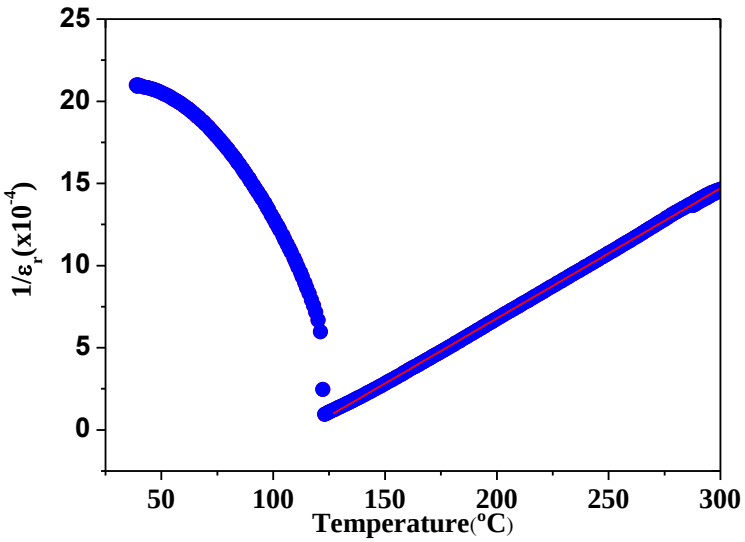

Figure 4.5 Inverse dielectric constant as a function of temperature for (001)-oriented $BaTiO_3$

4.3. FLEXOELECTRIC CHARACTERIZATION OF $BaTiO_3$.

The effective flexoelectric coefficients are plotted in Figure 4.6. The peaks at Tc mirror those observed in the permittivity. The maxima for the flexoelectric coefficient are in the 10-100 μC/m range, but these values fall sharply to 1-10 μC/m

immediately above T_C, coinciding with the disappearance of ferroelectricity. Once in the paraelectric phase, the flexoelectric coefficients continue to gradually decrease from 1-10 μC/m to ~0.1 μC/m.

The reported values for $BaTiO_3$ ceramics in this temperature range are much larger, between 50-5 μC/m [10], suggesting an important role of grain boundaries in enhancing the effective flexoelectric coefficient of the paraelectric phase – the grain boundaries of a closely related compound, $SrTiO_3$, are indeed known to be piezoelectric [23, 24], and in fact surfaces in general can be polar –or at least piezoelectric- even in non-polar materials [25, 26]. As we will show, there is evidence for surface piezoelectricity even in the flexoelectric polarization of thick single crystals such as ours, so it is not unreasonable to suspect that ceramics, with a larger concentration of grain boundaries and therefore of surface-piezoelectric contributions, can have a proportionally larger effective flexoelectricity.

Even above T_C, there is still some thermal hysteresis: flexoelectricity is higher on heating than on cooling up to a temperature labelled as T*. This hysteresis is reminiscent of the behaviour of relaxor ferroelectric PMN-PT described in the previos chapter [12]. Again, the hysteresis is consistent with the presence of polar nanoregions that contribute to the flexoelectric response: there are more residual polar domains when heating from the low-T polar phase than when cooling from the high-T paraelectric phase, explaining the larger bending-induced polarization on heating than on cooling.

Though polar domains are expected in relaxors, it may seem surprising to find them in "normal" ferroelectrics such as $BaTiO_3$. Yet, the existence of short range order in the paraphase of $BaTiO_3$ has been proposed before in order to explain the birefringence, acoustic emission and anelastic softening [16, 17, 27, 28]. The polar nanoregion contribution below T* has also been postulated by Bersuker [11], who proposes a bending-induced collapse along the gradient direction of the dynamic <111> polar fluctuations existing in the paraelectric phase (8-site model of the order-disorder phase transition of $BaTiO_3$ [2]). In this scenario the precursor polarization would be from dynamic rather than static polar nanoregions [21]).

For all samples, T* falls in the 200-225 ^{o}C range, which coincides with the range of T* measured by acoustic emission [28] and resonant ultrasound spectroscopy [29]. Importantly, the evidence does not allow discriminating whether such polar regions are located inside the bulk of the crystal or confined within polar surface layers [30, 31], and piezoelectric surface layers are in fact expected to respond in a manner that is functionally identical to flexoelectricity [13, 14, 32]. The fact that there was no evidence for precursor polarization in the dielectric constant suggests in fact that this precursor polarization effect may indeed be concentrated at the surfaces, which can indeed have a large contribution to flexoelectricity, as we discuss later, but have a negligible contribution to permittivity (series capacitor model).

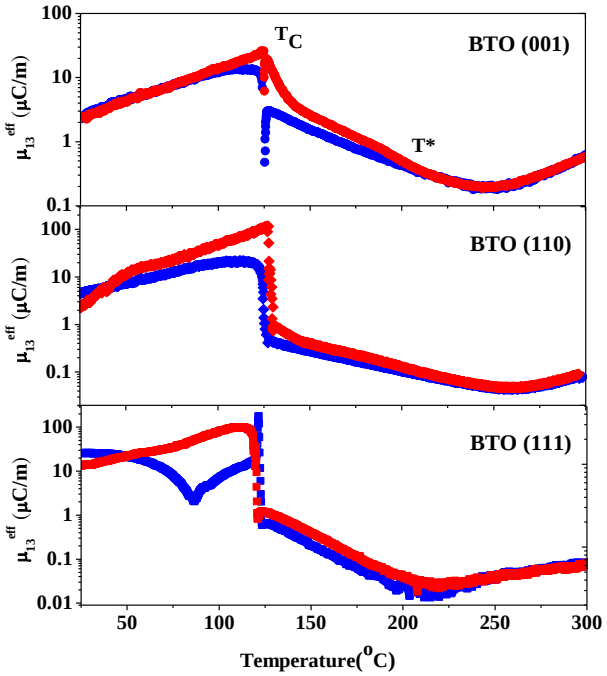

Figure 4.6 Effective flexoelectric coefficient as a function of temperature for $BaTiO_3$ crystals with different orientations. The red curves are measured on heating and the blue ones on cooling. There is a difference between flexoelectricity measured on heating and on cooling for temperatures up to T*~200-225 ^{o}C.

4.4. FLEXOCOUPLING CHARACTERIZATION OF $BaTiO_3$.

As discussed at the introduction, the flexoelectric coefficient normalized by the dielectric constant is known as flexocoupling (or flexovoltage) coefficient, f (Figure 4.7). Theoretically, for an intrinsic flexoelectric effect, f should be of the order of $1 < f < 20$V and temperature-independent [33-36]. Experimentally, we found f to be close to 10000V immediately below T_C, but this must clearly be due to the piezoelectric response of the ferroelectric phase and not a real flexoelectric effect; verification of this piezoelectric origin can be found in the 180 degree phase inversion of the low temperature signal upon turning the crystal upside down, shown in Figure 4.8. At T_C, the flexovoltage f decreases sharply (first order phase transition), and then more gradually up to T*, consistent with the aforementioned picture of gradual extinction of the precursor polar regions. Meanwhile, at temperatures around 250 ^oC or higher, leakage currents artificially increase the capacitance (Maxwell-Wagner model) and thus also the *effective* flexocoupling again. This correlation between high leakage and flexoelectric increase is in fact the first evidence that free charges inside a dielectric can contribute to effective flexoelectricity, something that we explore and exploit to great advantage in the next chapter of this thesis.

There has been a suggestion that some or all of the anomalous flexoelectric enhancement of dielectric $BaTiO_3$ and related compounds may be due to built-in piezoelectricity caused by gradients in defect concentration that appear during sample fabrication[10]. We have examined this hypothesis by looking at the phase angle of the bending-induced current: if the polarization is piezoelectric in nature, one would expect it to be inverted (i.e., the phase delay of the current with respect to the strain gradient should change by 180 degrees) when the crystal is turned upside-down. Here we must note that the absolute value of the phase angle is not meaningful because the preamplifier circuit introduces a phase lag. The relative change of phase, however, is robust, and a typical phase measurement is shown in Figure 4.8. At room temperature, there is indeed a difference of 180 degrees upon inverting the sample, consistent with the existence of a preferential macroscopic orientation of the ferroelectric polarization. However, above T_C there is no difference between the phase angles. Any macroscopic polarization, if it exists,

would appear to be switching in response to the strain gradient and is therefore not fixed in space. The invariance of the flexoelectric phase lag with respect to sample inversion is therefore more consistent with dynamically responsive polarization, and thus more suggestive of polar nanoregions than of a fixed polarity due to defect gradients.

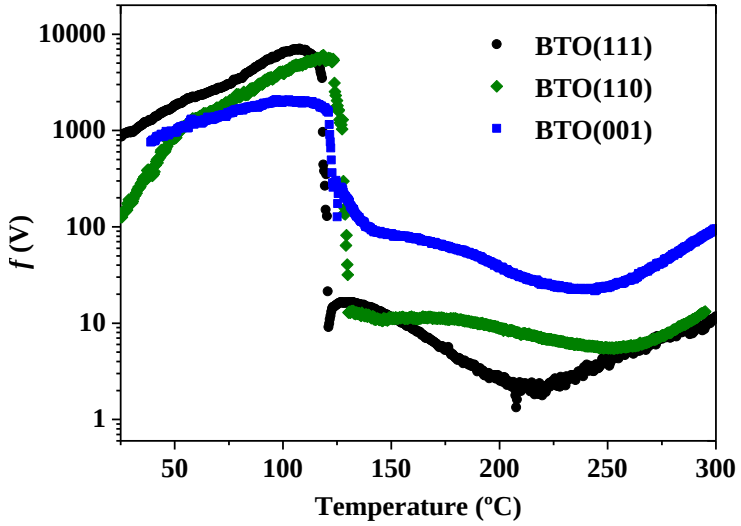

Figure 4.7 The flexocoupling coefficient as a function of temperature for (111), (110) and (001)-oriented BTO.

Even though the absolute value of the phase angle is, as said, not directly physical, we can compare the phase angle measured in the BTO samples to the phase angle that we measured in $SrTiO_3$ reference samples that we measured in the same setup. For STO the flexoelectric signs are known [37, 38], so it can be used as a callibration sample. This allows extracting the sign of the flexocoupling coefficients, shown in table 4.1. The experimental results show the minimum value measured above T* and therefore they place an upper limit for the intrinsic flexocoupling coefficient that is 22V for (001)-oriented BTO, -6 V for (110), and -2 V for (111). These values are consistent with intrinsic flexoelectricity and support the idea that, for perovskite dielectrics, the flexoelectric coefficient is a number of the order of ~10 V multiplied by the permittivity. Nevertheless, the outstanding feature is that even in the cubic phase there is a large and unexpected anisotropy: the flexovoltage is 10× bigger for (001) than for (111) crystals. The tenfold anisotropy is also bigger

than observed in homomorphic $SrTiO_3$, for which it is a factor smaller than three. We now turn our attention to the origin of this large anisotropy.

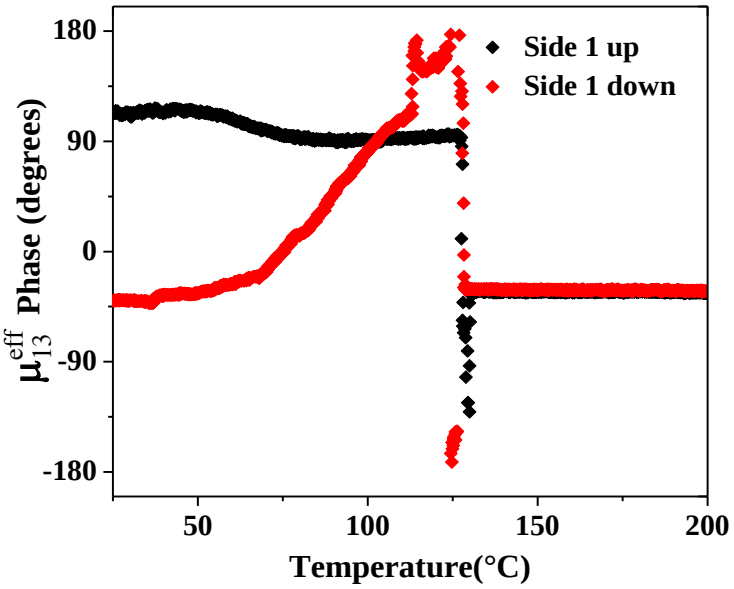

Figure 4.8 Phase angle between applied force and bending-induced current for a crystal measured twice consecutively, with its orientation flipped upside down between the two measurements. The room-temperature polarization changes phase by 180 degrees, consistent with the existence of a net macroscopic polarity. In contrast, above T_C the phase angle between force and current is identical for the two measurements, indicating that the flexoelectric enhancement in the paraelectric phase is not due to macroscopic built-in polarization.

Table 4.1 shows the orientation of the sample edges with respect to the crystallographic axes, determined using X-ray diffraction. As was previously reported [37], the effective coefficient for any given cubic crystal orientation is always a linear combination of the coefficients for the other two; in other words there do not exist three independent equations required to obtain the three independent tensor components in cubic symmetry. On the other hand, the linear dependence provides a "sanity check": if the measured coefficients are only dependent on the bulk properties of the sample (i.e., if there is no surface piezoelectricity), then the effective flexoelectric coefficient of, for example, the (001)-oriented sample can in principle be calculated from the effective flexoelectric coefficients measured for (111) and (011) orientations. Conversely, if the calculated and measured values do not coincide, it is a strong indication that non-bulk contributions must be present.

Table 4.1 The effective flexoelectric and flexoelectric coefficients for (100), ($\mathbf{1\bar{1}0}$) and ($\mathbf{10\bar{1}}$)-oriented single crystals of $BaTiO_3$

x_1	x_2	x_3	μ_{13}(μC/m)	f (V)
[100]	[010]	[001]	0.20	22
[1$\bar{1}$0]	[001]	[110]	-0.05	-6
[10$\bar{1}$]	[$\bar{1}$2$\bar{1}$]	[111]	-0.01	-2

Equation A.31 from the appendix relates the flexocoupling coefficient along (100) to the flexocoupling coefficients along (110) and (111):

$$1.47 f_{111}^{beam} - 1.24 f_{110}^{beam} = f_{100}^{beam} \qquad 4.1$$

The flexocoupling coefficients (table 4.1) are f (110) = -6V and f (111) = -2V, so, according to eq. 4.1, we should have f(100) = 4.5V, instead of which the experimental value is 22V (table 4.1): about five times as much. This large difference is experimentally robust (the variation of flexocoupling coefficients between different measurements was less than 10%) and indicates the existence of an additional effect that (i) cannot be bulk flexoelectricity and (ii) is above T*, so it is not due to precursor polar regions either. We therefore interpret this result as a first (indirect) indication of the contribution of surface piezoelectricity to the total effective flexoelectricity.

As discussed in section 1.6.2, surface piezoelectricity is a theoretically inevitable effect [13, 14] that can in principle be as big as or even bigger than bulk flexoelectricity even for bulk samples [39]. However, direct determination of surface piezoelectricity is experimentally difficult because it is largely independent of the thickness of the surface or the total thickness of the sample, and hence it behaves functionally identically to bulk flexoelectricity. Therefore, the only hope is to identify it by changing the type of surface, which is accomplished here by using different crystal orientations.

The results suggest that indeed the effect of surfaces can be even bigger than that of the bulk itself –sometimes much bigger, as is shown in the next chapter- and this has important practical consequences: maximizing flexoelectric performance requires not just optimizing material properties, but also careful surface engineering.

4.5. REFERENCES

1. B.A. Strukov, A. P. Levanyuk. Springer-Verlag: Berlin/ New York (1998)

2. R. Comes, M. Lambert, and A. Guinner, *Solid State Commun.* **6**, 715 (1968).

3. Y. Xu, North-Holland: Amsterdam (1991)

4. R. E. Cohen, H. Krakauer, *Phys. Rev. B.* **42**, 6416 (1990)

5. R. Blinc, *Struct Bond*. **124**, 51 (2007)

6. Kingery, Bowen & Uhlmann, *Introduction to ceramics*, 2nd edition, 913

7. W. Ma and L. E. Cross, *Appl. Phys. Lett*. **88**, 232902 (2006).

8. R. Marangati and P. Sharma, *Phys. Rev. B.* **80**, 054109 (2009).

9. J. Hong, G.Catalan, J.F.Scott and E. Artacho, *J. Phys.: Condens. Matter* **22**, 112201 (2010).

10. A. Biancoli, C. M. Fancher, J. L. Jones and D. Damjanovic. *Nature Materials* **14**, 224–229 (2015).

11. I. B. Bersuker, *Appl. Phys. Lett.* **106**, 022903 (2015).

12. J. Narvaez and G. Catalan, *Appl. Phys. Lett.*, **104** 162903 (2014).

13. A. K. Tagantsev and A. S. Yurkov, *J. Appl. Phys.* **112**, 044103 (2012).

14. M. Stengel, *Nat. Commun*. **4**, 2693 (2013); M.Stengel, Phys. Rev. B 90, 201112 (2014).

15. A. F. Devonshire, *Philos. Mag.* **40**, 1040, (1949).

16. M. Zenkner, U. Straube & G. Schmidt, *Ferroelectrics* **460**,1 (2014).

17. A. Ziebinska, D. Ryts, K. Szot, M. Gorny and K. Roleder, *J. Phys.: Condens. Matter* **20**, 142202 (2008).

18. G. Burns and F. H. Dacol, *Solid. State. Commun.* **42**, 9 (1982).

19. E. Dul'kin, J. Petzelt, S. Kamba, E. Mojaev and M. Roth, *Appl. Phys. Lett.* **97**, 032903 (2010).

20. E. K. H. Salje, M. A. Carpenter, G. F. Nataf, G. Picht, K. Webber, J. Weerasinghe, S. Lisenkov, and L. Bellaiche., *Phys. Rev. B*. **87**, 014106 (2013).

21. J. Hlinka, *J. Adv. Dielectrics.* **2**, 1241006 (2012).

22. W. Ma and L. E. Cross, *Appl. Phys. Lett.* **82**, 3293 (2003).

23. J. Petzelt, T. Ostapchuk, I. Gregora, I. Rychetský, S. Hoffmann-Eifert, A. V. Pronin, Y. Yuzyuk, B. P. Gorshunov, S. Kamba, V. Bovtun et al., *Phys. Rev. B*. **64**, 184111 (2001).

24. A. Kholkin, I. Bdikin, T. Ostapchuk and J. Petzelt, *Appl. Phys. Lett.* **93**, 222905 (2008).

25. J. F. Scott, *J. Chem. Phys.* **48**, 874(1968).

26. R. Munprom , P. A. Salvador , and G. S. Rohrer, *Chem. Mater* **26**, 2774(2014).

27. G. Burns and F. H. Dacol, *Solid. State. Commun.***42**, 9 (1982).

28. E. Dul'kin, J. Petzelt, S. Kamba, E. Mojaev and M. Roth, *Appl. Phys. Lett.* **97**, 032903 (2010).

29. E. K. H. Salje, M. A. Carpenter, G. F. Nataf, G. Picht, K. Webber, J. Weerasinghe, S. Lisenkov, and L. Bellaiche., *Phys. Rev. B.* **87**, 014106 (2013).

30. W. Känzing, *Phys. Rev.* **98**, 549 (1955).

31. G. Schmidt and F. Prokert, *Ann. der Physik* **7**, 120 (1966).

32. J. Hong and D. Vanderbilt, *Phys. Rev. B*. **84**, 180101 (2011).

33. I. Ponomareva, A. K. Tagantsev, and L. Bellaiche, *Phys. Rev. B*. **85**, 104101 (2012).

34. J. Hong and D. Vanderbilt, *Phys. Rev. B*. **88**, 174107 (2013).

35. M. Stengel, *Phys. Rev. B.* **88**, 174106 (2013).

36. P. Zubko, G. Catalan and A. K. Taganstsev, *Annu. Rev. Mater. Res.* **43** (2013).

37. P. Zubko, G. Catalan, A. Buckley, P. R. L. Welche, and J. F. Scott, *Phys. Rev. Lett.* **100**, 199906 (2008).

38. P. Zubko, G. Catalan, A. Buckley, P. R. L. Welche, and J. F. Scott, *Phys. Rev. Lett.* **99**, 167601 (2007).

39. M. Stengel *Phys. Rev. B*. **90**, 201112 (2014).

5 FLEXOELECTRICITY OF SEMICONDUCTOR SINGLE CRYSTAL $BaTiO_{3-\delta}$

5.1 INTRODUCTION.

Flexoelectricity, as we have been discussing, is a property of all dielectric materials, whereby they polarize in response to deformation gradients [1, 2, 3]. Although it is thought of as a property of electric insulators. Electrical insulation is not an actual requirement: semiconductors may in principle also redistribute their charge in response to strain gradients. The crucial difference between a dielectric and a semiconductor is that, while in the former only bound charge responds to gradients, in the latter free charge can also move, potentially leading to much bigger responses and hence solving the principal problem of flexoelectricity, which is its small magnitude compared to piezoelectricity. Here we show that, by vacancy-doping an insulating dielectric such as $BaTiO_3$ in order to increase its conductivity, its effective flexoelectricity is enhanced by more than 10000%, reaching the highest effective coefficient ever reported for any material.

The starting point for this investigation is the observation that the effective flexoelectric coefficient of normal (i.e. insulating) $BaTiO_3$ increases at the same temperature where dielectric losses (leakage) also increase. From Figure 5.1, we can see the flexoelectric coefficient and angle of flexoelectric coefficient as a function of temperature for (001)-oriented single crystal $BaTiO_3$, archetypical dielectric material, which was studied in detail in the previous chapter. Here we concentrate our attention in flexoelectric phase delay above 200 ^oC. Above this temperature, the phase angle of flexoelectric currents start to change, completing a 90 degree phase change by the time the highest temperature is reached. In theory, a phase difference of 90º must exist between the voltage and current for a purely capacitive AC circuit, i.e., in a perfectly insulating dielectric capacitor, while in a purely resistive circuit, voltage and current are in phase with one another. The high temperature increase in flexoelectricity is thus correlated with a change where BTO start to respond more like a conductor than like a dielectric. In other words, flexoelectricity (strain gradients) appears to act on free carriers just as it does on bound charge –put in polarization terms, the flexoelectric coupling between strain gradients and polarization affects not only dielectric polarization but also space charge polarization. From this observation, it follows that an increase in charge carrier density might lead to an increase in bending-induced current, and this is precisely our motivation for studying oxygen-deficient semiconductor $BaTiO_{3-\delta}$.

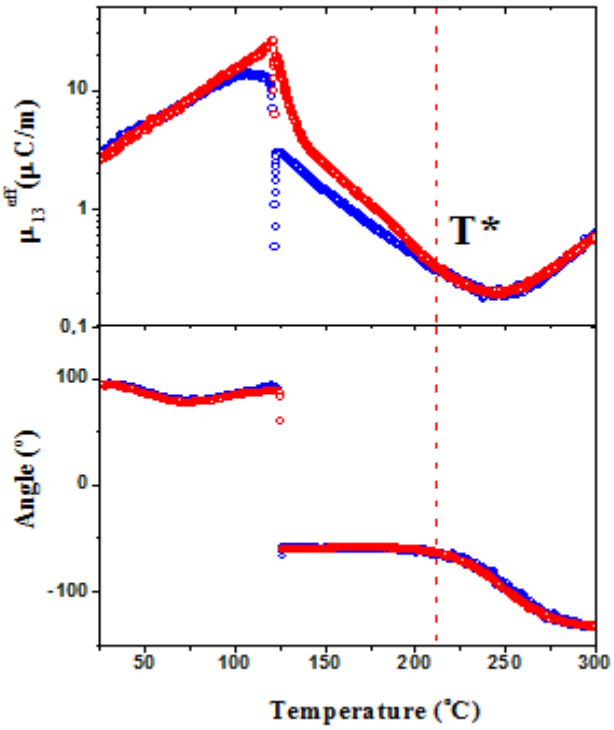

Figure 5.1. Flexoelectric constant and angle of flexoelectric constant as a function of the temperature for (001)-oriented single crystal $BaTiO_3$

Besides the purely fundamental interest, there is also a practical motivation for this study. Flexoelectricity, as we have also been seeing in previous chapters, is generally a small effect in bulk samples when compared to piezoelectricity, so there is an active search for ways to enhancing it. Currently, there are at least two tested strategies for achieving larger flexoelectricity. The first consists in exploiting the proportionality between flexoelectricity and permittivity [1, 2, 3]: materials with high dielectric constants, such as ferroelectric $BaTiO_3$, also have high flexoelectric coefficients [4, 5]. The second strategy, which can be used in conjunction with the first, consists in inducing larger strain gradients, which usually entails working at very small (nanoscopic) size scales [6, 7, 8], where achievable deformations are bigger. Here we explore a third way, which is to seek for flexoelectric responses in conductive samples.

5.2 THE MAXWELL-WAGNER MODEL OF OXYGEN-DEFICIENT $BaTiO_3$.

The polarization of an insulating dielectric is limited by how much can its positive and negative *bound* charges be separated. However, the effective polarizability of a device can be enhanced by many orders of magnitude if we also allow *free* charges to separate. The physics of this phenomenon has been well understood for more than a century and is described by the Maxwell-Wagner model [8]. The capacitor industry has been using the Maxwell-Wagner concept for decades in order to enhance effective capacitance in devices known as "barrier layer capacitors" [9, 10], and the Maxwell-Wagner mechanism can also enhance the effective piezoelectricity of heterogeneous semiconductors [11].

The macroscopic electric properties of materials are characterized by the dielectric constant ε and conductivity σ. The ratio $\tau = \varepsilon / \sigma$ gives a relaxation time for establishing the steady-state charge distribution after a change in the electric field. Charge accumulation is allowed at the interface between two materials with different relaxation times, and this explains the ability of Maxwell-Wagner capacitors to store more charge than homogeneous dielectrics.

The basic idea behind a barrier layer or Maxwell-Wagner capacitor is depicted in Figure 5.2: a low-frequency electric field (and by "low frequency" we mean one slower than the τ time constant of the bulk of the material) is applied to a heterogeneous material consisting of two thin insulating layers separated by a semiconducting bulk region, the conducting region responds by allowing its free charges to move across and accummulate at the interfaces with the insulating region, and thus the bulk effectively behaves as an intercalated electrode. In this scenario, only the thin barrier layers at the interface contribute to the total capacitance and, because capacitance is inversely proportional to thickness, colossal capacitances can be achieved [9, 10, 12, 13, 14]. Since effective flexoelectricity is proportional to capacitance (or effective permittivity) this mechanism should also yield ultra-high effective flexoelectric coefficients.

In order to explore this idea, we have examined the flexoelectricity of single crystal $BaTiO_3$, oxygen-reduced in order to create oxygen vacancies that act as electron donors, thus increasing its conductivity [15, 16]. Fully oxidized $BaTiO_3$ (BTO) is itself an archetypal ferroelectric with a high dielectric permittivity which, as we

have already seen in the previous chapter, already makes it one of the best flexoelectric materials its high temperature paraelectric phase [3, 5, 17]. But BTO is also a wide band-gap semiconductor that, when reduced with oxygen vacancies, becomes a doped n-type semiconductor with charge-depleted surfaces [15, 16, 18]. The combination of high conductivity in the core with interfacial charge depletion is the exact recipe for the Maxwell-Wagner effect, and it results in an enormous enhancement of effective permittivity. As we will show, the enhancement also affects the flexoelectricity, yielding the highest effective flexoelectric coefficient ever measured for any material.

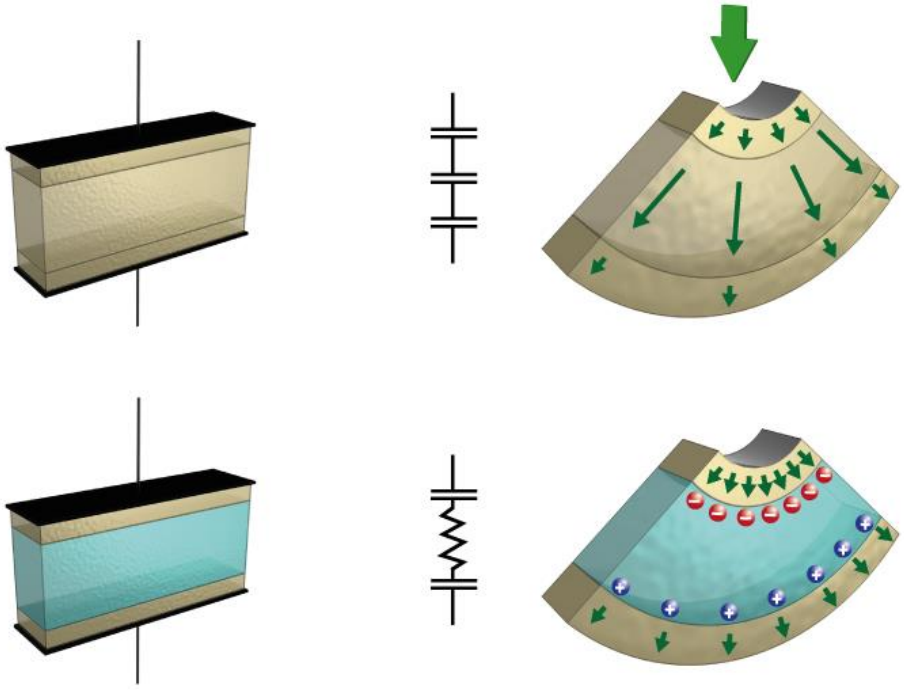

Figure 5.2: (top row): The capacitance of a dielectric insulator has contributions from its bulk and from its interfaces, behaving effectively as a series capacitor with two interfacial layers and one bulk layer. The same is true for its total (effective) flexoelectric polarization, which has contributions from the bulk and from the surface. (bottom row): when the bulk of the material is semiconducting, it behaves like an intercalated electrode, allowing free charges to travel through and accumulate near the interfacial insulating layers. This results in a bigger capacitance (barrier layer capacitor model) and also in a much bigger polarization at the surface, thus yielding a giant effective flexoelectricity – which is polarization divided by bending.

5.3 Dielectric Characterization Of $BaTiO_3$.

The sample used in this work was a single crystal of (001)-oriented BTO, commercially acquired from SurfaceNet. The sample dimensions were: 1mm wide, 10 mm long and 0.46 mm thick. Measurements made on the as-received sample are referred to hereon as BTO. Measurements made after reducing the as-received sample at 900ºC for 2 hours in vacuum atmosphere, are referred to hereon as $BTO_{-\delta}$. Measurements made after reoxidizing the reduced sample, at 800ºC, for 30 hours in pure (99.9999%) O_2 atmosphere, are referred to hereon as $BTO_{+\delta}$. The method for measuring the capacitive impedance and flexoelectric coefficient is exactly the same as in the measurements described in the previous chapters: a dynamic mechanical analyser connected to a lock-in amplifier was used to measure the bending-induced displacement current, and an LCR-meter was used to measure the capacitance and dielectric loss.

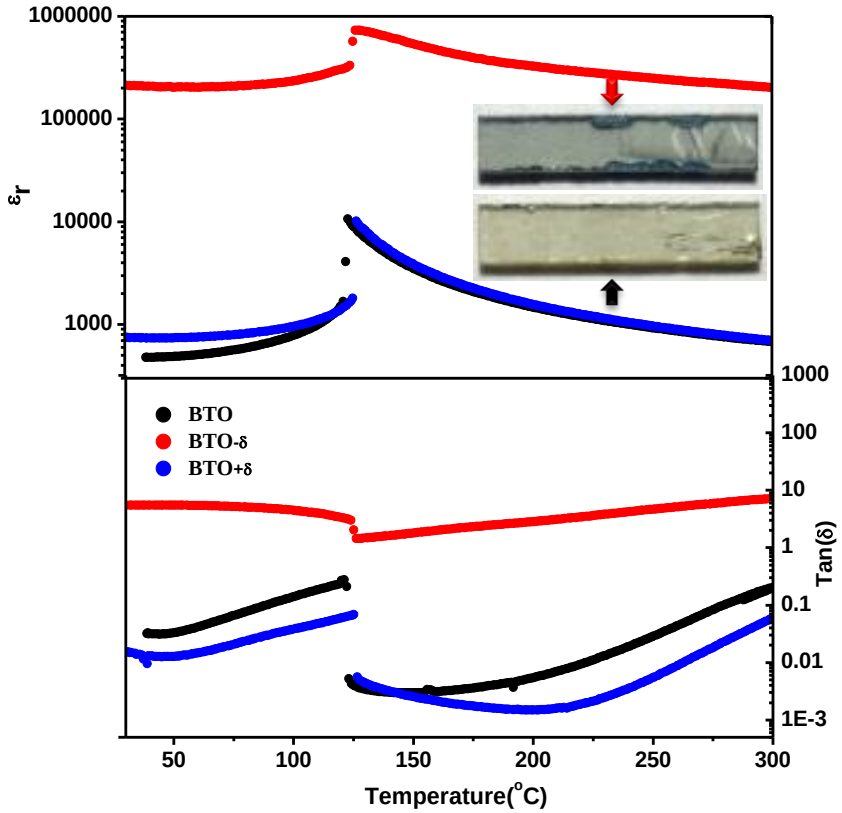

Figure 5.3 . Dielectric constant and dielectric loss as a function of temperature for BTO, $BTO_{-\delta}$ and $BTO_{+\delta}$.

Evidence that $BTO_{-\delta}$ was reduced is already visible in the inset in Figure 5.3: the reduced crystal is darker, signalling an increase in light absorption due to the larger concentration of free carriers, as also reported for $SrTiO_3$ [19]. Impedance analysis confirms the increased conductivity: Figure 5.3 shows the effective permittivity (real part of the capacitance multiplied by thickness and divided by area) and dielectric loss as a function of temperature for BTO, $BTO_{-\delta}$ and $BTO_{+\delta}$. The peak corresponding to the ferroelectric transition is observed around 125ºC for all three cases; however, the dielectric loss and dielectric constant of reduced $BTO_{-\delta}$ are orders of magnitude larger compared to fully oxidized BTO and $BTO_{+\delta}$. Both high loss and giant effective permittivity are classic signatures of the Maxwell-Wagner effect, whereby increased conductivity inside the crystal results in high dissipation (high loss tangent), while the reduced thickness of the charge-depleted interfacial barrier results in high capacitance (high effective permittivity) [8, 9, 10, 13, 14, 15]. The fact that the intrinsic dielectric properties of the as-received sample can be recovered upon reoxidation ($BTO_{+\delta}$) shows that the enhancement is due to vacancies and reversible.

5.4 Flexoelectric Characterization Of $BaTiO_3$.

The effective flexoelectric coefficient μ_{13}^{eff}, defined as the measured polarization (charge density at the electrodes) divided by the strain gradient (bending) [3] is plotted as a function of temperature in Figure 5.4. When we compare Figure 5.3 and Figure 5.4, we see an enhancement of flexoelectricity that mirrors that of the permittivity: the maximum effective flexoelectric coefficient both for as-received BTO and for re-oxidized $BTO_{+\delta}$ are in the range of ~ 20 - 30 μC/m, whereas the flexoelectric coefficient of reduced $BTO_{-\delta}$ is over 2 orders of magnitude bigger, a similar enhancement to what we observed in the capacitance. The effective flexoelectric coefficient of reduced BTO is the largest ever measured for any material [3].

On a purely phenomenological level, flexoelectricity is proportional to permittivity, so any mechanism that enhances the effective permittivity of a material may in principle be expected to enhance its flexoelectricity, but we can also examine the effect from a more microscopic point of view. Like giant effective permittivity, the

ultra-large effective flexoelectricity of semiconducting $BTO_{-\delta}$ can be explained by the existence of conductivity with insulating interfacial barrier layers.

Bending always generates at least two electromechanical responses: the bulk flexoelectric polarization and a surface piezoelectric polarization caused by the straining of the opposite surface layers (compression on the concave side, tension on the convex side) [2, 3, 20, 21]. Surface piezoelectricity is itself a necessary consequence of the fact that interfaces are asymmetric: the material above the interface (electrode) is different from the material below (BTO). In principle, there can also be a contribution from surface flexoelectricity, but this is small compared to the other two for bulk samples [17]: the surface-flexoelectric polarization is of the same order of magnitude as the bulk flexoelectric polarization, but the thickness ratio of surface to bulk is small, hence we can neglect it (notice that in surface piezoelectricity this argument cannot be made, because even though the surface to bulk ratio is still small, the actual surface polarization grows in direct proportion to the bulk thickness). The $BTO_{-\delta}$ crystal is conducting, and this has two important consequences: (1) The bulk polarization is screened by free charges [18, 21], so bulk flexoelectricity cannot contribute to the total polarization, and (2) the free charges help screen the polar discontinuity between the interfacial layer and the bulk of the crystal, thus reducing the depolarization field and increasing the piezoelectric polarization that can be generated by the surface. In effect, the system behaves as if there were two piezoelectric layers attached to the opposite surfaces of a conducting slab that acts as an intercalated electrode. Usefully, the surface piezoelectricity is intrinsic and must exist at all temperatures, irrespective of whether or not the material is ferroelectric, as we can see from the fact that the large polarization persists also in the paraelectric phase above the Curie temperature.

In this scenario, the bending-induced charge density is just the product of the surface piezoelectric coefficient (e) times the surface strain, while the surface strain itself is the product of the curvature (the strain gradient, G) times the half-thickness of the crystal, $t/2$. Thus, the bending-induced surface polarization is

$$P = eG\frac{t}{2} \qquad 5.1$$

And therefore, the effective flexoelectric coefficient, defined as the polarization divided by the strain gradient G, is:

$$\mu_{eff} = e\frac{t}{2} \qquad 5.2$$

It is also possible to arrive at equation (5.2) by starting from the general expression for surface piezoelectricity in a dielectric material [20], $\mu_{eff} = e\lambda\frac{t\varepsilon_b}{2\lambda\varepsilon_b + t\varepsilon_\lambda}$ (where λ is the thickness of the surface layer, and ε_b, ε_λ are respectively the dielectric constants of the bulk and the surface layers), and setting up the effective permittivity of the bulk to infinite. Physically, an infinite permittivity is equivalent to a perfect screening efficiency, so we see that the effect of the conducting layer is indeed to screen the depolarization field of the piezoelectric interface, thus enhancing the maximum polarization that can be achieved. Conversely, when the crystal is an insulating dielectric with a finite permittivity, the contribution from surface polarization becomes smaller, due to the imperfect screening of the polar discontinuity. The key message here is therefore that bulk conductivity does not just allow us to isolate the contribution from surface piezoelectricity (itself a difficult problem [20, 21, 22, 23], as we discussed in the previous chapter), but to greatly amplify it to reach values that would be unattainable in insulators.

Usefully, the large bending-induced polarization measured in semiconducting $BTO_{-\delta}$ does NOT require an anomalously large surface piezoelectric coefficient. We can see this by inverting equation.5.2 in order to calculate the size of the surface piezoelectric coefficient: $e = \frac{2\mu_{eff}}{t}$, where, t is the thickness of our crystal (0.46mm) and μ_{13}^{eff} is the experimentally measured effective flexoelectric coefficient of the semiconducting crystals (Figure 5.4). Here e is the strain-polarization piezoelectric coefficient, which can be converted into the more familiar force-charge coefficient (d_{ij}) by multiplying times the elastic compliance [24] ($s_{11} \approx 8.5\text{x}10^{-12}$ Pa^{-1} for BTO [25]), hence $d_{13}^{surf} = s_{11}\frac{2\mu_{13}^{eff}}{t}$. Substituting the experimentally measured values, we see that d_{13}^{surf} ranges from 37 pC/m at T_c down to 0.6 pC/m at 300 °C. These are modest piezoelectric coefficients by electroceramic standards: the maximum is still smaller than the bulk piezoelectricity of $BaTiO_3$ (85 pC/m) [16], while the minimum

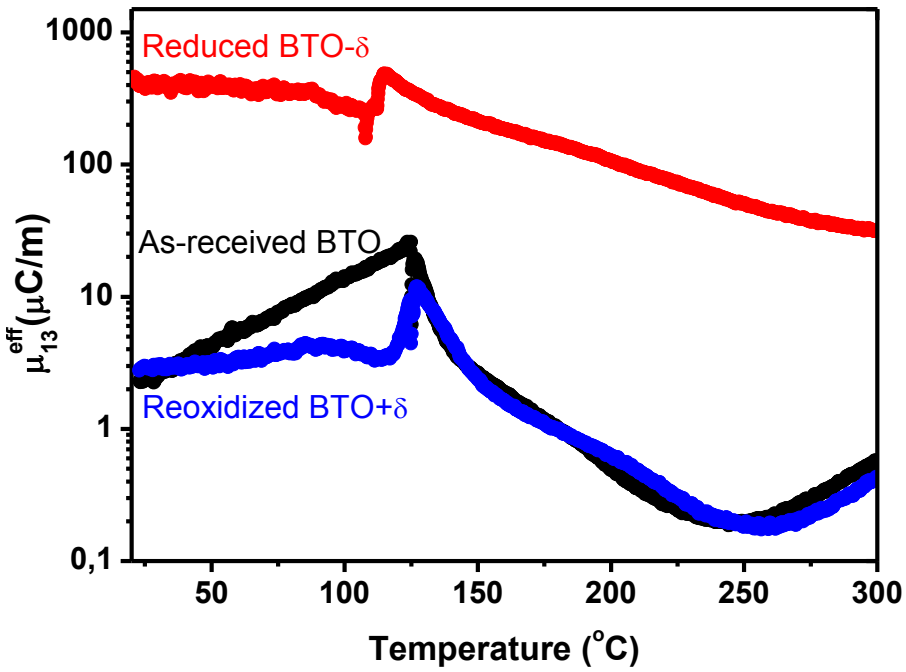

Figure 5.4. Effective flexoelectric coefficient as a function of temperature for BTO, $BTO_{-\delta}$ and $BTO_{+\delta}$.

is smaller even than the piezoelectric coefficient of quartz; and yet these fairly modest piezoelectric coefficients enable effective flexoelectric polarizations orders of magnitude bigger than would be attainable from the bulk effect alone, as shown in Figure 5.4.

The conclussions from this investigation into the flexoelectricity of semiconducting crystals are manifold:

i) Tough in dielectric insulators the contributions from bulk and surface are inextricably linked [20, 21, 22], by making the bulk conductive it is experimentally possible to isolate the surface contribution, hitherto an unsolved scientific problem [23].

ii) Importantly for technological applications, we find that the surface role is not just comparable to that of the bulk, but it can be much larger, thanks to screening of the polar discontinuity by the conducting medium: for barium titanate, the combination of bulk conductivity with modest surface

piezoelectricity yields much larger effective flexoelectricity than for the same crystals in insulating form.

iii) Finally, it is also important to notice that the surface contribution to the effective flexoelectricity is directly proportional to the thickness (equation 5.2). This cancels the inverse thickness dependence of the strain gradients [20], and therefore the enhanced bending-induced polarization is independent of sample size. This means that the enhanced bending-induced polarization can be important not only at the nanoscale, where conventional flexoelectricity is already competitive, but also at the macroscale.

iv) The barrier layer mechanism therefore not only breaks beyond the limits of bulk flexoelectricity in insulators [1, 3, 21] but also, because of its thickness dependence, it can do so across all device size scales.

5.5 REFERENCES.

1. S. M. Kogan, *Sov. Phys. Solid. State* **5**, 2069 (1964).

2. E. V. Bursian, N.N. Trunov, *Sov. Phys. Sol. State* **16**, 760 (1974).

3. P. Zubko, G. Catalan and A. K. Taganstsev, *Ann. Rev. Mater. Res.* **43**, 387 (2013).

4. E. Bursian and O. I. Zaikovskii, *Sov. Phys. Solid State* **10**, 1121 (1968).

5. W. Ma and L. E. Cross, *Appl. Phys. Lett.* **88**, 232902 (2006).

6. G. Catalan, A. Lubk, A. H. G. Vlooswijk, E. Snoeck, C. Magen, A. Janssens, G. Rispens, G. Rijnders, D. H. A. Blank, and B. Noheda, *Nat. Mater.* **10**, 963 (2011).

7. D. Lee, A. Yoon, S. Y. Jang, J.-G. Yoon, J.-S. Chung, M. Kim, J. F. Scott, and T. W. Noh, *Phys. Rev. Lett.* **107**, 057602 (2011).

8. H. Lu, C.-W. Bark, D. Esque de los Ojos, J. Alcala, C. B. Eom, G. Catalan, A. Gruverman, *Science* **336**, 59-61 (2012).

9. D. C. Sinclair, T. B. Adams, F. D. Morrison, and A. R. West, *Appl. Phys. Lett*. **80**, 2153 (2002).

10. R. M. Glaister, *IEE - Part B: Electronic and Communication Engineering*, **109**, 423 (1962).

11. D. Damjanovic, M. Demartin Maeder, P. Duran Martin, C. Voisard, and N. Setter, *J. Appl. Phys.* **90**, 5708 (2001).

12. A. V. Hippel. *Dielectrics and Waves,* London: Artech House, (1995).

13. D. O'Neill, R. M. Bowman, J. M. Gregg, *Appl. Phys. Lett*. **77**, 1520 (2000).

14. G. Catalan, J. F. Scott. *Nature*. **448**, 7156 (2007).

15. W. Heywang, *J. Mater. Science.* **6**, 1214 (1971).

16. T. Kolodiazhnyi, A. Petric, M. Niewczas, C. Bridges, A. Safa-Sefat, and J. E. Greedan, *Phys. Rev. B*. **68**, 085205 (2003).

17. L.E. Cross, *J. Mater. Sci.* **41**, 53 (2006).

18. Y. A. Genenko, O. Hirsch and P. Erhart, *J. Appl. Phys*. **115**, 104102 (2014)

19. J. Mannhart, D. G. Schlom, *Nature.* **430**, 620-621 (2004).

20. A.K. Tagantsev, A.S. Yurkov, *J. Appl. Phys*. **112**, 044103 (2012).

21. M. Stengel, *Nat. Comm.* **4**, 2693 (2014).

22. J. Hong and D. Vanderbilt, *Phys. Rev. B.* **84**, 180101 (2011).

23. J. Narvaez, S. Saremi, J. Hong, M. Stengel, G. Catalan, *Phys. Rev. Lett.* **115**, 037601 (2015)

24. D. Damjanovic, *Rep. Prog. Phys*. **61,** 1267 (1998).

25. D. Berlincourt and H. Jaffe, *Phys. Rev.* **111**, 143 (1958).

6 CONCLUSIONS AND FUTURE DIRECTIONS

This thesis is a contribution to research on previously unexplored or unclear experimental flexoelectricity phenomena on single crystals. We started off by making the set-up for this type of measurements since is not commercially available. This setup allowed us to successfully study flexoelectricity on three types of materials: relaxor ferroelectrics (PMN-PT), ferroelectrics (BTO) and semiconductors (oxygen-defficient BTO). For each one of the materials, this thesis work gives an answer to a scientific open question.

In the relaxor-ferroelectric $Pb(Mg_{1/3}Nb_{2/3})O_3$-$PbTiO_3$ single crystals, we were able to measure the flexoelectric coefficient as a function of temperature and distinguish specific phenomena in three ranges of temperature; in the range from 0º to T_c, we found that the contribution of the polarization was not only flexoelectric but also piezoelectric; from T_c to T*, we saw a clear evidence of the polar nanoregions contribution not only from flexoelectric behaviour but also from young's modulus curves. The latter statement, confirms the existence of *flexoferroelastic* contribution that enhances the polarization in this range of temperature. Finally from T* to 300ºC, we could measure an intrinsic value of flexoelectricity which was according with the theoretical predictions, with a temperature-independent flexocoupling coefficient of the order of f =10V. The key message from this investigation is that the anomalously large flexoelectric enhancement between T_c (or T_m) and T* is due to mechanically-induced reorientation of ferroelastic polar nanoregions.

In ferroelectric $BaTiO_3$ single crystals, we also saw an enhancement of the flexoelectric coefficient in the paraelectric phase between T_c and T* attributable to polar nanoregions as in the case of the relaxor-ferroelectric PMN-PT, but we also saw an additional and unexpected orientational dependence. By measuring different orientations of single crystals, we were able to observe a strong anysotropy of the flexoelectric coefficient in the paraelectric cubic phase that is not consistent with bulk flexoelectricity in a cubic medium. Using theoretical calculations and comparing it with experimental data, we conclude that this anisotropy is an indirect evidence of the surface piezoelectricity contributing to the total effective flexoelectricity.

Finally, in the n-type semiconductor $BaTiO_{3-\delta}$ single crystal, we observed a colossal value of the effective flexoelectric coefficient (polarization divided by strain

gradient) which is not only much larger than theoretical predictions but is in fact the largest ever measured. The latter result has been explained by a barrier-layer model, in which the bulk of the crystal provides free charges charges that help screening the polar discontinuity between the piezoelectric interfacial layer and the bulk of the crystal, thus reducing the depolarization field and increasing the piezoelectric polarization that can be generated by the surface. Therefore in this case, the flexoelectricity measured comes entirely from the surface piezoelectricity, since the bulk flexoelectricity is cancelled. The main conclusion is therefore that, appropriately engineered, surface piezoelectricity can be a much more powerful generator of bending-induced charge than bulk flexoelectricity, even in bulk samples.

This last result, lead to the question about how is the behaviour of flexoelectricity in archetypal known semiconductors such as silicon and germanium. These materials are the mainstay of the electronics industry. Silicon is by far the major player in today's electronic market, dominating the microelectronics industry with about 90% of all semiconductor devices sold worldwide being silicon-based. Silicon is a semiconductor material with the band gap of 1.12eV, and it possesses two outstanding natural dielectrics, silicon dioxide (SiO_2) and silicon nitride (Si_3N_4), which are essential for device formation. In particular, SiO_2, which is basis of the metal-oxide – semiconductor devices (MOS) can be grown thermally on a silicon wafer; it is chemically very stable and can achieve a very high breakdown voltage. The interface defects of the thermally grown SiO_2 by reaction of oxygen with a silicon wafer are several orders of magnitude lower than those of any deposited film. Silicon is also non-toxic, relatively inexpensive (Silicon comprises about 26% of the earth's crust which makes it second in abundance only to oxygen), easy to process (a very well established industrial infrastructure in silicon processing exists around the world), and has quite good mechanical properties (strength, hardness, thermal conductivity, etc.). For these reasons, and considering the large enhancement of flexoelectricity in the semiconducting state of BTO, measuring the flexoelectricity of silicon seems like an obvious next step, and we have taken preliminary measurements in this direction, which we show below.

Figure 6.1 shows our measured flexoelectricity in a single crystal of silicon with 100-orientation, doped with phosphor in dopant concentration of 8.8×10^{11} cm^{-3}. The

crystals were acquired in Sil'tronix-ST, a specialist on silicon wafers. The wafer came factory-metalized on both sizes, and cut with dimension of 25 x 1.5 x 0.3 mm^3. Finally, the bending-induced charge was measured in our set-up at room temperature as a function of strain gradient applied to the sample. From Figure 6.1, it can be seen the polarization is indeed linearly proportional to the strain gradient as:

$$P_3 = \mu^{eff} \frac{\partial \epsilon_{11}}{\partial x_3} \qquad 7.1$$

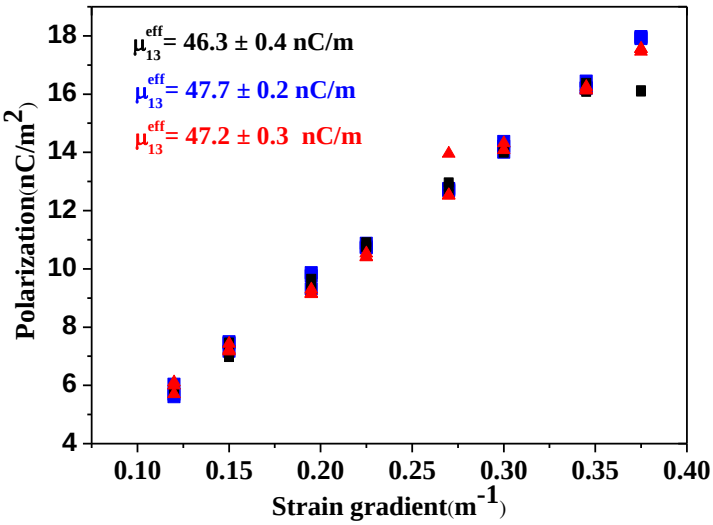

Figure 6.1 Curve of Polarization vs Strain gradient for a single crystal of silicon 100-oriented

The latter statement is evidence that there exists flexoelectricity (in the effective sense of bending-induced polarization) in silicon. The effective flexoelectric coefficient value obtained for this sample was around 47nC/m; this value is even almost one order of magnitude higher than the flexoelectric coefficient of $SrTiO_3$. Figure 6.1 shows three different measurements in order to confirm the reproducibility of the result. The flexoelectric coefficient was extracted from a lineal fit, where the slope is the flexoelectric coefficient. Therefore, the next step will be to query about the origin of this behaviour. Following the discussion in Chapter 5, the dominating mechanism of flexoelectricity in semiconductor materials is expected to be surface piezoelectricity. However to confirm this point; it is needed to perform

more experiments as a function of the thickness. Additionally to elucidate the role of conductivity in flexoelectricity measurements, we also measured the polarization as a function of the strain gradient at room temperature for samples with different dopant concentration such as $1.5x10^{17}$, $7.2x10^{15}$ and $8.8x10^{11}$ cm^{-3} (Figure 6.2).

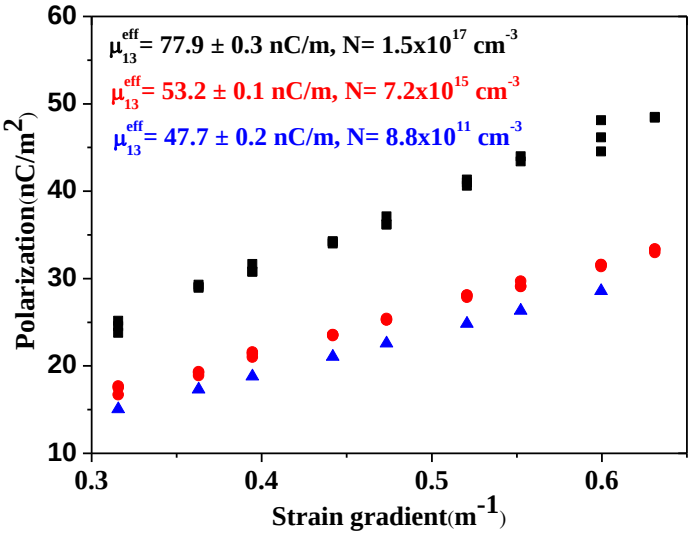

Figure 6.2. Curves of polarization as a function of the strain gradient for samples with different dopant concentration of silicon 100-oriented

Figure 6.2 shows that there does not exist a strong dependency with the dopant concentration, because between each samples there are orders of magnitude in dopant concentration and yet the flexoelectric coefficient values are similar. For understanding better these results, it is necessary to perform a theoretical calculations to match our experimental results with the flexoelectricity in semiconductor materials. Nonetheless, this is an amazing and promising starting point to open the world of the flexoelectricity to semiconductor materials, envisaging a huge impact for both fundamental science and technology applications.

Appendix A: Calculation Of The Interdependence Between Flexoelectric Coefficients For Different Crystal Orientations In Cubic Symmetry.

These calculations were provided by Professor M. Stengel and are important for the discussion of the results in chapter 5 (flexoelectricity of insulating BTO).

We shall assume, in all cases, that the axis 3 (primed quantities indicate the rotated frame, to distinguish them from the pseudocubic crystallographic axes) corresponds to the surface normal, while 1 and 2 lie in the surface plane and are, respectively, perpendicular and parallel to the main bending axis. In such a reference, given a strain-gradient tensor of the type

$$\varepsilon'_{\beta\gamma,\lambda} = \frac{\varepsilon'_{\beta\gamma}}{r'_{\lambda}} \qquad \text{A. 1}$$

The principal component of the (externally applied) bending deformation corresponds to the transverse $\varepsilon'_{11,3}$ component. We shall work in the beam-bending limit, i.e. suppose that at mechanical equilibrium the main bending is accompanied by (i) a longitudinal strain-gradient of the type $\varepsilon'_{33,3}$ and (ii) an anticlastic bending of the type $\varepsilon'_{22,3}$. The relative amplitude of (i) and (ii) with respect to the main deformation is given by the Poisson's ratios of the material in the rotated frame, ν'_{ji}, which we define as the amplitude of the linear transverse contraction - ε'_{ii} following a tensile strain ε'_{jj}. The effective flexovoltage coefficient corresponding to a specific orientation is then given by

$$f^{beam} = f'_{33,11} - \nu'_{13} f'_{33,33} - \nu'_{12} f'_{33,22} \qquad \text{A. 2}$$

where the prime is indicated, again, to stress that the above quantities refer to the rotated Cartesian system. We are now left with the task of deriving the explicit formulas of the Poisson's ratios (based on the three independent components of the elastic tensor, $c_{11} = c_{ii,ii}$, $c_{12} = c_{ii;jj}$ and $c_{44} = c_{ij,ij}$, where $i \neq j$) and of the flexovoltage tensor in the rotated frame (we shall indicate the three independent components as $f_{11} = f_{ii;ii}$, $f_{12} = f_{ii;jj}$ and $f_{44} = f_{ij;ij}$, where $i \neq j$). We shall do this in the following for each of the three cases that are relevant for our experimental samples.

(100) ORIENTATION

This is the simplest case - no rotation of the crystal axes is needed here. We have, for the Poisson's ratios

$$\nu = \nu_{13} = \nu_{12} = \frac{c_{12}}{c_{11} + c_{12}} \qquad \text{A. 3}$$

Then, we can immediately write

$$f_{100}^{beam} = (1 - \nu) f_{12} - \nu f_{11} \qquad \text{A. 4}$$

This coincides with the result of Zubko et al [1].

(110) ORIENTATION

First, we define the rotated reference frame,

$$\hat{\mathrm{x}}_1' = \frac{1}{\sqrt{2}}(\bar{1}, 1, 0) \qquad \text{A. 5}$$

$$\hat{\mathrm{x}}_2' = (0, 0, 1) \qquad \text{A. 6}$$

$$\hat{\mathrm{x}}_3' = \frac{1}{\sqrt{2}}(1, 1, 0) \qquad \text{A. 7}$$

where, as above, 3' is the longitudinal (normal to the surface) direction, 1' is the transverse direction, and 2' is the main bending axis. (Recall that, as we are working in the beam limit, there is an anticlastic bending about the 1' axis).

The Poisson's ratios are easiest to express in term of the compliances, $\nu'_{ji} = -s_{ij}/s_{jj}$. In our case, this yields

$$\nu'_{13} = -\frac{s_{11} + s_{12} - \frac{s_{44}}{2}}{s_{11} + s_{12} + \frac{s_{44}}{2}} \quad \text{A. 8}$$

$$\nu'_{13} = -\frac{2s_{12}}{s_{11} + s_{12} + \frac{s_{44}}{2}} \quad \text{A. 9}$$

This can be expressed in terms of the stiffness coefficients by using the following relationships,

$$s_{11} = \frac{c_{11}+c_{12}}{(c_{11}-c_{12})(c_{11} + 2c_{12})} \quad \text{A. 10}$$

$$s_{12} = \frac{-c_{12}}{(c_{11}-c_{12})(c_{11} + 2c_{12})} \quad \text{A. 11}$$

$$s_{44} = \frac{1}{c_{44}} \quad \text{A. 12}$$

This leads immediately to

$$s_{11} + s_{12} \pm {}^{s_{22}}/_{2} = \frac{c_{11}}{(c_{11}-c_{12})(c_{11} + 2c_{12})} \pm \frac{1}{2c_{44}}$$

Straightforward algebra leads then to

$$\nu'_{13} = \frac{(c_{11}-c_{12})(c_{11} + 2c_{12}) - 2c_{11}c_{44}}{(c_{11}-c_{12})(c_{11} + 2c_{12})+2c_{11}c_{44}} \quad \text{A. 13}$$

$$\nu'_{13} = \frac{4c_{12}c_{44}}{(c_{11}-c_{12})(c_{11} + 2c_{12})+2c_{11}c_{44}} \quad \text{A. 14}$$

[As a test, we can check that the factors and signs are correct by taking the hypothetical limit of an isotropic solid, where c_{11} - c_{12} = $2c_{44}$. By plugging this ansatz in the above formulas, we obtain the correct result, $\nu'_{13} = \nu'_{12} = c_{12}/(c_{11} + c_{12})$].

For the flexoelectric coefficients we have, more simply,

$$f'_{33,11} = \frac{f_{11} + f_{12} - 2f_{44}}{2} \qquad \text{A. 15}$$

$$f'_{33,33} = \frac{f_{11} + f_{12} + 2f_{44}}{2} \qquad \text{A. 16}$$

$$f'_{33,22} = f_{12} \qquad \text{A. 17}$$

By plugging these values of *f'* and ν' in Eq. (5.2), we recover, again, the formula of Zubko et al. [1](the explicit expression is reported in Sec. 4.5.4).

(111) ORIENTATION

Here, we have

$$\hat{\mathrm{x}}'_1 = \frac{1}{\sqrt{2}}(1, 0, \bar{1}) \qquad \text{A. 18}$$

$$\hat{\mathrm{x}}'_2 = \frac{1}{\sqrt{6}}(1, \bar{2}, 1) \qquad \text{A. 19}$$

$$\hat{\mathrm{x}}'_3 = \frac{1}{\sqrt{3}}(1, 1, 1) \qquad \text{A. 20}$$

The system is hexagonal, and hence isotropic, in plane. This means that there is only one relevant Poisson ratio,

$$\nu' = \nu'_{13} = \nu'_{12} = -\frac{s_{11} + 2s_{11}\frac{s_{44}}{2}}{s_{11} + 2s_{11} + s_{44}} \qquad \text{A. 21}$$

In terms of the stiffness coefficients, this can be written as

$$\nu' = \frac{1}{2}\frac{c_{11} + 2c_{12} - 2c_{44}}{c_{11} + 2c_{12} + c_{44}} = \frac{c'_{12}}{c'_{11} + c'_{12}} \qquad \text{A. 22}$$

We also have

$$1 - \nu' = \frac{1}{2}\frac{c_{11} + 2c_{12} - 4c_{44}}{c_{11} + 2c_{12} + c_{44}} \qquad \text{A. 23}$$

The result is

$$f_{111}^{beam} = \frac{c_{44}}{c_{11} + 2c_{12} + c_{44}}(f_{11} + 2f_{12}) - \frac{c_{11} + 2c_{12}}{c_{11} + 2c_{12} + c_{44}} f_{44} \qquad \text{A. 24}$$

SUMMARY OF CALCULATIONS AND COMPARISON TO RESULTS

In summary, we have for the beam-bending case

$$f_{100}^{beam} = -\frac{c_{12}}{c_{11} + c_{12}} f_{11} + \frac{c_{11}}{c_{11} + c_{12}} f_{12} \qquad \text{A. 25}$$

$$f_{110}^{beam} = \zeta f_{11} + \xi f_{12} - 2(1 - \zeta) f_{44} \qquad \text{A. 26}$$

$$f_{111}^{beam} = \frac{c_{44}}{c_{11} + 2c_{12} + c_{44}}(f_{11} + 2f_{12}) - \frac{c_{11} + 2c_{12}}{c_{11} + 2c_{12} + c_{44}} f_{44} \qquad \text{A. 27}$$

Where

$$\zeta = \frac{2c_{11}c_{44}}{(c_{11} - c_{12})(c_{11} + 2c_{12}) + 2c_{11}c_{44}} \qquad \text{A .28}$$

$$\xi = \frac{2(c_{11} - 2c_{12})c_{44}}{(c_{11} - c_{12})(c_{11} + 2c_{12}) + 2c_{11}c_{44}} \qquad \text{A. 29}$$

So, let's check the linear dependence above. We need to multiply f_{110} by

$$\frac{(c_{11}-c_{12})(c_{11}+2c_{12})+2c_{11}c_{44}}{2(c_{11}-c_{12})}$$

and then subtract $f_{111}(c_{11} + 2c_{12} + c_{44})$. We have, for the coefficient of f_{11},

$$\frac{c_{11}c_{44}}{c_{11}-c_{12}} - c_{44} = \frac{c_{12}c_{44}}{c_{11}-c_{12}}$$

Regarding f_{12}, we have

$$\frac{(c_{11}-2c_{12})c_{44}}{c_{11}-c_{12}} - 2c_{44} = \frac{-c_{11}c_{44}}{c_{11}-c_{12}}$$

The result is

$$-\frac{(C_{11}-C_{12})(C_{11}+2C_{12})+2C_{11}C_{44}}{2C_{44}(C_{11}-C_{12})} f_{110}^{beam}$$

$$+\frac{(C_{11}+2C_{12}+4C_{44})(C_{11}-C_{12})}{C_{44}(C_{11}+C_{12})} f_{111}^{beam} = f_{100}^{beam} \qquad \text{A. 30}$$

One can check the consistency of the above in the isotropic case, where we have $3f_{111}^{beam} - 2f_{110}^{beam} = f_{100}^{beam}$. To apply this to $BaTiO_3$ we use the following experimental values for the elastic (stiffness) contants: c_{11} = 173 GPa, c_{12} = 82 GPa, c_{44} = = = 108 GPa. We obtain

$$1.47f_{111}^{beam} - 1.24f_{110}^{beam} = f_{100}^{beam} \qquad \text{A. 31}$$

REFERENCES

1. P. Zubko, G. Catalan, A. Buckley, P. R. L. Welche, and J. F. Scott, *Phys. Rev. Lett.* **99**, 167601 (2007).